Superconductors in high magnetic fields:

Ising protection in WS_2 monolayers and critical currents in superconducting tapes

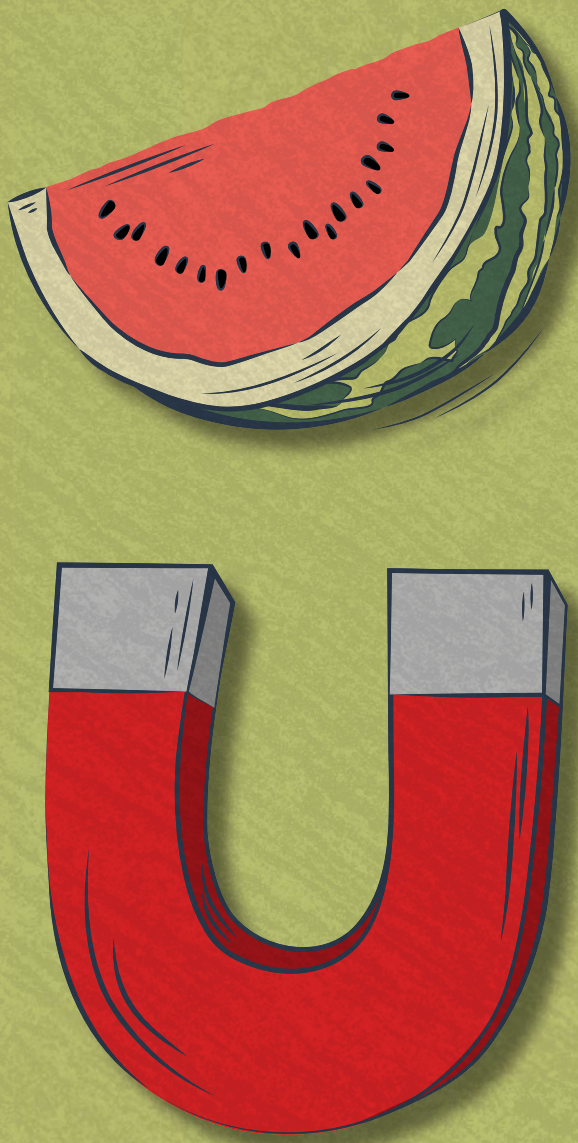

Emily Leonie Quinlyn
Nowalaja Ammerlaan

Institute for Molecules and Materials

RADBOUD UNIVERSITY PRESS

Radboud Dissertation Series

Superconductors in high magnetic fields: Ising protection in WS_2 monolayers and critical currents in superconducting tapes

Emily Leonie Quinlyn Nowalaja Ammerlaan

Superconductors in high magnetic fields: Ising protection in WS_2 monolayers and critical currents in superconducting tapes
Emily Leonie Quinlyn Nowalaja Ammerlaan

Radboud Dissertation Series
ISSN: 2950-2772 (Online); 2950-2780 (Print)

Published by RADBOUD UNIVERSITY PRESS
Postbus 9100, 6500 HA Nijmegen, The Netherlands
www.radbouduniversitypress.nl

Design: Emily Leonie Quinlyn Nowalaja Ammerlaan
Cover: Proefschrift AIO | Guntra Laivacuma
Printing: DPN Rikken/Pumbo

ISBN: 9789465152233
DOI: 10.54195/9789465152233
Free download at: https://doi.org/10.54195/9789465152233

RADBOUD
UNIVERSITY
PRESS

Superconductors in high magnetic fields:
Ising protection in WS_2 monolayers and critical currents in superconducting tapes

Proefschrift

ter verkrijging van de graad van doctor
aan de Radboud Universiteit Nijmegen
op gezag van de rector magnificus prof. dr. J.M. Sanders,
volgens besluit van het college voor promoties
in het openbaar te verdedigen op

vrijdag 17 april 2026
om 10:30 uur precies

door

Emily Leonie Quinlyn Nowalaja Ammerlaan

geboren op 23 juni 1997
te Nijmegen

Promotor:
Prof. dr. U. Zeitler

Manuscriptcommissie:
Prof. dr. A.I. Kiriliouk
Prof. dr. A. McCollam (University College Cork, Ierland)
Prof. dr. ir. A. Brinkman (Universiteit Twente)
Dr. E. Pardo (Slovenská akadémia vied, Slowakije)
Prof. dr. M.E. Diniz Guimaraes (Rijksuniversiteit Groningen)

Superconductors in high magnetic fields:
Ising protection in WS_2 monolayers and critical currents in superconducting tapes

Dissertation

to obtain the degree of doctor
from Radboud University Nijmegen
on the authority of the Rector Magnificus prof. dr. J.M. Sanders,
according to the decision of the Doctorate Board
to be defended in public on

Friday, April 17, 2026
at 10:30 am

by

Emily Leonie Quinlyn Nowalaja Ammerlaan

born on June 23, 1997
in Nijmegen, the Netherlands

Supervisor:
Prof. dr. U. Zeitler

Manuscript Committee:
Prof. dr. A.I. Kiriliouk
Prof. dr. A. McCollam (University College Cork, Ireland)
Prof. dr. ir. A. Brinkman (University of Twente)
Dr. E. Pardo (Slovac Academy of Science, Slovakia)
Prof. dr. M.E. Diniz Guimaraes (University of Groningen)

Contents

Part I

General introduction

Chapter 1

Overview

One of the major driving forces behind technological advancement in society is the continuously growing knowledge of materials. This exploration of materials and how their behaviour changes in extreme conditions is what enables us to design new materials and find new applications for existing materials. Simultaneously, it is this technological advancement that allows physicists to put known and unknown materials into more and more extreme conditions and to push the boundaries of our knowledge even further. A prominent example of this symbiotic relationship between technology and material physics is perfectly illustrated by the achievements of Heike Kamerlingh Onnes, who in 1908 succeeded in liquefying helium at the University of Leiden.

Liquid helium has a boiling point of 4.2 K at atmospheric pressure. Therefore, by using helium as a refrigerant, this technological breakthrough enabled experiments at unprecedentedly low temperatures. It is with this new tool in hand that Heike Kamerlingh Onnes found something unexpected in 1911. While measuring the temperature dependence of the resistivity of mercury, he found that just below 4.2 K the resistance suddenly started to rapidly decrease until it vanished completely [49]. And thus superconductivity was discovered. In the following years, with the aid of the newly discovered cryogenic liquid helium, many other materials were found to become superconducting as well at sufficiently low temperatures.

More than 110 years after this first observation of superconductivity, this field of research still remains a fascinating puzzle with many mysteries yet to be properly explained. The prospect of eliminating resistance offers many futuristic sounding promises; think of ultra-fast computers that do not overheat or electricity grids with near-zero losses. The holy grail in this field is of course finding an ambient-pressure room-temperature superconductor that is relatively easy to mass produce and maintain. Due to the sheer size of the material-space to search, the final discovery of this enigmatic substance is likely to be a task for future generations. Nonetheless, in this dissertation we aim to contribute to this epic quest by further exploring a fascinating special case from the family of superconductors, and by testing a new candidate material for the next generation of superconducting magnets.

This dissertation is organised into three parts. Before getting into the details of the experiments that we performed, we will first take a look at our tools and refresh our knowledge in the next chapters of this Part I. Then Part II deals with our experiments on Ising-protected superconductors and Part III addresses superconducting critical currents in technically relevant high-temperature superconductors.

After the initial experimental observation of superconductivity, it would take several more decades before the first theory was proposed to explain this phenomena. In 1957 John Bardeen, Leon Cooper, and John Robert Schrieffer presented their *Bardeen-Cooper-Schrieffer theory* [55], for which they would receive the Nobel prize in 1972. They explained that through electron-phonon interaction, two electrons of opposite spin could be paired together in a *Cooper pair*. This quasi-particle consisting of two fermions would itself not be a fermion and therefore it would not be subject to the *Pauli exclusion principle*. And thus many of these pairs could occupy the same energy levels in a *Bardeen-Cooper-Schrieffer condensate*. This *Bardeen-Cooper-Schrieffer condensate* is a first step in intuitively explaining superconductivity

Electron spin is an essential part of the BCS theory, and therefore it stands to reason that we can use magnetic fields to destroy the spin pairing and thus destroy the superconductivity. This brings us to our experiments on superconductors in high magnetic fields. In Chapter 2 we introduce the magnets and the cryogenic setup at HFML-FELIX, we will use these experimental tools to expose our samples to extremely low temperatures and high magnetic fields. This allows us to characterise them and enables us to improve our understanding of their superconducting phase.

We have already briefly mentioned the Bardeen–Cooper–Schrieffer (BCS) theory. In Chapter 3, we will review this theory in more detail and discuss the remaining theoretical concepts and models that we need to know and understand in order to interpret our experimental results.

With our knowledge of superconductivity refreshed and our experimental tools understood, we move on to Part II. Here we shift focus and deep dive into a special form of superconductivity that is found in materials from the *Transition Metal Dichalcogenide* (TMD) family. These *Transition Metal Dichalcogenides* are layered materials with a stacked hexagonal structure. By adding extra electrons to the material a superconducting phase may be induced. This superconducting phase will strengthen, meaning the superconducting transition temperature will go up, as the charge carrier concentration is increased further. Until it reaches a maximum and from there on starts to decrease again. Due to its shape, we call this region of superconductivity the *superconducting dome*.

About 10 years ago, two-dimensional layers of the *Transition Metal Dichalcogenide* MoS_2 were found to have an extremely high superconducting critical magnetic field [33] when gated using an ionic liquid and when the applied magnetic field was parallel to the two-dimensional layers of the sample. The superconducting critical magnetic field in this material extended well beyond the *Pauli limit*. This *Pauli limit* depends on the superconducting critical temperature and usually describes the highest possible value for the superconducting critical magnetic field. Above the *Pauli limit* the *Zeeman energy* aligning the spins of the two Cooper paired electrons in the direction of the applied magnetic field, exceeds the binding energy of the Cooper pairs thereby effectively destroying the superconductivity. However, it is theorised that the hexagonal structure and strong spin-orbit coupling of these *Transition Metal Dichalcogenides* pins the spins of the electrons to opposite valleys, effectively strengthening the Cooper pairing that would otherwise be destroyed by magnetic field induced spin flips.

In Chapter 4 we introduce this *Ising protected superconductivity* in more detail and review what is known so far from theory and experimental research. For this part of the dissertation we have collaborated intensively with the Zernike Institute for Advanced Materials of the University of Groningen. In Groningen we fabricated the sample devices that we measured in our experiments, the procedure we followed is described in Chapter 5. One of the major challenges in this PhD project was the development of a reliable setup for performing the ionic liquid gating procedure in the resistive Bitter magnets at HFML-FELIX. This method of ionic liquid gating is vital to our experiments, and has also been successfully

applied in other experiments, because it allows us to reach doping levels far beyond what is attainable with a traditional solid gate. In doing so ionic liquid gating allows us to access and to map the entire superconducting dome of the *Transition Metal Dichalcogenides*. In Chapter 5 we shall describe these advancements we have made in our measurement setup and explain how an ionic liquid gate is applied in detail.

Next, in Chapter 6, we will show the results from the various experiments we have performed on the samples we have made. We start with initial characterisation experiments and critical current measurements which will allow us to extract the various parameters describing the superconducting phase in this material. Then we turn on the magnetic field and map the superconducting phase as a function of temperature and magnetic field in both the parallel and perpendicular direction. We find that the strength of the Ising protection is only weakly modified throughout the superconducting dome. The Ising protection is slightly reduced by the Rashba effect which is the strongest in the centre of the superconducting dome, and decreases as we move towards the edges of the superconducting dome. We summarise our conclusions in Chapter 7 and also list some practical challenges we faced and how these may be surmounted in order to get better experimental results in the future.

In our final Part III we will continue pushing the boundaries of superconductivity, though on a completely different class of materials and using completely different techniques. In Chapter 8 we introduce briefly the SuperEMFL project and its aim of developing a 40 T or higher all-superconducting magnet. When developing a new superconducting magnet it is of course essential to first understand the properties of the superconducting phase in the material that will be carrying the current. To that end we wish to measure the magnetic moments resulting from superconducting critical currents in this material as a function of applied magnetic field. We meet our tools in Chapter 9, the in-house built *Vibrating Sample Magnetometer* and *Torque Magnetometer*, both are relatively standard magnetometry techniques. We will explain how these tools work and then in Chapter 10 we will use them to measure the magnetic response of superconducting tapes developed by THEVA GmbH, a candidate material for the next generation of superconducting magnets.

These experiments were performed in collaboration with the Institute of Electrical Engineering of the Slovak Academy of Sciences and the University of Geneva. We will show that we are able to measure superconducting critical currents in these superconducting tapes, but we will also find that our results are significantly smaller and contradicting with the results from identical low-field measurements in superconducting magnets. We hypothesise that this apparent partial suppression of the superconducting phase is due to additional electromagnetic noise in the resistive magnets. Nonetheless, our results can be interpreted as a lower boundary for the superconducting critical currents in the THEVA tapes. Possible future improvements of the experimental setup will help to push this boundary closer to reality. Finally, in Chapter 11 we draw our conclusions and formulate several key points for improvement and further exploration in the future.

Chapter 2

Experiments in extreme conditions at HFML-FELIX

As we shall see in more detail in Chapter 3, there are two main physical quantities that destroy the superconducting phase, these are: (electro)magnetic field and temperature. Therefore, to be able to understand the superconducting phase in some material and to learn about its limitations, we need two tools: magnets and cryogenics. In this chapter we briefly introduce these tools.

2.1 High magnetic fields

The experiments described in this dissertation have been performed in the Florida poly-Bitter magnets of HFML-FELIX (High Field Magnet Laboratory - Free-Electron Lasers for Infrared eXperiments). This type of magnet was invented by *Francis Bitter* in 1933 and is built by alternately stacking conducting Copper plates and insulating plates as shown schematically in Figure 2.1.1. At the time of writing, the Bitter magnets at HFML-FELIX can reach a maximum magnetic field of 38 T [1]. This is accomplished by driving a current of up to 40 kA at a maximum of 550 V through the coils of the magnet.

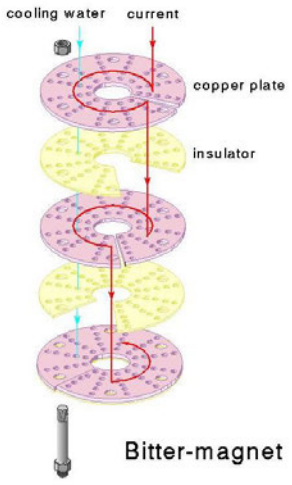

Figure 2.1.1: Schematic representation of HFML-FELIX's bitter magnets [1][42].

The required electrical power is drawn from the 50 kV 50 Hz AC grid via an on-site transformer which will first scale this down to 10 kV 50 Hz AC. This is then connected through 10 kV switches to a set of two 11 MW power-converters to convert this AC to up to 20 kA of DC [42, 31, 30].

Naturally since such a large quantity of electrical power goes in, an equally large amount of generated heat must come out. In order to extract this heat and prevent the magnet from melting, each winding of the magnet is fitted with a set of cleverly engineered holes. The spacing and location of the holes in the plates are designed such that a precise balance is

found between the structural integrity of the whole magnet and the internal temperature profile of the magnet.

To dissipate the produced heat, the magnets are cooled by a continuous flow of up to $160\,\mathrm{L\,s^{-1}}$ of demineralised water which is being pushed through the holes in the plates. In this process this cooling water typically heats up from about 10 °C to about 40 °C. A combination of heat-exchangers, chillers, and cooling towers is used to extract this heat from the cooling water. The extracted heat is partially used for heating campus buildings and partially released into the environment.

In addition to this high-field installation, two standard low-field commercial superconducting magnets are also available at HFML-FELIX. Being powered from the standard electricity grid, these superconducting magnets consume considerably less electrical power during operation. However, they also have a much lower upper limit for the magnetic field, typically 10 to 14 T. The superconducting magnets are usually used for initial characterisation experiments, and have also been used for the experiments described in this dissertation.

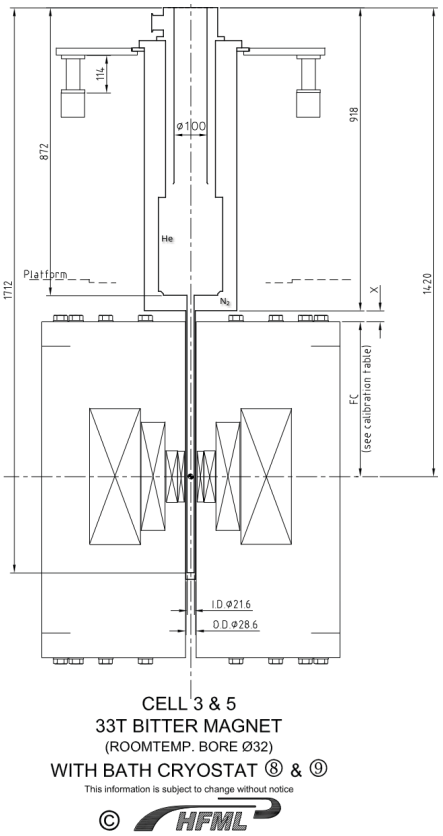

Figure 2.1.2: Schematic representation of a typical cryostat mounted on top of a typical HFML-FELIX magnet cell. The main body of the cryostat consists of a helium and nitrogen bath surrounded by thin vacuum chambers (not depicted). The tail of the cryostat consists of a heat shield thermally connected to the nitrogen bath and is also surrounded by the vacuum chamber. The experimental probe may be inserted directly in the helium bath, or an additional intermediary (for example a flow-cryostat (not depicted)), may be used for better temperature control [1].

2.2 Low temperatures

For low-temperature experiments cryostats are mounted on top of the magnet cells, as schematically depicted in Figure 2.1.2. The outer chamber of the cryostat is filled with liquid nitrogen (77 K) first and then, after the system has reached equilibrium again, the inner chamber is filled with liquid helium (4.2 K). However, by themselves the cryostats only provide cooling power and offer limited temperature control for experiments. Proper temperature control is gained by using either:

- a ^{3}He-jacket (>300 mK) or ^{4}He-jacket (>1.3 K): Allows for controlling two parameters which effectively control the temperature, namely a) heat load from a resistive heater, and b) the helium gas pressure inside the jacket.

- a flow-cryostat: For the widest possible range of operating temperatures (2.1 to 400 K). In a flow-cryostat the temperature of the sample is controlled by using a continuous flow of heated ^{4}He gas. The helium gas flows from the bath of the main cryostat through a thin capillary along a resistive heater and then enters the flow-cryostat where it is in direct thermal contact with the experimental probe.

- a dilution refrigerator: For reaching ultra-low temperatures (<100 mK). A dilution refrigerator utilises the spontaneous phase separation of a mixture of ^{3}He and ^{4}He to effectively extract heat from the sample.

Let us look at these techniques in more detail in the remainder of this section.

Controlling the temperature using a ^{3}He-jacket or ^{4}He-jacket is relatively simple. The experimental probe is inserted into the jacket and the jacket is then pumped vacuum. Inserting a small amount of helium contact gas into the jacket containing the probe provides thermal coupling to the helium bath of the main cryostat and therefore cooling power. A small heater on the probe provides heating power and this combination enables temperature controlled experiments between 1.3 K and about 20 K. The vapour pressure of ^{3}He is significantly higher than that of ^{4}He, which means that by exchanging ^{4}He with ^{3}He the lower boundary of the operating temperature can be lowered from 1.3 K to 300 mK.

A flow-cryostat is similar to a jacket but it has a small capillary that allows helium to travel from the bath of the main cryostat into the flow-cryostat chamber containing the probe. The flow through this capillary is controlled by the pressure inside the flow-cryostat and by a needle valve which can close off the inlet of the capillary. A heater allows for controlling the temperature of the helium gas flowing through the capillary which effectively controls the temperature inside the flow-cryostat and thus controls the temperature of the experimental probe.

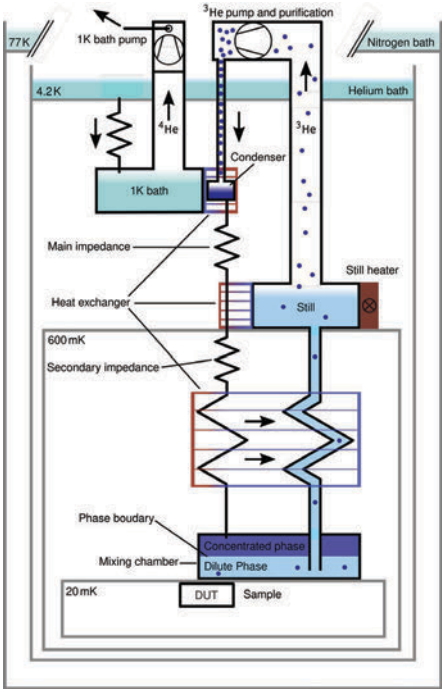

Figure 2.2.1: Schematic illustration of the operating principle of a dilution refrigerator. [22]

The dilution refrigerator, depicted schematically in Figure 2.2.1, is a bit more complicated. Below a temperature of about 870 mK a mixture of ^{3}He and ^{4}He undergoes a spontaneous phase separation, meaning that the mixture will separate into a concentrated (rich in ^{3}He) and a dilute (poor in ^{3}He) part. The system does this because the combined thermodynamic enthalpy of the separated parts is lower then that of the mixture. Hence, between the two parts a phase boundary is formed. The process of ^{3}He crossing this phase boundary from the concentrated to the dilute part is endothermic, meaning that if this crossing is driven it can be used to extract heat from this *mixing chamber*.

This phase boundary crossing forms the core of the dilution refrigerator. It is driven by a pump at room temperature, that forces ^{3}He gas through a liquid nitrogen (77 K) trap which purifies the gas. And then through a liquid helium (4.2 K) bath to pre-cool it. Next this ^{3}He is liquefied in the *condenser* which is cooled by a pumped ^{4}He bath at about 1 K. Then a series of heat exchangers cools down the ^{3}He approaching the *mixing chamber* using the colder ^{3}He leaving the *mixing chamber*. The pre-cooled ^{3}He enters the *mixing chamber* in the concentrated phase and is then pulled across the phase boundary into

the dilute phase, absorbing energy and extracting heat from the environment in the process. The ^{3}He is then extracted from the *mixing chamber* in the dilute phase. It passes again the heat exchangers, absorbing heat from the ^{3}He travelling in the opposite direction before it is heated in the *still*, boils, and returns to the pump in gaseous form to close the cycle.

2.3 Transport experiments

Measuring resistance is an excellent starting point to learn more about a certain material and how it changes under extreme conditions. As such, electrical transport experiments are a relatively common type of experiment performed in the high-field installation at HFML-FELIX. The origin of electrical resistance was first explained by Paul Drude in 1900 by his *Drude model* [64]. He tells us that as an electron, the carrier of electrical current, travels through a material it will at some point hit a scattering point which will cause a change in the electrons velocity and direction of motion. The *Drude model* is particularly noteworthy in that it was proposed years before the structure of the atom was explained by Niels Bohr in his *Bohr model* in 1913 [60, 61, 62].

It is this microscopic scattering that macroscopically results in a loss of electrical potential as a current is forced through a material. The energy lost in the collision events ends up in the scattering points and effectively warms up the material which then must dissipate this heat. Mathematically we can describe this as [64]:

$$\vec{J} = \frac{nq^2\tau}{m}\vec{E} \tag{2.3.1}$$

Where $\vec{J}$ is the current density, n is the charge carrier concentration, q is the electrical charge of the carriers, τ is the mean free time between collision events, m is the charge carrier mass, and $\vec{E}$ is the applied electrical field.

Now when we subject this electrical current to a magnetic field something interesting happens. As we know, electrons are charged particles [63], and in 1895 Hendrik Lorentz mathematically described how such a moving charged particles respond to magnetic field [65]:

$$\vec{F} = q\left(\vec{E} + \vec{v} \times \vec{B}\right) \tag{2.3.2}$$

Where $\vec{F}$ is the *Lorentz force* exerted on the charged particle, $\vec{v}$ is its velocity and $\vec{B}$ is the applied magnetic field.

Because of the cross product in Equation (2.3.2) we know that if the applied magnetic field is perpendicular to the current direction, then the charge carriers will experience a bending force deviating them away from their usual current path. This causes an overall build up of charge on one side of the current carrying material. Macroscopically this creates a measurable voltage difference perpendicular to the electrical current path. This effect was discovered in 1879 by Edwin Hall and is therefore called the *Hall effect* [66]. Mathematically we can describe the induced Hall electric field E_H as:

$$\vec{E_H} = \frac{-1}{nq}\left(\vec{J} \times \vec{B}\right) \tag{2.3.3}$$

Where the quantity $1/nq$ is often called the Hall resistance R_H. We can immediately see from Equation (2.3.3) that by measuring the Hall effect we effectively measure the charge carrier concentration in the material, which is the main use case for a Hall effect measurement.

Combining Equations (2.3.1) and (2.3.3) we can write the following for the total electric field vector:

$$\vec{E_{total}} = \begin{pmatrix} \sigma_{xx} & \sigma_{xy} \\ -\sigma_{xy} & \sigma_{xx} \end{pmatrix} \vec{J} = \boldsymbol{\sigma}\vec{J} \tag{2.3.4}$$

Where we have defined the conductivity matrix $\boldsymbol{\sigma}$, consisting of the elements $\sigma_{xx} = nq\mu$, with μ defined as the charge carrier mobility, and $\sigma_{xy} = -B/nq$. These elements represent the longitudinal and transversal conductivity respectively and are usually measured in a *Hall bar* configuration consisting of at least six measurement terminals as shown in more detail in Section 5.1.

Now that we have recapped the basics of longitudinal (Drude) and transversal (Hall) resistivity, let us look at a more exotic phenomena that we can observe when measuring resistance.

2.3.1 Quantum oscillations

During the authors PhD journey all of the cryogenic techniques described earlier in Section 2.2 were successfully applied in numerous collaboration projects with other users of the high-field magnet installation at HFML-FELIX. In this section we will briefly outline a couple of typical experiments we have performed that are only weakly related to the main subject matter of this dissertation, yet still deserve to be mentioned due to the authors involvement in the acquisition of a subset of the experimental data.

As a first example, in Zheliuk et al. [12] the ^{3}He-jacket technique was used to measure Shubnikov-de Haas (SdH) oscillations and the Quantum Hall Effect (QHE) in Bi_2O_2Se. With this technique, magnetic fields of up to 38 T can be combined with temperatures as low as 300 mK. These low temperatures are useful here since the resolvability of the Quantum Hall Effect scales inversely with temperature and can only be observed at high magnetic fields. Below we will briefly explain this Quantum Hall Effect and show a selection of the results from the experiment.

Both the Quantum Hall Effect (QHE) and the Shubnikov-de Haas (SdH) oscillations find their origin in the quantisation of (two-dimensional) electron orbitals under the influence of a magnetic field. As already explained above, electrons, being charged particles, experience a bending force called the *Lorentz force* when moving through a magnetic field perpendicular to their direction of motion. This effectively causes a charge accumulation on one side of a current carrying conductor, and a charge depletion on the other side. On a macroscopic level this results in a voltage build-up perpendicular to both the applied magnetic field and to the current, this is the *classical Hall effect*.

Considering now that electrons are quantum mechanical particles we must conclude that when the *Lorentz force* is sufficiently strong to force the electrons into closing *cyclotron orbitals*, then these orbitals must be quantised. The energy levels associated with these quantised microscopic orbitals are called *Landau Levels* (LL) and their radius depends on the magnetic field strength [58]. Therefore, as the strength of the magnetic field is increased, more and more *Landau Levels* will surpass the *Fermi Energy* and as this happens the electrons currently in that Landau level will redistribute themselves over the lower lying Landau levels. Since the macroscopic properties of a material depend strongly on this microscopic electron distribution, the end result is $(1/B)$ periodic oscillations of properties such as

the resistivity (Shubnikov-de Haas (SdH) oscillations [59]) and the magnetisation (de Haas-van Alphen (dHvA) oscillations [57]).

Let us now consider what this quantisation into Landau levels means for the Hall effect in systems where the electrons are strongly constrained to two dimensions (as is the case in the studied Bi_2O_2Se devices). In this case the total energy of each electron in the system is now fully determined by the Landau levels. After all, the third dimension that is not influenced by the applied magnetic field and could otherwise provide an additional energy degree of freedom is not accessible in such a two dimensional system. This additional constraint means that the system can only conduct current when the magnetic field strength is such that a Landau level aligns exactly with the *Fermi level*, after all this is the only situation in which this system has free carriers available at the *Fermi energy*.

Let us now define a *filling factor* (v) which represents the ratio between the total density of states in the system (n_{2D}) and the density of states in the Landau levels. When this *filling factor* is exactly integer, then all Landau levels must be filled and therefore no Landau level is at the *Fermi level* and there is no conductance in the system. On the other hand if the filling factor is exactly half-integer then the highest Landau level must be half full and this level must therefore be exactly at the *Fermi level*. It is at this point that the conductivity thus reaches a maximum.

Classically we know that the Hall effect is described by $\rho_{xy} = B/qn_{2D}$. Using then our definition for the filling factor ($v = hn_{2D}/qB$) we can substitute the density of states and find then that the Hall resistivity depends only on this filling factor $\rho_{xy} = h/vq^2$ (or inversely $\sigma_{xy} = vq^2/h$). Thus when all Landau levels are completely filled, and v is therefore integer, the Hall conductance must be an integer multiple of q^2/h. This effective quantisation is what is called the *Quantum Hall Effect* (QHE) [50].

What is especially remarkable about the quantum Hall effect is that it does not depend on the material parameters at all. The observed Hall conductance is always an integer multiple of q^2/h, and exhibits

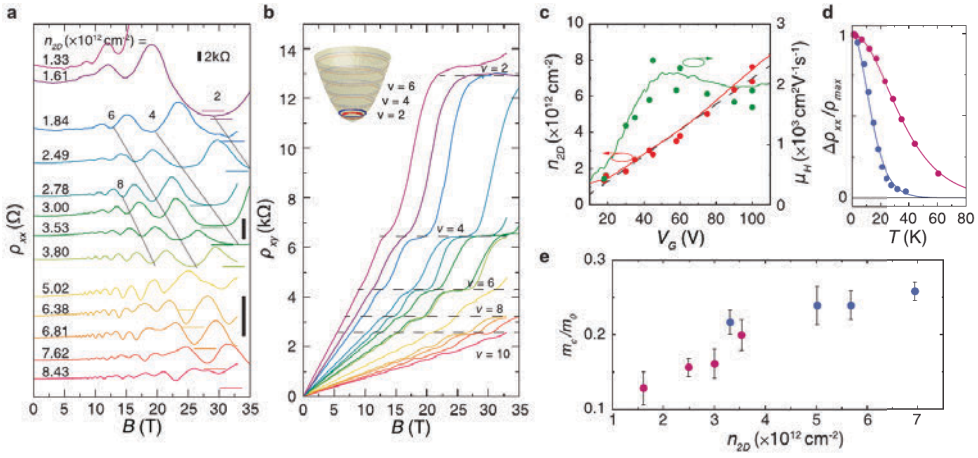

Figure 2.3.1: a. Longitudinal resistivity of a 11 nm thick Bi_2O_2Se sample at different carrier concentrations. Offset for clarity. b. Transversal resistivity (Hall effect) measured simultaneously (same colour scheme as in a.). c. Induced charge carrier concentration as a function of the applied gating voltage. d. Decay of the Shubnikov-de Haas oscillation amplitude at 30 T. e. Cyclotron mass at different electron concentrations for a 11 nm thick sample (pink) and a 10 nm thick sample (blue). Figure taken from Zheliuk et al. [12].

$1/B$ periodic steps as the applied magnetic field is increased. For this reason q^2/h is considered a standard for electrical conductance (or inversely h/q^2 a standard for electrical resistance). This constant ($h/q^2 = 25\,812.807\,\Omega$) has been named the *von Klitzing constant* after physicist Klaus von Klitzing who first observed it [50] and nowadays serves as a metrological quantum for defining the value of an Ohm.

As mentioned earlier, Zheliuk et al. [12] have measured Shubnikov-de Haas oscillations and the quantum Hall effect in Bi_2O_2Se. Bi_2O_2Se belongs to the oxychalcogenide family which are two-dimensional layered materials. Layers of the chalcogen Se alternate with layers of BiO, where the layers of Se effectively restrict the electrical transport to two dimensions and also protect the underlying BiO layers from air-contamination. These properties make Bi_2O_2Se a great platform to observe the quantum Hall effect. By means of applying an electric field with a Si/SiO_2 gate the charge carrier concentration in these layers can be manipulated, which will effect the Shubnikov-de Haas oscillations but crucially will not change the quantum Hall effect since as we have seen this quantisation is universal.

In Figure 2.3.1 we briefly showcase the results from our experiment. Panel a of this figure shows very clear Shubnikov-de Haas oscillations. These oscillations in the longitudinal resistivity shift to lower magnetic fields as the two-dimensional charge carrier concentration is decreased. In order to track this shift, guides for the eye are added to the figure for several filling factors. The second Panel b shows the transversal resistivity measured simultaneously, here we can clearly see the quantum Hall effect expressed by the occurrence of quantised plateaus in the Hall effect. Once again each plateau is labelled by the corresponding filling factor.

This successful observation of the Quantum Hall Effect in Bi_2O_2Se provides the research community with a new material system to study quantum Hall physics. In particular, the layered structure of this oxide family allows for controlled adjustments of the two-dimensional electron confinement. Readers who wish to know more details about the Quantum Hall Effect that was observed in Bi_2O_2Se are invited to read Zheliuk et al. [12].

Another experiment where Shubnikov-de Haas oscillations were observed was performed by Rubi et al. [11]. Here the dilution refrigerator was used to measure quantum oscillations in the Two-Dimensional Electron Gas (2DEG) formed at the interface between the complex oxides $LaAlO_3$(LAO)/$SrTiO_3$(STO) and EuO(EuO)/$KTaO_3$(KTO). Once again these low temperatures attainable with the dilution refrigerator (100 mK) aid to better resolve the quantum oscillations. The measured quantum oscillations, depicted in Figure 2.3.2 for different tilting angles, are rather unusual since there is some degree of aperiodicity. As we have mentioned earlier, normally quantum oscillations are exactly periodic with the inverse of the magnetic field. In order to properly understand what is going on here, a thorough theoretical analysis was required.

The experimental data, together with a thorough theoretical analysis, allowed us to gain deeper insight in the electronic band structure of the Two-Dimensional Electron Gas at the LAO/STO interface. Moreover, we were able to identify that, while these interfaces exhibit electron confinement in the two-dimensional plane at the interface, a portion of the charge carriers penetrate deep into the STO. Our experimental findings and the proposed model hold promise for aiding in understanding similar observations in other materials where non-trivial electronic states are found. To learn more about the details of this experiment and the theoretical model describing our results the reader is invited to read Rubi et al. [11].

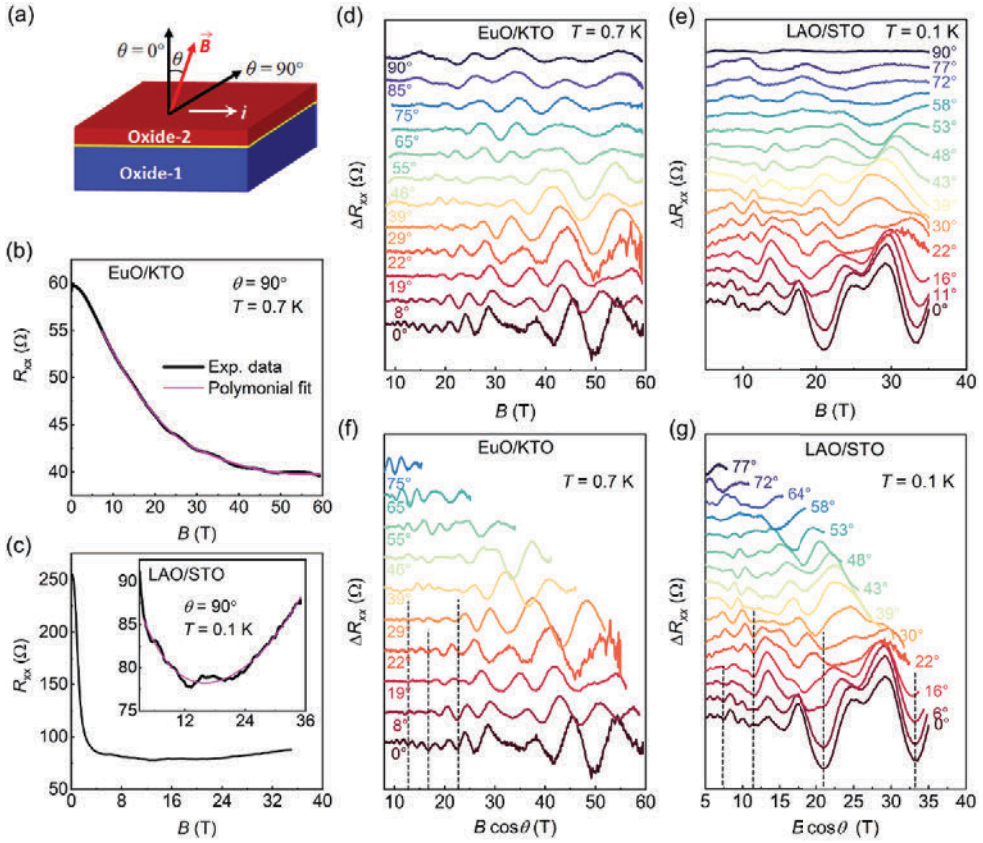

Figure 2.3.2: (a) schematic illustration of the angle between the sample plane and the applied magnetic field. (b) and (c) longitudinal resistance of the 2-Dimensional Electron Gas (2DEG) at the interfaces of $LaAlO_3$(LAO)/$SrTiO_3$(STO) and EuO(EuO)/$KTaO_3$(KTO) respectively. (d) and (f) quantum oscillations at different angles for EuO/KTO plotted as a function of magnetic field and effective perpendicular magnetic field. (e) and (g) same for LAO/STO. Figure taken from Rubi et al. [11].

Chapter 3

Superconductivity, a general introduction

In this chapter we will briefly recap the theory of superconductivity as it has been established so far. We will need to understand these fundamental concepts in order to be able to properly interpret our experimental results and put our research in the context of what has been done before.

The superconducting phase is broadly defined by three properties. The first of these properties is of course the vanishing of all resistance. The next property is a very sharp jump in the specific heat at the superconducting transition. And the final property of the superconducting phase is called the *Meissner effect*. This *Meissner effect* we will describe in Section 3.4, in the next section let us first focus on resistance and see why this completely disappears in the superconducting phase.

3.1 The pathway towards vanishing resistance

A material has resistance because (normally) an electron moving through a material will sooner or later bump into some atom, phonon (a crystal lattice vibration quantum), or other electron, and scatter as described in more detail in Section 2.3. As a result of this scattering the electron might change its velocity and direction of motion and thus in these inelastic scattering events the electron loses energy. When sending current through a material this microscopic loss of kinetic energy manifests itself macroscopically as a voltage drop over the material, or in other words: resistance.

This scattering may be minimised at low temperatures, since due to the reduced thermal energy there are less phonons in the system. It may then become possible for the motion of the electrons through a crystalline material to become more organised as the main source of scattering events shifts from phonons to impurities in the crystal structure. To intuitively illustrate this, let us imagine an electron moving through a crystal lattice. Being negatively charged, this electron will attract the positively charged atomic cores comprising the crystal lattice. This distortion creates a localised positively charged region in the crystal, which may attract a second electron to closely follow the path of the first electron. The motion of this first and second electron thus becomes bound together and therefore the electrons are said to be paired. Scattering of one or both of the electrons may destroy the pair, and thus thermal energy is detrimental to superconductivity. With this simple picture in mind superconductivity can be somewhat understood.

Of course such a mental picture can only get us so far, in order to properly understand the theory of superconductivity we must also consider a more mathematical perspective. Consider that electrons are fermions (spin $\frac{1}{2}$). If we now introduce some crystal lattice mediated interaction between two electrons pairing them together, the resulting quasi-particle (called a *Cooper pair*) will be boson-like with an integer spin (usually spin 0, meaning *singlet*). Unlike electrons, *Cooper pairs* thus do not adhere to the *Fermi exclusion principle* and therefore multiple of these *Cooper pairs* may occupy the same state. Consequently, this pairing may result in an overall reduction of the occupation of the higher energy states in the system, effectively a superconducting energy gap is opened with respect to the *Fermi energy level* of the normal state. When (almost) all *Cooper pairs* are in the lowest possible energy state (called a *Bardeen-Cooper-Schrieffer condensate*), the movement of *Cooper pairs* through the crystal must be resistance free. After all, a (quasi-)particle that is already in the lowest possible energy state cannot loose any energy. Hence superconductivity is achieved.

3.2 Superconductivity and magnetic fields

As we have seen, the spin of the (quasi-)particles plays an essential role in the formation of the superconducting state. Since the property of spin represents magnetic fields on a quantum level, it stands to reason that magnetic fields must have some effect on superconductivity.

And indeed, external magnetic fields may cause the electrons in a material to flip from spin up to spin down or the other way around. In a superconductor this effectively breaks the otherwise energetically favourable Cooper pairing between electrons of opposing spin, and therefore destroys superconductivity. In addition to this spin-flip induced destruction of superconductivity, magnetic fields also interact with the orbitals of the electrons (the Zeeman effect) and thus they may also destroy the superconducting state by forcing the electrons into orbitals that complicate Cooper pairing. Hence the superconducting state is not only limited by the temperature at which the thermal energy exceeds the binding energy of the Cooper pairs, it is also limited by the external magnetic field at which the Zeeman energy exceeds this binding energy of the Cooper pairs.

These points where the superconductivity disappears and normal resistive behaviour is restored we call the superconducting critical temperature (T_c) and the superconducting critical magnetic field (B_{c_2}). For a "regular" superconductor, meaning one that (mostly) adheres to the Bardeen–Cooper–Schrieffer (BCS) theory, this critical magnetic field cannot exceed the *Chandrasekhar-Clogston* [53, 54] (or *Pauli*) *limit* for Zeeman-induced Cooper pair breaking [51]. This Pauli limit is obtained by equating the Zeeman energy resulting from the applied magnetic field with the superconducting energy gap.

$$\frac{1}{2}\frac{g^2 N_0}{2} B_{c_2}^2 = \frac{1}{2} N_0 \Delta_0^2 \tag{3.2.1}$$

Here N_0 is the density of states at the Fermi level, g is the Landé g-factor, and Δ_0 is the superconducting energy gap which according to *Bardeen–Cooper–Schrieffer theory* is equal to $1.764 k_B T_c|_{B=0\,\mathrm{T}}$ [55]. For the case of a free electron the Landé g-factor is equal to 2, which is the value we will use here for simplicity. Plugging all of this into Equation (3.2.1) and simplifying, results in the equation below, where T_{c_0} is the superconducting critical temperature at zero magnetic field:

$$B_{c_2}|_{T=0\,\mathrm{K}} = \left(1.86\,\mathrm{T\,K^{-1}}\right) T_c|_{B=0\,\mathrm{T}} = \left(1.86\,\mathrm{T\,K^{-1}}\right) T_{c_0} \tag{3.2.2}$$

Since both temperature and magnetic field can destroy superconductivity it is not surprising that combining the two influences the values for the critical points. In other words, the superconducting critical magnetic field decreases as the temperature is increased. And conversely, the superconducting critical temperature decreases as the applied magnet field is increased. This relation between the superconducting critical temperature and the superconducting critical magnetic field can be approximated with the *Ginzburg-Landau model* [56, 48]:

$$B_{c_2} = \frac{\phi_0}{2\pi\ \xi^2|_{T=0\,\mathrm{K}}} \left(1 - \frac{T_c}{T_{c_0}}\right) = \frac{\phi_0}{2\pi\xi_0^2} \left(1 - \frac{T_c}{T_{c_0}}\right) \tag{3.2.3}$$

Which holds for a three-dimensional system. For a two-dimensional system, such as the *Transition Metal Dichalcogenides* we will be studying, the linearity in the *Ginzburg-Landau model* changes to a square root behaviour [13, 18, 36]:

$$B_{c_{2_{2D}}} = \frac{\sqrt{3}\phi_0}{\pi\xi_0^2 d_{SC}} \sqrt{1 - \frac{T_c}{T_{c_0}}} \tag{3.2.4}$$

Here d_{SC} represents the thickness of the two-dimensional superconducting layer. One way in which these models are useful is because they introduces a new quantity ξ that can be used to directly compare different superconductors. This new quantity ξ is the superconducting coherence length and it can be thought of as the size of the *Cooper pairs*, or more accurately, it represents the distance within which the superconductivity would be destroyed if the electron density would change drastically. ξ_0 represents this superconducting coherence length at zero magnetic field. This quantity ξ_0 can be easily extracted from a measurement of the superconducting critical temperature as a function of magnetic field by looking at the slope at zero magnetic field [43] where the linear approximation of the *Ginzburg-Landau model* model is the most accurate, as we shall also do in Chapter 6.

A more precise relation between the superconducting critical temperature and the superconducting critical magnetic field is given by the *Werthamer–Helfand–Hohenberg (WHH) model* [52]. This model has previously been used by Ding et al. [15] to analyse the superconducting phase in the *Transition Metal Dichalcogenides* (TMDs) and we shall therefore also use it to analyse our results in Chapter 6. The application of this model is particularly helpful for *dirty superconductors* [10, 13, 17] where it has been found to provide better theoretical predictions compared to the *Ginzburg-Landau model* [52]. This distinction between a *dirty superconductor* versus a *clean superconductor* is defined by the ratio of the *superconducting coherence length* and the *mean free path*. Where a *superconducting coherence length* longer than the *mean free path* defines a *dirty superconductor*, and the other way around, a *clean superconductor* is defined as having a *superconducting coherence length* that is shorter than the *mean free path*. For the case of a one-band two-dimensional superconductor this WHH model reduces to the *Maki-de Gennes equation* [19] shown below:

$$\ln \frac{T_{c_0}}{T_c} = U(h) = \psi\left(\frac{1}{2} + \frac{\hbar B_{c_2} D}{2\phi_0 k_B T_c}\right) - \psi\left(\frac{1}{2}\right) \tag{3.2.5}$$

Here, $\hbar$ is the reduced Planck constant, D represents the diffusivity of the superconducting band, ϕ_0 is the magnetic flux quantum, k_B is the Boltzmann constant and ψ is the digamma function. T_c is the superconducting critical temperature and it varies as a function of the applied magnetic field. Conversely, B_{c_2} is the superconducting critical magnetic field and it varies as a function of the temperature. Finally,

T_{c_0} represents the superconducting critical temperature at zero magnetic field. Because of the digamma function in Equation (3.2.5) this model cannot be rewritten into a simpler form for use with a standard fitting algorithm, we shall therefore use this model numerically and fit by minimalisation of the difference between the right hand side and the left hand side of the equation.

3.3 Currents in a superconductor

From *Ampère's circuital law* we know that any current always results in an associated magnetic field:

$$\mu_0 \int_\Sigma \vec{J} \cdot \mathrm{d}\vec{S} = \oint_{\partial\Sigma} \vec{B} \cdot \mathrm{d}\vec{l} \tag{3.3.1}$$

Here μ_0 is the vacuum permeability, Σ represents a surface through which a current density $\vec{J}$ flows (integrated with the differential of that surface $\mathrm{d}\vec{S}$), and $\partial\Sigma$ is the contour of the surface along which the associated magnetic field $\vec{B}$ is formed (line integrated with the differential of that path $\mathrm{d}\vec{l}$).

Given that magnetic fields are detrimental to superconductivity and currents always imply magnetic fields, it comes as no surprise that there is a limit to the current density that a superconductor can support. For a two-dimensional Type-II *s-wave* superconductor (a superconductor where the cooper pairs have a combined spin of 0, meaning that the electrons making up the Cooper pair have opposing spins) this superconducting critical current density J_c can be accurately described with the following model developed by Talantsev et al. [28], given by Equation (3.3.2) [2, 14, 25, 28]. This model is based on the *Bardeen–Cooper–Schrieffer theory* [55] and was also used by Zheliuk et al. [23] and Liu et al. [26] to analyse superconducting critical current measurements in MoS_2 and $PdTe_2$ respectively, and therefore we shall apply it as well for our experiments on the similar material WS_2 in Chapter 6.

$$J_c = \frac{\phi_0(\ln\left(\frac{\lambda_0}{\xi_0}\right)+0.5)}{4\pi\mu_0\lambda_0^3}\left(1-\frac{1}{2k_BT_c}\int_0^\infty \frac{d\epsilon}{\cosh^2\left(\frac{\sqrt{\epsilon^2+\left(\Delta_0\tanh\left(\frac{\pi k_B T_{c0}}{\Delta_0}\sqrt{\frac{2}{3}\frac{\Delta C}{C}\left(\frac{T_{c0}}{T_c}-1\right)}\right)\right)^2}}{2k_BT_c}\right)}\right)^{\frac{3}{2}} \tag{3.3.2}$$

Here ϕ_0 is the magnetic flux quanta, μ_0 is the vacuum permeability and k_B is the Boltzmann constant. In addition to the zero-field superconducting coherence length ξ_0 that we have already seen, there are several other parameters describing the superconductivity that enter into this model.

The first is the superconducting energy gap Δ_0, which is the result of the boson-like *Cooper pairs* forming a *Bardeen-Cooper-Schrieffer condensate* as described earlier in Section 3.1. As a result of this shifting of the occupation of the energy levels and the opening of the energy gap, there is also an associated jump in the specific heat at the superconducting transition, this is represented in the quantity $\Delta C/C$. The final new quantity introduced here is the superconducting penetration depth λ_0. As the name suggests, this quantity represents how deep an externally applied magnetic field will penetrate into the surface of the superconductor. We shall discuss the magnetic response of superconductors and this superconducting penetration depth in more detail in Section 3.4 below.

Equation (3.3.2) looks very impressive and one might think that the quantity of the parameters entering this model will significantly complicate fitting this model to real data. However, if we consider some of the limiting cases of this model the complexity quickly reduces. Let us first consider the limit where the temperature approaches the zero-field critical temperature T_{c_0}. Intuitively we expect the superconducting phase to disappear here and therefore J_c must be zero. And indeed, as $T_c \to T_{c_0}$ the argument in the hyperbolic tangent will go towards zero and Equation (3.3.2) reduces to:

$$J_c = \lim_{T_c \to T_{c_0}} \frac{\phi_0(\ln\left(\frac{\lambda_0}{\xi_0}\right) + 0.5)}{4\pi\mu_0\lambda_0^3} \left(1 - \frac{1}{2k_BT_c}\int_0^\infty \frac{d\epsilon}{\cosh^2\left(\frac{\epsilon}{2k_BT_c}\right)}\right)^{\frac{3}{2}} \tag{3.3.3}$$

The integral has become solvable, the solution results in $(1-1)$, and therefore J_c does indeed reduce to zero:

$$J_c = \lim_{T_c \to T_{c_0}} \frac{\phi_0(\ln\left(\frac{\lambda_0}{\xi_0}\right) + 0.5)}{4\pi\mu_0\lambda_0^3} \left(1 - \frac{1}{2k_BT_c} 2k_BT_c \left[\tanh\left(\frac{\epsilon}{2k_BT_c}\right)\right]_0^\infty\right)^{\frac{3}{2}} = 0 \tag{3.3.4}$$

This shows that the T_{c_0} parameter of the model is the only parameter involved in determining the crossing of the axis at $J_c = 0$ as might be expected.

Let us now look at the more interesting opposite limit where temperature approaches zero. In this case the argument of the hyperbolic tangent diverges to infinity, which means the hyperbolic tangent itself evaluates to one:

$$J_c = \lim_{T_c \to 0\,\mathrm{K}} \frac{\phi_0(\ln\left(\frac{\lambda_0}{\xi_0}\right) + 0.5)}{4\pi\mu_0\lambda_0^3} \left(1 - \frac{1}{2k_BT_c}\int_0^\infty \frac{d\epsilon}{\cosh^2\left(\frac{\sqrt{\epsilon^2+\Delta_0^2}}{2k_BT_c}\right)}\right)^{\frac{3}{2}} \tag{3.3.5}$$

To evaluate this limit properly we must Taylor expand this hyperbolic cosine:

$$J_c = \lim_{T_c \to 0\,\mathrm{K}} \frac{\phi_0(\ln\left(\frac{\lambda_0}{\xi_0}\right) + 0.5)}{4\pi\mu_0\lambda_0^3} \left(1 - \frac{1}{2k_BT_c}\int_0^\infty \frac{d\epsilon}{\left(1 + \frac{1}{2}\left(\frac{\sqrt{\epsilon^2+\Delta_0^2}}{2k_BT_c}\right)^2 + \mathcal{O}\left(\left(\frac{\sqrt{\epsilon^2+\Delta_0^2}}{2k_BT_c}\right)^4\right)\right)^2}\right)^{\frac{3}{2}} \tag{3.3.6}$$

Combining the denominators inside and outside of the integral we find that the combined denominator diverges to infinity as the temperature reduces to zero, and therefore the integral evaluates to zero and we are left with:

$$J_c = \lim_{T_c \to 0\,\mathrm{K}} \frac{\phi_0(\ln\left(\frac{\lambda_0}{\xi_0}\right) + 0.5)}{4\pi\mu_0\lambda_0^3} \tag{3.3.7}$$

And hence the crossing with the other axis, and also the maximum J_c is entirely determined by the superconducting coherence length ξ_0 and the superconducting penetration depth λ_0. The remaining two

parameters, the superconducting energy gap Δ_0 and the relative jump in the specific heat $\Delta C/C$, control the shape of the curve between the two extremes of $T_c = 0, J_c = J_{max}$ and $T_c = T_{c_0}, J_c = 0$. Thus the effective complexity of the model is reduced, keeping this in mind will greatly simplify fitting this model to real data [28].

The ratios of some of the mentioned parameters in this model provide additional information about the superconducting state. One such ratio is the gap ratio, the ratio of the zero-field superconducting critical temperature and the superconducting energy gap $2\Delta_0/k_B T_{c_0}$. *Bardeen–Cooper–Schrieffer theory* [55] predicts a value of 3.528 for this ratio. This value is called the *weak-coupling limit* because values smaller then this limit indicate that the electron-phonon coupling that is fundamental to superconductivity is relatively weak [38]. Whereas if the gap ratio is larger then this limit, the electron-phonon coupling is relatively strong. Similarly, *Bardeen–Cooper–Schrieffer theory* also predicts that the relative shift in the specific heat at the superconducting transition temperature, $\Delta C/C$, is 1.42 [55]. Superconductors with relatively strong electron-phonon coupling have values larger than this BCS-theory prediction, and superconductors with relatively weak electron-phonon coupling have values smaller than predicted by BCS-theory.

Another interesting ratio to look at is the ratio of the superconducting penetration depth and the superconducting coherence length λ_0/ξ_0, this ratio is called the *Ginzburg-Landau parameter* κ. The *Ginzburg-Landau theory* [48, 56] specifies that superconductors with a *Ginzburg-Landau parameter* $\kappa < 1/\sqrt{2}$ are *Type-I* superconductors, whereas values of $\kappa > 1/\sqrt{2}$ are associated with *Type-II* superconductors (Figure 3.4.1b). More on the distinction between *Type-I* and *Type-II* superconductors will follow in the next section.

3.4 Magnetisation of superconductors: Type-I and Type-II

We have already briefly touched upon a distinction between *Type-I* and *Type-II* superconductors. To understand this difference we must fist explore the behaviour of the magnetic response of a superconductor. As a rule of thumb, crystals consisting of only a single element tend to be *Type-I* superconductors, whereas alloys and compounds tend to be *Type-II* superconductors.

3.4.1 The Meissner phase

The magnetic response of a *Type-I* superconductor is perfectly diamagnetic. When a *Type-I* superconductor is put in a magnetic field, the magnetic field is completely nullified in the bulk interior of the superconductor. This occurs because *screening currents* manifest on the surface of the superconductor opposing the external magnetic field and effectively shielding the bulk interior from the magnetic field [48, 56]. This effect is called the *Meissner effect*, and the superconducting phase of a *Type-I* superconductor is therefore also referred to as the *Meissner phase*.

Though the *Meissner effect* is phenomenologically perfectly diamagnetic, the *Meissner effect* itself has no relation to regular diamagnetism. Regular diamagnetism is a microscopic effect resulting from the magnetic field interacting with electron orbitals in the material. This quantum mechanical effect is small since electron orbitals are strongly constrained due to the *Pauli exclusion principle* and *Coulomb repulsion* between individual electrons. The *Meissner effect*, on the other hand, is a macroscopic thermodynamic effect, where the currents opposing the magnetic field are large and purely localised on the surface of the superconductor. To illustrate this further let us first consider how a regular conductor responds to

a magnetic field.

From the *Maxwell-Faraday equation* we know that a changing magnetic flux through a surface is equivalent to an electric field along the edge of this surface:

$$\int_{\Sigma} \frac{\partial \vec{B}}{\partial t} \cdot \mathrm{d}\vec{S} = -\oint_{\partial\Sigma} \vec{E} \cdot \mathrm{d}\vec{l} \tag{3.4.1}$$

Here Σ represents a surface penetrated by the magnetic field $\vec{B}$ which is integrated over the differential of that surface $\mathrm{d}\vec{S}$. And $\partial\Sigma$ is the contour of this surface along which the electric field $\vec{E}$ travels, this in turn is path integrated over the differential of that contour $\mathrm{d}\vec{l}$.

In a conductor, where the electrons are able to move relatively freely, this means that a changing magnetic field will cause charge carriers to be subject to an electric field forcing them to move in circles. These induced electrical currents are called *Eddy currents*. As any other current, these *Eddy currents* have an associated magnetic field described by *Ampère's circuital law* (Equation (3.3.1)). This associated magnetic field opposes the original change in magnetic field as a result of the minus sign in Equation (3.4.1).

The end result is that free electrons in a conductor "resist" changes in magnetic field. How strong this opposing response is, depends on how much circular current $\vec{J}$ (Equation (3.3.1)) is created by the electric field $\vec{E}$ (Equation (3.4.1)). Or, more concretely, since $\vec{J} = \sigma\vec{E}$, the magnitude of the induced *Eddy currents* depends on the conductivity σ, and therefore inversely on the resistivity ρ, of the material. With that in mind, a conductor with zero resistance would be expected to react to a change in the magnetic field with very large[1] *Eddy currents* opposing and nullifying the change in magnetic field.

This, however, is not what happens in superconductors. A superconductor is distinct from this imaginary zero resistance conductor in two ways. Firstly, the currents opposing the magnetic field are localised exclusively on the surface of the superconductor because this is thermodynamically favourable and because the vanishing of the resistance facilitates that the surface currents can be large enough to shield the entire interior volume. The bulk of the superconductor thus remains current and field free. Secondly, whereas the zero resistance conductor would merely react to changes in the applied magnetic field, a superconductor always expels **all** magnetic field from its interior. In other words, if magnetic field is applied before the material is cooled down to the superconducting state, the magnetic field will still be completely expelled once the material becomes superconducting even though the applied magnetic field is not changing. Both of these differences can be intuitively understood by considering that the circular electrical currents induced by a magnetic field introduce vorticity in the material. Vorticity is energetically costly, therefore the energetically most favourable configuration is to have a minimal amount of vorticity (i.e. screening currents) on the surface in order to reduce the vorticity (i.e. magnetic field) in the bulk to zero. A superconductor can do this, as opposed to a regular conductor which cannot, since the resistivity is zero and therefore the energetic cost associated with moving a current to a different part of the superconducting material is greatly reduced.

[1] In fact, looking at the equation here, zero resistance would mean infinite conductivity. Implying infinitely large *Eddy currents*, which of course is not physical. It is thus not surprising that this linear relation between current and electric field breaks down at high conductivity.

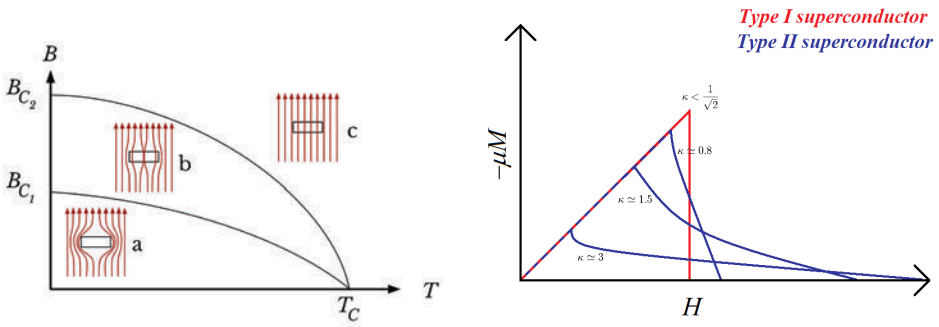

(a) Illustration of the behaviour of magnetic field lines around a superconducting material in the *Meissner*, *Shubnikov*, and normal state. Presented in a magnetic field versus temperature plot. Illustration by Bobroff et al. [37].

(b) Illustration of the magnetic response of a *Type-I* and *Type-II* superconductor for different values of the *Ginzburg-Landau parameter* κ. Illustration by Eynar [40].

Figure 3.4.1

3.4.2 The Shubnikov phase

As we have already seen, above a certain critical magnetic field (B_{c_2}) the electrons that form the superconducting *Cooper pairs* will align their spins with the magnetic field, effectively breaking the Cooper pairing and therefore destroying the superconductivity. Some superconductors however approach this critical magnetic field in two steps, these superconductors are called *Type-II* superconductors. Before the superconducting phase fully terminates (at B_{c_2}) these *Type-II* superconductors have a second lower magnetic field ($B_{c_1} < B_{c_2}$) where they leave the *Meissner* superconducting phase and enter the *Shubnikov* superconducting phase[2] [48, 56]. This phase is sometimes also called the *mixed state* or *vortex state*. In the *Shubnikov* superconducting phase, quanta[3] of magnetic flux (i.e. vortices) start penetrating the superconductor, as illustrated in Figure 3.4.1a. Effectively this makes parts of the material non-superconducting while the material as a whole mostly retains superconducting properties. After all, current will take the path of least resistance hence as long as a zero resistance path through the material still exists the overall resistance to current will remain zero.

In this vortex state, more and more vortices will penetrate the superconductor as the magnetic field is increased, up till the second critical magnetic field value (B_{c_2}) where the superconductivity is completely destroyed. Therefore, in this vortex state the diamagnetic response of the superconductor will gradually decrease from the perfect diamagnetism of the *Meissner* phase to the regular background diamagnetism of the non-superconducting state, as illustrated in Figure 3.4.1b. The latter of course being many orders of magnitude smaller then the former, as we have already explained in the previous section.

When current is flowing through a superconductor in the *Shubnikov* phase, this current may cause the vortices to move. After all, per Equation (3.3.1), every current has its associated magnetic field. And this

[2] From a thermodynamic perspective this is not a *real* phase transition. Hence "state" is technically a more appropriate word then "phase" to describe *Type-I* (*Meissner*) versus *Type-II* (*Shubnikov*). Nonetheless, "phase" is what is almost always used, and therefore it is what we will use here as well.

[3] A vortex in a superconductor must be quantised, and therefore the penetrating magnetic field must be too. This can be intuitively understood by considering that a super-current flowing in a circle cannot scatter (else it would be resistive). This means that after completing the full circle the phase of the charge carrier must match what it started the circle with, otherwise there would be destructive interference. Only certain constructively interfering circular super-currents are allowed, and hence there must be quantisation.

associated magnetic field can interact with the effective magnetic moments of the penetrating vortices. Since inside the vortex there is a non-zero magnetic field, movement of the vortices is effectively movement between magnetic field and charge carriers in the non-superconducting part of the material. This means a *Lorentz force* must act on the vortices, causing them to move, collide and scatter, dissipating energy[4]. This effectively creates a pseudo-resistance even though the material is technically still superconducting.

This pseudo-resistance is problematic for applications, the dissipating energy heats the superconductor which may cause it to exit the superconducting phase well before the critical field has been reached. This problem is reduced when the crystal structure of the superconductor has pinning points where the flux vortices get "stuck", preventing them from moving and therefore dissipating energy. These *flux pinning* points may be intrinsic to the crystal structure, or they may be artificially introduced via doping or intentional crystal defects. When the vortices are pinned in this manner they form a "lattice" which has the side-effect of altering the magnetic response of the superconductor. This change in magnetic response can be understood by considering that around each pinning point a circular super-current opposes changes in the magnetic field, similarly to the *Eddy currents* we see in regular conductors, as described before in Equation (3.4.1). Since the resistivity is zero, the only limit for this current is the maximum, or *critical*, current the superconductor can sustain. Naturally, as the external magnetic field is increased, the critical current the superconductor can sustain must go down. After all, per Equation (3.3.1), each current is accompanied with a magnetic field and for the material to remain superconducting the total magnetic field cannot exceed the critical magnetic field.

Therefore the magnetic response of a superconductor with flux-pinning points in the *Shubnikov* phase consists of two parts. The first part is the diamagnetic response, and it is called the *reversible* part of the magnetisation. This part decays as the external magnetic field is increased and more magnetic flux penetrates the material. The second part is is called the *irreversible* part of the magnetisation. This part opposes *changes* in the magnetic field. The magnitude of this part is almost[5] entirely determined by the critical current (J_c)[6] at a given field. It is irreversible because it depends not on the strength of the applied magnetic field but on the direction of change of the applied magnetic field. This irreversible magnetisation causes hysteresis in the magnetisation curve since it will flip sign when the sweeping direction of the magnetic field changes ($\vec{M} \propto -\left|\vec{J_c}\right| \rightarrow \vec{M} \propto \left|\vec{J_c}\right|$) [41].

As we have seen, the pinning of a vortex is the result of some pinning force holding it in place, but if this pinning is relatively weak then the *Lorentz force* may exceed the pinning force. When this happens the "vortex-lattice" breaks up and the vortices are free to move and as a result will dissipate energy and cause a pseudo-resistance in the superconductor. In superconductors that exhibit this breakdown of vortex pinning the pinned and free state are often referred to as the "vortex solid" and "vortex liquid" state because the breaking[7] of this "vortex-lattice" resembles the phase transition of a real crystal lattice to a liquid. The result for the magnetisation curve is the disappearance of the hysteretic part of the magnetisation and a return to the regular diamagnetic response of a *Type-II* superconductor. The magnetic field where this happens is called the *irreversibility field* (B_{irr}), since for higher magnetic fields the magnetisation curve is reversible (i.e. non-hysteretic) again. If the flux-pinning is particularly strong,

[4] This kind of energy dissipation is often called *flux creep*.

[5] Since macroscopic currents are involved, the exact relation between the magnetisation and the critical current also depends on the geometry of the superconducting device. Additionally, since no pinning can be perfect, there is still some small vortex movement and therefore induced currents do eventually decay causing the magnetisation to slowly decay with time (i.e. *flux creep*).

[6] This is **not** the same as the critical current density presented previously in Equation (3.3.2), that equation applies specifically to the two-dimensional case considered there. Here we are considering macroscopic superconductors with a bulk.

[7] This is also not a "real" phase transition, it just resembles one.

then the destruction of the superconducting phase may occur before the *Lorentz force* can overcome the pinning force and destroy the "vortex-lattice". In that case the *irreversibility field* (B_{irr}) will be the same as the critical magnetic field (B_{c_2}).

Part II

Ising protected superconductivity in Transition Metal Dichalcogenides - Tuning electronic phases by means of liquid-ion gating

Chapter 4

Introduction

Now that we have recapped the theory of superconductivity and have introduced the HFML-FELIX magnet setup in the previous Part I, we can deep dive into our first experimental subject. This Part II focusses on a type of superconductivity that strongly violates the *Pauli limit* (Equation (3.2.2)) introduced in Chapter 3. In other words, the superconductors we study here have a superconducting critical magnetic field that is more than 10 times higher than would usually be expected from *Bardeen–Cooper–Schrieffer* (BCS) theory. We aim to better understand this type of superconductivity, and specifically to investigate whether the mechanism that causes this protection of the superconducting phase changes as a function of the doping level, and if so how it changes.

4.1 Ising Protected Superconductivity

It is in the materials from the family of *Transition Metal Dichalcogenides* (TMDs) that this rather unusual form of superconductivity is found. A *Transition Metal Dichalcogenide* consists of one atom from the transition metal group, and two chalcogen atoms (S, Se, or Te) in a layered hexagonal lattice as illustrated in Figure 4.1.1.

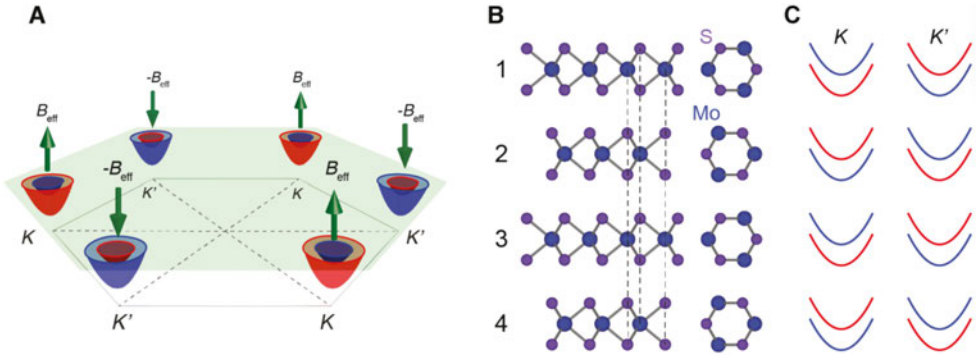

Figure 4.1.1: A: schematic structure of a MoS_2 unit cell showing the opposite internal effective magnetic fields at the K and K' valleys. B: schematic stacking structure of multiple MoS_2 layers, note the alternating pattern of the stacking. C: Band structure of multilayer MoS_2 at the K and K' valleys, note again the alternating pattern. This structure is common to all TMDs, though the size of the superconducting phase differs strongly within this family. Figure from Lu et al. [33].

Previous research on the *Transition Metal Dichalcogenides* WS_2 [27] and MoS_2 [33] has shown these materials exhibit *Ising Protected Superconductivity* at cryogenic temperatures [21]. This protection protects the superconductive phase from being destroyed by magnetic fields and as a result the critical magnetic field in these TMD devices is extremely high. To illustrate this, let us consider superconductivity in a typical monolayer WS_2 device. The superconducting critical temperature depends strongly on the doping level as illustrated in Figure 4.1.2, at optimal doping we typically find a critical temperature of about 5 to 6 K [15] depending on sample quality and possibly on the substrate.

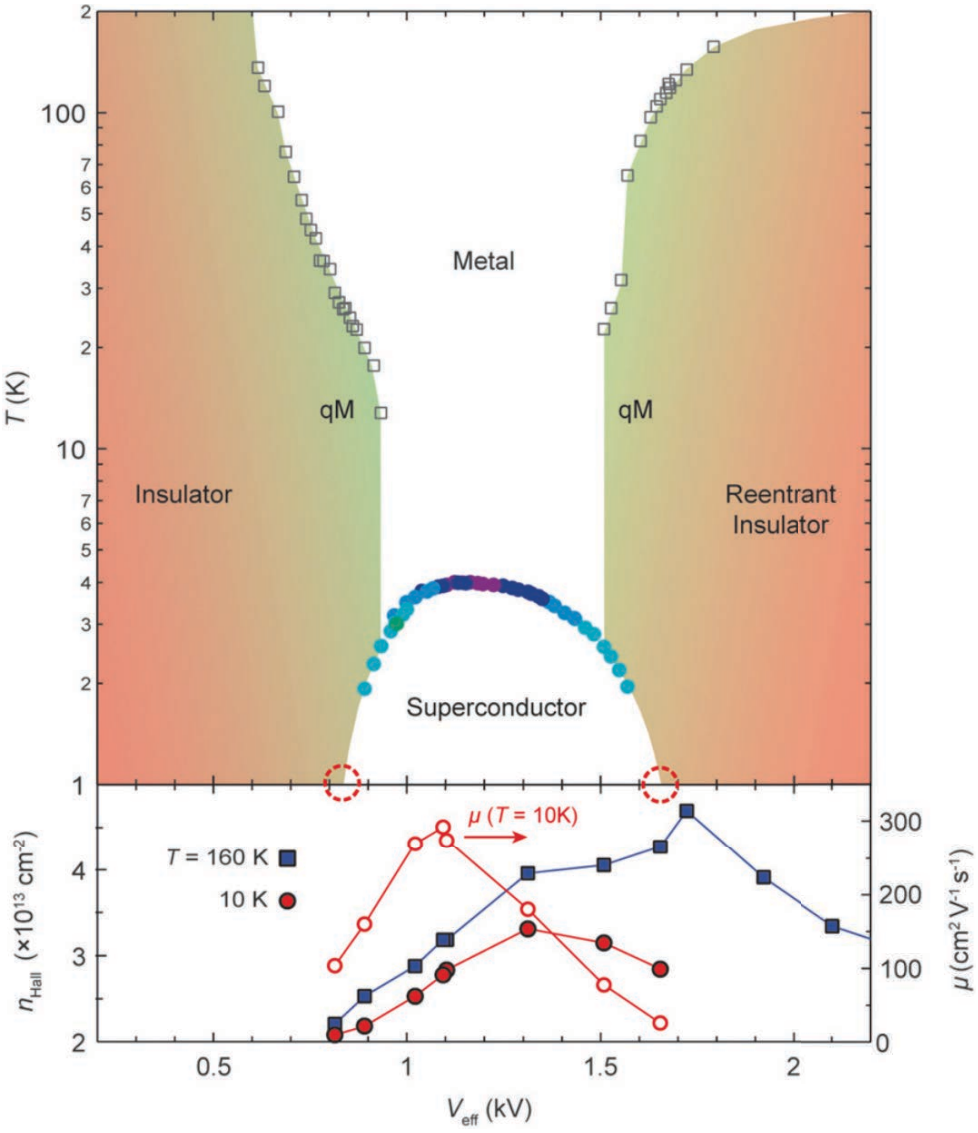

Figure 4.1.2: Phase diagram overview of the superconducting critical temperature versus the effective applied gate (qM = quasi-metal). The lower pane shows the change of the charge carrier concentration and the charge carrier mobility in response to this gating. Figure from Lu et al. [27].

Considering *Bardeen–Cooper–Schrieffer theory* and the usual definition of the *Pauli limit* (Equation (3.2.2)) we would thus expect that the superconducting critical magnetic field of monolayer WS_2 is 9 to 11 T at most. This contrasts sharply with the experimental reality, where we find that the critical magnetic field[1] is instead well above 35 T [27], far beyond what is experimentally measurable in our resistive magnets. Clearly this is not a "regular" BCS-type superconductor as described previously in Chapter 3. In the *Transition Metal Dichalcogenides* the superconducting phase is protected from externally applied magnetic fields that in most other materials are detrimental to superconductivity.

This Ising protection finds its origin in a very strong spin-orbit interaction that pins the spins of the electrons to the K and K' valleys and therefore protects the *Cooper pairs* from breaking due to magnetic spin flips. The Ising protection effect is illustrated in Figure 4.1.1: A. depicts the large alternating effective internal magnetic field B_{eff} ($\sim$100 T [33]) resulting from the strong spin-orbit coupling ($\sim$6 meV [33]) which pins the spins of the electrons to opposite directions in the K and K' valleys. B. shows that the individual layers stack in an alternating pattern; the result of this is that in multilayer *Transition Metal Dichalcogenides* the effective magnetic field of each layer is reduced by the neighbouring layers. Consequently, in TMD devices consisting of many layers (bulk devices) the Ising protection is generally greatly reduced. Finally, C. sketches the band structure at the K and K' valleys, and illustrates again the alternating pattern of the stacking.

4.1.1 Mean-Field model for Ising protection

The Ising protection can be modelled using a Mean-Field model accounting for *Rashba-type* (in-plane) and *Zeeman-type* (out-of-plane) spin-orbit coupling. We shall use these terms *Rashba-type* and *Zeeman-type* throughout this dissertation. The former is defined [27] as the in-plane spin-orbit coupling resulting from the *Rashba effect*. The latter effect is defined [27] as belonging to the spin pinning that pins the electron spins at the K and K' valleys, this pinning results in an effective internal *Zeeman-type* magnetic field. This model is described by Equation (4.1.2) and was also used by Lu et al. [27] for their experiments on WS_2. We shall use this model in Chapter 6, though once again due to the presence of the digamma function in this model we must apply it numerically.

We start by describing the lowest conduction band in a monolayer *Transition Metal Dichalcogenide* (TMD)[27]:

$$H(\vec{k}) = \frac{|\vec{k}|^2}{2m-\mu} \pm \beta_{SO}\sigma_{\mathbf{z}} + \alpha_R \vec{g}\cdot\vec{\sigma} + \vec{b}\cdot\vec{\sigma} \tag{4.1.1}$$

Where m is the effective electron mass, μ is the chemical potential, β_{SO} and α_R represent the respective strengths of the *Zeeman-type* and *Rashba-type* spin-orbit coupling, $\vec{\sigma} = (\sigma_{\mathbf{x}}, \sigma_{\mathbf{y}}, \sigma_{\mathbf{z}})$ are the *Pauli matrices*, $\vec{b} = \mu\vec{B}$ represents the applied magnetic field, $\vec{g} = (k_y, -k_x, 0)$ is the (always in-plane) *Rashba vector*, and the $\pm$ denotes the valley (either K (+) or K' (−)). This results in the following relation between the superconducting critical temperature (T_c) and the superconducting critical magnetic field (B_{c_2}) [27]:

$$0 = \ln\frac{T_c}{T_{c_0}} + \Phi(\rho_-) + \Phi(\rho_+) + [\Phi(\rho_-) - \Phi(\rho_+)]\frac{\left(\vec{g_F} + \vec{\beta_{SO}}\right)^2 - \vec{b}^2}{\left|\vec{g_F} + \vec{\beta_{SO}} - \vec{b}\right|\left|\vec{g_F} + \vec{\beta_{SO}} + \vec{b}\right|} \tag{4.1.2}$$

[1] that is, for magnetic fields parallel to the WS_2 layers.

Here the function $\Phi(\rho_{\pm})$ is defined as:

$$\Phi(\rho_{\pm}) \equiv \frac{1}{2}\Re\left[\psi\left(\frac{1+i\rho_{\pm}}{2}\right) - \psi\left(\frac{1}{2}\right)\right]$$

Where ψ is the digamma function and its argument $\rho_{\pm}$ is specified as:

$$\rho_{\pm} \equiv \frac{\left|\vec{g_F} + \vec{\beta_{SO}} + \vec{b}\right| \pm \left|\vec{g_F} + \vec{\beta_{SO}} - \vec{b}\right|}{2\pi k_B T_c}$$

And the vectors $\vec{g_F}$, $\vec{\beta_{SO}}$ and $\vec{b}$ are given by:

$$\vec{g_F} = (\alpha_R k_F, -\alpha_R k_F, 0) \quad \vec{\beta_{SO}} = (0, 0, \beta_{SO}) \quad \vec{b} = (\mu_B B_{c_2}, 0, 0)$$

Which makes that we can write the following for $\left|\vec{g_F} + \vec{\beta_{SO}} \pm \vec{b}\right|$:

$$\left|\vec{g_F} + \vec{\beta_{SO}} \pm \vec{b}\right| = \sqrt{\left(\mu_B B_{c_2} \pm \alpha_R k_F\right)^2 + \left(\alpha_R k_F\right)^2 + \beta_{SO}^2}$$

Where μ_B is the Bohr magneton, k_B is the Boltzmann constant, k_F is the Fermi wave vector, and $\alpha_R k_F$ and β_{SO} represent the *Rashba-type* and *Zeeman-type* spin-orbit coupling energies respectively.

In the next chapters we further explore Ising protected superconductivity in *Transition Metal Dichalcogenides*, specifically in WS_2. First we introduce our experimental setup, and we will learn about the sample fabrication and gating process. Then we will show our experimental results, draw our conclusions and mention points for further improvement.

Chapter 5

Experimental techniques: Ionic liquid gating and sample device fabrication

In the previous chapter we have learned about the theory underlying our experiments on Ising protected superconductivity in WS_2 as it has been established so far. In this chapter we will take the next step and introduce the techniques, methods and setup we used. We will limit ourselves to the specifics of this particular experiment, a more general outline of the resistive magnets and cryogenic equipment was already presented in Chapter 2.

5.1 Ionic liquid gating

Transition Metal Dichalcogenides (TMDs) become superconducting at high doping levels (meaning the charge carrier concentration is largely enhanced with respect to the usual level) as also illustrated in Figure 4.1.2. In order to achieve this high electron doping level we utilise the *Ionic Liquid Gating* technique.

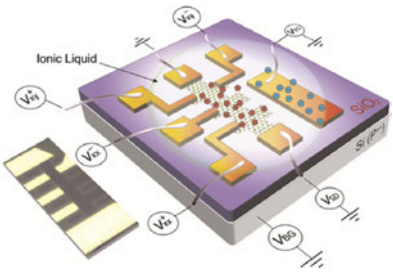

Figure 5.1.1: Schematic of a characteristic *Transition Metal Dichalcogenide* (TMD) device using ionic liquid gating. Figure from Lu et al. [27]

A typical device consists of at least six terminals, a (solid) back gate and a (liquid) top gate on a Si/SiO_2 substrate. An example device is depicted in Figure 5.1.1. Two terminals are used to apply a source-drain current (I_{SD}), while the remaining four terminals are used to measure the voltage across the device (V_{XX}) and the *Hall voltage* (V_{XY}). A droplet of ionic liquid is deposited on top of the device, covering both the TMD sample and the top gate terminal (V_{TG}). Upon applying a voltage to this top gate terminal the ions in the liquid will move; one charge will move to the V_{TG} terminal and the opposite charge will accumulate on the surface of the TMD sample. As a consequence counter-charges will build up in the uppermost layer of the TMD sample. Using this method we can achieve an extremely high ($n \propto 10^{13}/\text{cm}^2$) local charge carrier concentration on the surface of the TMD device, and thus reach

doping states which are not achievable using traditional solid state gates. By combining both ionic liquid gating (the top gate) with a traditional solid gate (the back gate) (V_{BG}) we achieve both high effective gating voltages (from the top gate) and fine control (using the back gate).

The ionic liquid gating technique presents some experimental challenges. For the superconducting phase to manifest we require cryogenic temperatures. However, the ionic liquid is in a glass state within this temperature range making it impossible to apply any gating directly using this method in the relevant temperature range. In order to successfully apply the gate, the temperature must be well above the glass transition point of the ionic liquid, which is around 190 K. On the other hand, if the temperature is too far above the glass transition point, the increased mobility of the ions causes the charge carrier concentration accumulated on the sample to decrease and be less homogeneous. Furthermore, higher temperatures increase the chemical reactivity of the ionic liquid which increases the chance of permanent degradation of the sample. Experimental experience has shown that, for the ionic liquid we used, 220 K is a reasonable choice for the temperature at which to perform the gating procedure.

Consequently, to achieve the highest possible carrier concentration and to ensure the reproducibility of the experiment it is important to have highly accurate temperature control when applying the ionic liquid gate. Then, after the gate voltage has been applied, a relatively fast but controlled cool down is required to freeze the separated ions in place. Once the ionic liquid has gone through the glass transition at 190 K, the ions can no longer move and therefore the gating voltage may be removed.

The combination of fine temperature control, controlled cooling, and sensitive monolayer samples presents a technical and experimental challenge. The solution that was developed as part of the author's PhD project, is to use a large heating element well above the liquid helium bath of a cryostat to keep the temperature stable while applying the gate, as described in more detail in Section 5.3. Once the gate is applied, the probe is lowered from the heating element into the liquid helium bath, reducing the temperature with a cooling rate that is simply controlled by the average velocity of the probe.

The setup we used for our experiments is described in more detail in Section 5.3, let us first focus on how the samples are made in the next section.

5.2 Sample fabrication

Fabrication of monolayer WS_2 devices starts with cleaving bulk WS_2 using the scotch-tape technique. Scotch-tape is carefully pressed onto to the bulk crystal and then pealed off. This piece of scotch-tape is attached to another piece of scotch-tape, aligning the part with the WS_2 flakes to the upper left corner of the new piece of scotch-tape. The two pieces of scotch tape are peeled off, and the procedure is repeated while now aligning the WS_2 flakes on the first piece of tape right next to where the flakes where deposited the first time. This is repeated until the scotch-tape contains an array of flakes comparable in size to the target Si/SiO_2 wafer.

The target Si/SiO_2 wafer is baked at 400 °C for 3 h to remove water and other contaminations before a fresh piece of scotch-tape is used to transfer the cleaved WS_2 flakes from the scotch-tape onto the Si/SiO_2 wafer. The next step is to locate monolayer flakes of sufficient size on the Si/SiO_2 wafer. It is in principle possible to do this with an optical microscope, there is sufficient contrast between monolayer, bilayer and thicker flakes (Figure 5.2.1a). However, to be absolutely sure that a flake is monolayer photo-luminescence microscopy is used. Gutiérrez et al. [34] have shown that WS_2 transitions from an *indirect bandgap* to a *direct bandgap* as the number of layers decreases to one. This results in more efficient recombination of electrons and holes, and thus the yield of the photo-luminescence is increased by several orders of magnitude, as illustrated in Figure 5.2.1b where we see the monolayer part of the WS_2 flake light up bright red.

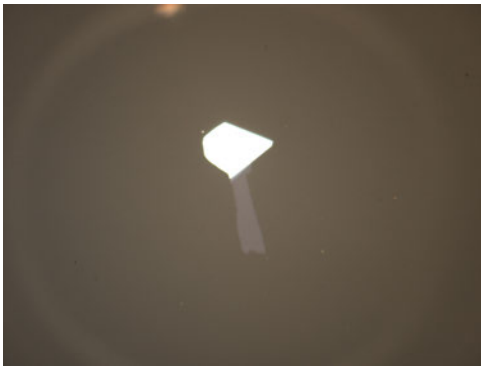

(a) An example flake of WS_2 on a Polydimethylsiloxane substrate. The "tail" of this flake is a monolayer, the "head" at the top is several layers thick. The dimensions are depicted in Figure 5.2.2a below.

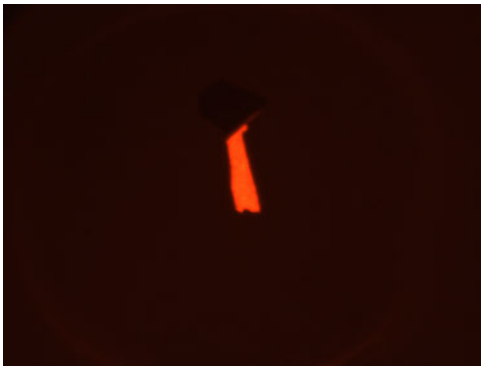

(b) The photo-luminescence of the same WS_2 flake on a Polydimethylsiloxane substrate. Only the "tail" is visible due to the strongly enhanced photo-luminescence of WS_2 monolayers with respect to bulk WS_2.

Figure 5.2.1

Ding et al. [15] have indicated that a Si/SiO_2 substrate may introduce strain and impurities in the hexagonal lattice of the *Transition Metal Dichalcogenides*. This source of disorder reduces the carrier mobility and somewhat suppresses the superconducting phase. The proposed solution is to add a relatively thick layer of hexagonal Boron Nitride (hBN) between the Si/SiO_2 wafer and the WS_2 monolayer flake. Hexagonal Boron Nitride is chemically inert and its' layered hexagonal lattice closely resembles the structure of the Transition Metal Dichalcogenides (Figure 4.1.1b). It is hypothesised that this reduces the stress in the WS_2 lattice, allowing the Q valleys to participate in the charge transport, and therefore potentially enhancing the superconducting critical temperature. When using hBN as an intermediary in this way, an increase of the superconducting critical temperature of as much as 30 % has been reported [15].

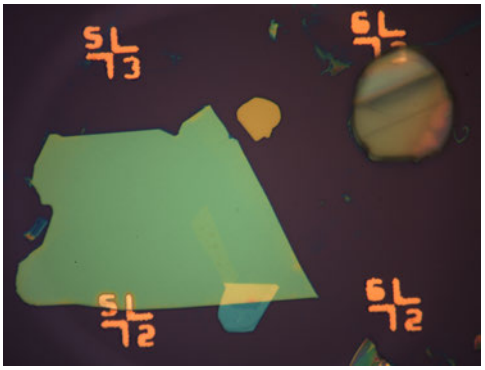

(a) The WS_2 flake from Figure 5.2.1a deposited onto a hBN substrate on a Si/SiO_2 wafer. Note that the WS_2 flake is mirrored and rotated with respect to Figure 5.2.1a. The distance between the shown coordinate markers is 100 µm.

(b) The photo-luminescence of the WS_2 flake from Figure 5.2.1b deposited onto a hBN substrate on a Si/SiO_2 wafer. Note that the intensity of the photo-luminescence has decreased because of the addition of the extra layer of hBN and note also that the flake has been mirrored and rotated with respect to Figure 5.2.1b.

Figure 5.2.2

The procedure to add hBN as an intermediate layer between the Si/SiO_2 wafer and the WS_2 sample starts with cleaving hBN onto a Si/SiO_2 wafer similar to what was described above for WS_2. A hBN flake of suitable size and thickness is then selected. Next, the WS_2 is cleaved, also as described above, but onto a substrate of *Polydimethylsiloxane* (PDMS) instead of directly on the Si/SiO_2 wafer. The PDMS containing the selected WS_2 monolayer flake is then flipped upside-down and, using an optical microscope, carefully aligned with the chosen hBN flake. Once the alignment is correct the PDMS is carefully lowered on the the Si/SiO_2 wafer. The transfer process of the WS_2 from the PDMS to the hBN can be monitored using an optical microscope, special care must be taken to avoid bubbles. When the WS_2 flake is in contact with the hBN the PDMS substrate may be carefully lifted off. Since the adhesion of WS_2 to hBN is stronger then the adhesion of WS_2 to PDMS, the WS_2 monolayer flake will remain on the new hBN substrate (Figure 5.2.2a).

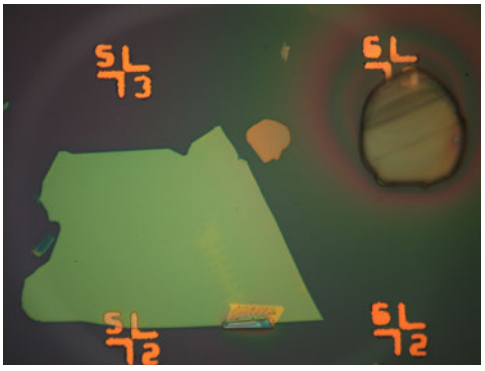

(a) The plasma-etched hBN/WS_2 device from Figure 5.2.2a, shown on the same scale.

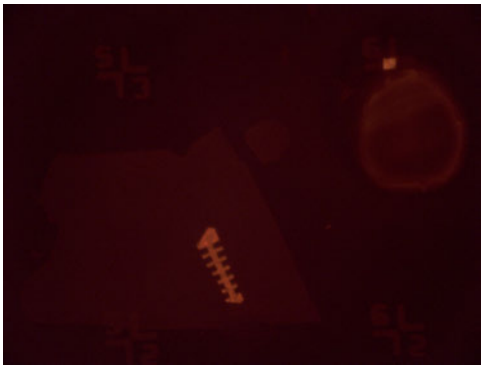

(b) The photo-luminescence of the plasma-etched hBN/WS_2 device from Figure 5.2.2b.

Figure 5.2.3

The prepared WS_2 flake, whether on hBN or directly on the Si/SiO_2 wafer, must be etched into a suitable *Hall-bar* geometry to ensure uniform electrical transport properties. To do this, the device is first coated with *Poly(methyl methacrylate)* (PMMA), after which the inverse of the desired Hall-bar pattern is exposed onto the device using *Electron Beam Lithography* (EBL). Next the pattern is developed using a 1:3 mixture of *Methyl Isobutyl Ketone* (MIBK) and *Isopropanol* (IPA), this removes the areas of the PMMA that were exposed to the electron beam. The exposed and developed pattern is then etched using *Induction Coupled Plasma - Reactive Ion Etching* (ICP-RIE). While etching, the remaining unexposed PMMA protects the parts of the monolayer WS_2 flake that should be kept, while the bare WS_2 under the exposed and removed PMMA is etched away. Once the etching process has been completed the remaining PMMA is removed with *Acetone* (Figure 5.2.3a).

The next step is to create electrodes that will facilitate the electrical connection between the chip-carrier and the hBN/WS_2 device. This is done by coating the device again with PMMA, exposing the desired electrode pattern with EBL, and developing with the MIBK/IPA solution, as described above. Note that in this round of EBL the desired pattern itself should be exposed to the electron beam, as opposed to the previous round of EBL where the **inverse** of the desired pattern was exposed. After all, this round we want to control areas where we deposit the electrodes, whereas in the previous round we wanted to control the areas that should **not** be etched away. After exposure to the electron beam, the developed pattern is coated with Titanium and then Gold. The remaining PMMA is finally removed again with *Acetone* (Figure 5.2.4a and Figure 5.2.5).

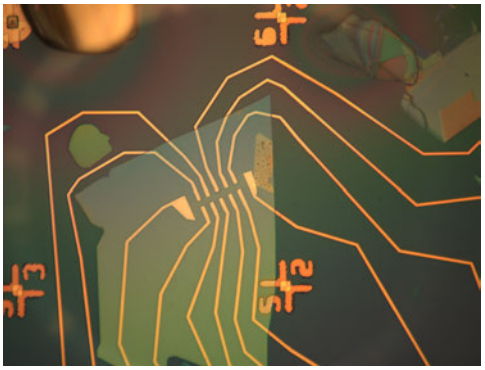

(a) The plasma-etched hBN/WS_2 device from Figure 5.2.3a with Ti/Au electrodes, shown on the same scale. Note the device is rotated 90° anticlockwise with respect to Figure 5.2.3a.

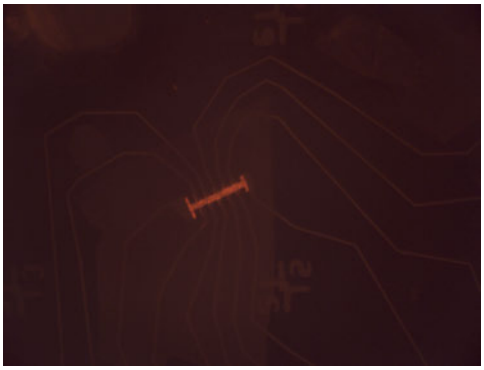

(b) The photo-luminescence of the plasma-etched hBN/WS_2 device from Figure 5.2.3b with Ti/Au electrodes. Note the device is rotated 90° anticlockwise with respect to Figure 5.2.3b.

Figure 5.2.4

The completed wafer is glued on a *Leaded Chip Carrier* (LCC) and a wire-bonder is used to electrically connect the electrodes on the wafer with individual terminals on the chip carrier. A droplet of *Diethylmethyl(2-methoxyethyl)ammonium bis(trifluoromethylsulfonyl)imide* (DEME-TFSI) ionic liquid is deposited on the wafer, covering the WS_2 sample and the top-gate electrode, shown in the top left of Figure 5.2.5. The ionic liquid is air-sensitive, and may over time chemically react with the WS_2 sample. Therefore, from this point onwards special care must be taken when storing the sample. Best practice is to store and transport the completed devices dry and at temperatures well below the glass-transition temperature of DEME-TFSI (i.e. well below 190 K). This prevents the droplet from moving on the wafer, and reduces the air-sensitivity and chemical-reactivity of the completed device. The easiest way

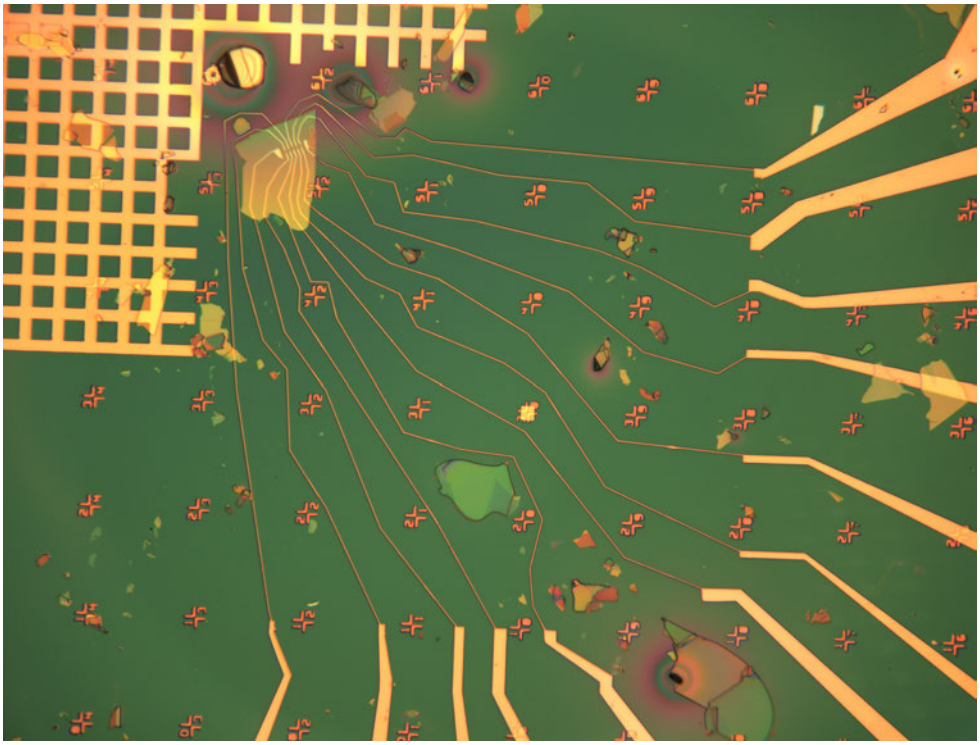

Figure 5.2.5: The completed plasma-etched hBN/WS_2 device from Figure 5.2.3a with Ti/Au electrodes. Zoomed out with respect to Figure 5.2.4a, showing also the larger electrodes and the liquid gate in the top right. The distance between the shown coordinate markers is 100 µm.

to accomplish this is to store the entire box containing the completed devices in a bath of liquid nitrogen. This is also the method we used to transport the completed devices from the fabrication facility in Groningen to the HFML-FELIX laboratory in Nijmegen. That being said, to reduce the risk of, for example, broken electrodes or unwanted chemical reactions ruining the devices, the completed devices should be measured as soon as possible and storage time must be minimised.

5.3 Experimental Setup

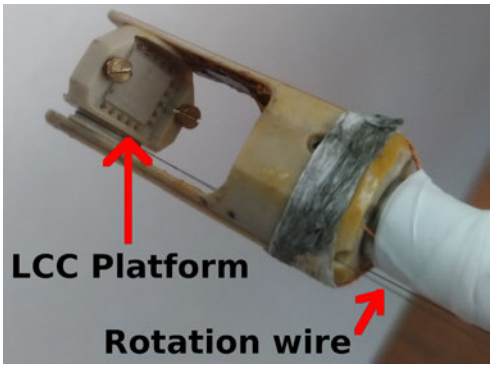

Figure 5.3.1: Photograph of the head of the LCC rotator probe. Showing the LCC socket where the sample device will be mounted and the rotation wire that may be used to rotate the entire platform in the magnetic field. The LCC socket has 20 terminals and fits a standard 9 mm by 9 mm LCC.

The chip carrier containing the completed WS_2 device is mounted on the rotatable head of the probe shown in Figure 5.3.1. This probe in turn is inserted into a jacket, the inside of which is then pumped vacuum before a small amount of ^{4}He contact gas is added. By replacing the top of a regular cryostat with a new top featuring a heating element (Heater A, and its associated Thermometer A, as depicted in Figure 5.3.2) we can use a small crane to carefully position the tip of the probe containing the sample device within the heating element. We can now control the temperature of our sample device by either, making small adjustments to the height of the probe moving it closer or further away from the helium bath, by adjusting the current through our large heating element (Heater A, Figure 5.3.2), or by adjusting the current through our smaller secondary heater on the probe itself (Heater B, Figure 5.3.3a).

By tweaking these three variables we can reproducibly stabilise the temperature of our sample device, our target is (220.0 ± 0.5) K which is sufficiently far above the glass transition point of the DEME-TFSI ionic liquid (190 K). These stable temperature conditions enable the controlled creation of the liquid top gate. It is essential to verify that the application of the liquid top gate is reproducible by repeatedly sweeping the voltage on the top gate electrode up and down, as demonstrated in Figure 5.3.4. A sample that is not responding reproducibly indicates either, temperature instability, flaky electrodes, or chemical reactions changing the sample properties. If the sample does respond in a reproducible manner to the application of the top gate, then the desired set point for the top gate can be applied. Next the probe can be lowered into the liquid helium bath while keeping the top gate voltage applied. Once the temperature drops well below 190 K, the glass transition temperature of DEME-TFSI, the ions are frozen in place and thus the gate voltage can be released.

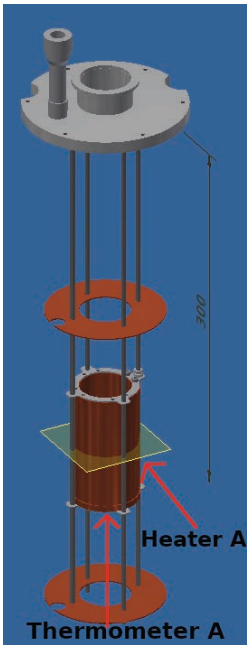

Figure 5.3.2: Schematic of the Copper heating element (Heater A) used for temperature control while gating. The associated Thermometer A is on the inside of the cylindrical heating element. Dimensions shown in the figure are in mm. Design by Lijnis Nelemans.

During the cool down the trend of the resistance is monitored (as demonstrated in Figure 6.1.1). In order for the sample device to become superconducting at helium temperatures, it must be in a metallic state. This is indicated by a continuously decreasing resistance as the temperature drops. If at any point during the cool down, the resistance starts to increase then this indicates that the sample device is entering a insulating state meaning the superconducting dome has been missed and the applied ionic-liquid top gate is either too high or too low [27]. If this happens then the probe may be slightly lifted, increasing the temperature. When the temperature again

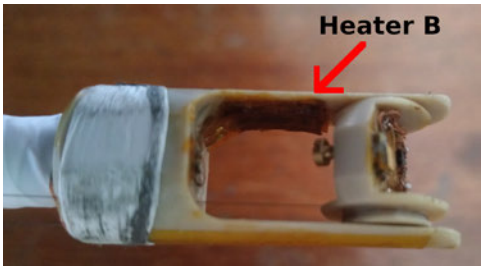

(a) Photograph of the strain-gauge heater on HFMLs LCC rotator probe (Heater B).

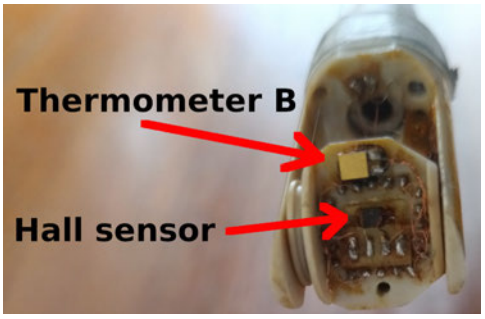

(b) Photograph of the bottom of the rotation platform on HFMLs LCC rotator probe. Showing a Cernox thermometer (Thermometer B) and a Hall sensor for measuring the angle of the rotation platform.

Figure 5.3.3

approaches the melting point of 190 K, the ionic liquid will slowly melt and in doing so the top gate is partially released. If the resistance starts to decrease then this indicates that the starting point of the ionic liquid top gate was too high and the superconducting dome was overshot. At this stage, this is a problem that can be fixed by slowly partially melting the ionic liquid. Once the resistance reaches a value that looks more reasonable with respect to the starting point the probe can be lowered again, decreasing the temperature and stopping the melting of the ionic liquid top gate.

This partial-gate-release process may be repeated several times if the gating induced by the ionic liquid is still too high. However, care must be taken to not overdo it because if the gate is too low then the sample will become insulating again (Figure 4.1.2). This procedure, when compared to simply warming

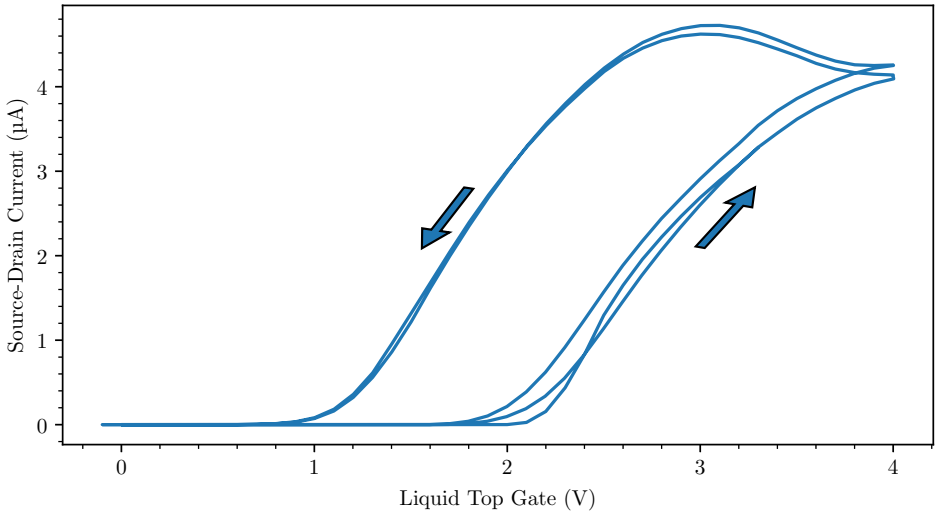

Figure 5.3.4: Example response of a typical WS_2 monolayer device to the application of the liquid top gate at 220 K. As the loop is repeated multiple times, the transfer curve becomes more reproducible.

up all the way to 220 K and re-gating from scratch, has the advantage that it is a lot faster and that it is easier to monitor the response of the sample with respect to the top gate in real-time. However, it has the disadvantage that there is less control and that the information on the state of the top gate is lost. Effectively, the reproducibility of the path to a specific superconducting state, which is already low to begin with, is lost completely.

Once the gate is released, the sample has finished cooling down, and a proper state has been established, all the electrodes on the device must be tested to find out which ones have the best conductance and which ones are not working at all. To do this a pair of lock-in amplifiers are used, the first one will create a sinusoidal voltage. Which is converted to a stable current by a pre-resistor and then sent through a selected pair of electrodes. The second lock-in amplifier measures the voltage across two different electrodes that cross the current path. By iterating over different pairs of current and voltage electrodes the performance of the electrodes can be compared. An ideal device has at least six working electrodes, a pair to apply current (i.e. the source and drain), a pair to measure the longitudinal voltage drop (i.e. the resistance), and a pair to measure the transversal voltage difference (i.e. the Hall voltage).

In the frozen state, the top gate can no longer be changed, therefore further fine-tuning must be done with the solid back gate. This allows for measuring the sample device at multiple charge carrier concentration states without thermal cycling to change the ionic liquid top gate.

The sample device is now ready for the experiment. Typically an experiment on these Transition Metal Dichalcogenides devices involves controlled changes of the applied current, the applied back gate, the external magnetic field, or the temperature. Specifically for temperature controlled measurements in a magnetic field we need to account for the effect the magnetic field will have on the temperature sensors (Thermometer A and B). These Cernox thermometers operate by measuring the resistance of the sensor and converting this to temperature using a predetermined calibration file. However, in a magnetic field this simple calibration of resistance to temperature will require an additional correction since there is a magnetic field dependent component to the resistance which is especially relevant at low temperatures.

As a consequence of this magneto-resistance effect we cannot use PID control to keep the temperature stable when varying the magnetic field at cryogenic temperatures. Therefore, to perform these magnetic field sweeps, we stabilise the temperature first at the desired set point and then switch to a constant current mode where we simply apply a constant amount of heating power through Heater B. Within the time-frame of the experiment we can safely assume that the temperature remains constant with this approach.

However, when performing experiments at a constant magnetic field with a changing temperature, we have no choice but to use the PID control in order to guarantee a stable cooling or heating rate. As a consequence we must, when analysing the data, perform a magneto-resistance correction to convert the measured temperature to the actual temperature. We do so by using a set of calibration measurements where we have measured the behaviour of the thermometer at a constant temperature in a varying magnetic field. To assist with this correction we have created a set of Python tools to semi-automatically create calibration files to convert between measured temperature and actual temperature as a function of magnetic field, and to apply this calibration to existing datasets as well as in real-time by directly hooking into the data-acquisition software of HFML-FELIX [7].

Chapter 6

Results: Ising protection across the superconducting dome

We have thoroughly investigated the properties of the superconductivity in monolayer WS_2 samples in several different gating states. As previously stated, our final aim is to characterise if and how the Ising protection of the superconducting phase in WS_2 changes as a function of doping level. To that aim we have preformed several experiments which we will describe in this chapter.

First, we will present the results from current-voltage measurements as well as the temperature dependence of the resistance without applying any magnetic field. From these measurements we shall extract several parameters describing the superconducting phase in ion-gated monolayer WS_2, similar to what was done by Zheliuk et al. [23] for MoS_2. After this initial characterisation we will move on to measurements in perpendicular and parallel magnetic fields. The measurements in perpendicular magnetic field allow us to determine the charge carrier concentration of a given state using the *Hall effect*. Furthermore, these perpendicular magnetic field measurements also enable us to determine the superconducting coherence length, and may teach us more about the distribution of the electrical transport over different electronic bands. Then finally, the measurements in parallel magnetic field make it possible to extract the parameters describing the Ising protection of the superconductivity.

From the critical current measurements we will learn that WS_2 is a *Type-II* superconductor with strong electron-phonon coupling. For the measured states we will find a superconducting critical temperature that varies from 1.7 K to 4.9 K, where the WS_2 samples that are on a hBN substrate tend to have higher transition temperatures compared to the samples where the WS_2 monolayer is directly on a Si/SiO_2 substrate.

Similar to what was done by Ding et al. [15], we will use the one-band *Werthamer–Helfand–Hohenberg (WHH) model* introduced in Chapter 4. When fitting the perpendicular magnetic field data to this model we will find that it fits well to the data belonging to the samples which are directly on a Si/SiO_2 substrate, but fits noticeably worse to the samples on a hBN substrate. Ding et al. [15] have suggested that there could be some multi-band character to the superconducting phase introduced by the addition of the hBN substrate. This theory could explain our findings, but unfortunately at this stage we cannot offer conclusive evidence in support of this claim as we were unable to fit our data to the two-band *Werthamer–Helfand–Hohenberg (WHH) model*.

Furthermore, we shall find that the *Zeeman-type* spin-orbit coupling energy (β_{SO}) associated with each state is constant throughout the superconducting dome within the measurement accuracy. The *Rashba-type* spin-orbit coupling energy ($\alpha_R k_F$), on the other hand, increases with the superconducting critical temperature. This finding suggests that the Ising protection associated with the superconducting phase decreases in relative strength towards the centre of the superconducting dome compared to both edges of this superconducting dome.

6.1 Zero-field measurements

Superconductivity in ionic liquid gated WS_2 was first reported by Jo et al. [32], and later Lu et al. [27] confirmed the presence of Ising protection in the superconducting state of WS_2. However, to the best of our knowledge, a thorough analysis to determine the properties describing this superconducting state has not been performed yet. Therefore, before we use any magnetic field we first perform characterisation measurements to determine the properties of the superconductivity in WS_2. Such measurements without magnetic field already allow us to extract several parameters describing superconductivity in this material. First of all, by measuring the temperature dependence of the resistance we can determine the zero-field critical temperature (T_{c_0}). Next we determine the superconducting critical current (J_c) by measuring the current-voltage response of the superconducting phase. Using the superconducting coherence length (ξ_0) that we will determine later, this allows us to obtain: the magnetic penetration depth (λ_0), the superconducting energy gap (Δ_0) and the relative change in the specific heat at the superconducting transition ($\Delta C/C$). For all states a similar procedure was followed, and in this chapter we consistently use one of these states to showcase our results in detail before comparing the end results of all measured states with each other.

6.1.1 Temperature dependence of the resistance

As described in detail in Section 5.3 we establish a specific gating state in the WS_2 device by applying a voltage of around 2 to 4 V to the ionic liquid top gate at a temperature of 220 K. The established state is then fixed by reducing the temperature of the sample to below 190 K which freezes the ionic liquid. As the ions in the ionic liquid are now frozen in-place, the gating voltage that was applied to the top gate can now be removed. The cooling is then continued by lowering the probe further down towards the helium bath of the cryostat with a target cooling rate of about 1 to 3 K min^{-1}. During this cool down the sample resistance is monitored as shown in Figure 6.1.1. We see that the resistance steadily decreases which shows that the sample device is gated into the metallic regime. For these systems this metallic behaviour is a strong indicator for the eventual occurrence of superconductivity in this state at cryogenic temperatures [27]. And indeed, around 4 K we find that the sample device enters the superconducting phase and the resistance starts to decrease rapidly. The sample device was briefly fully grounded during the final stage of lowering the probe into the cryostat to avoid possible discharges as the probe enters, and comes into direct electrical contact with, the tail of the cryostat. In this stage no resistance values can be recorded, and thus this results in a brief gap in the cool down curve.

Once the jacket is fully inserted, the sample is ungrounded and the measurement is continued. The inset of Figure 6.1.1 zooms in on the superconducting transition, where we see the resistance quickly decreasing towards zero. Note that a completely zero resistance state is not reached, this is likely the result of some degree of inhomogeneity in the sample and/or the top-gate causing the superconductivity to be filamentary. Such inhomogeneities may cause that, while part of the sample is in the superconducting

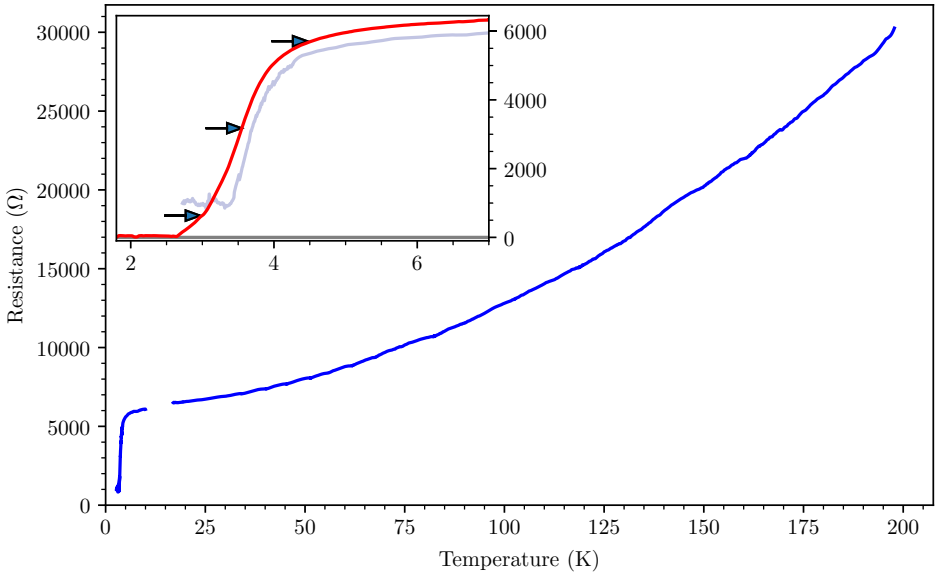

Figure 6.1.1: Resistance of a WS_2 monolayer sample versus the sample temperature during an initial fast free cool down after the ionic liquid top gate has been fixed and frozen. There is a small gap in the curve due to a brief interruption in the measurement during the cool down, as described in more detail in the main text. The inset zooms in on the superconducting transition. The blue curve represents the initial fast free cool down. The red curve shows the subsequent slower controlled measurement that was performed after reheating the sample and finding the best contact pair. Arrows indicate the 10 %, 50 %, and 90 % points in the superconducting transition.

state, another part of the sample has a slightly different charge carrier concentration and remains resistive. If such areas of the sample are in series with each other with respect to the current direction then the end result will be a non-zero remnant resistance in a state that is otherwise superconducting. In other words, the zero-resistance *percolation path* is shorter than the distance between the electrodes that are being used in this measurement.

For comparison, and to get a more consistent result for the superconducting critical temperature at zero-field, we also depict in red a slower temperature controlled measurement that was performed after the initial fast cool down. For this measurement we use a new pair of electrodes that was carefully selected after testing all possible combinations one-by-one and determining which pair performed best. We find that this new pair does not exhibit the same remnant resistance issue; instead the resistance does decrease all the way to zero. Since the red temperature controlled curve was measured at a slower rate, the measured temperature is also more accurate as the temperature difference between the sample and the thermometer is minimised. This has the effect of not only resulting in a much smoother curve but it also shifts the curve slightly to lower temperatures. From this slow curve we determine the zero-field superconducting critical temperature $T_{c_0} = 3.54\,\mathrm{K}$ using the 50 % criterion as indicated with an arrow in the inset of Figure 6.1.1. By finding the 10 % and 90 % points of the superconducting transition as well, we can define the zero-field superconducting transition width $\Delta T_{c_0} = 1.50\,\mathrm{K}$ by taking the difference between these two extremes.

Sample	State	hBN	Dome Side	V_{BG} (V)	T_{c_0} (K)	n ($\times 10^{13}$/cm^2)	$\Delta T_c/T_{c_0}$	$\alpha_R k_F$ (meV)	β_{SO} (meV)	D (cm^2 s^{-1})	ξ_0 (nm)	λ_0 (nm)	Δ_0 (meV)	$\Delta C/C$
4	2	N	R	0	1.73	2.587 ± 0.011	0.11 ± 0.03	1.5 ± 0.2	11.5 ± 1.2	-	-	-	-	-
2	1	Y	R	50	1.96	2.531 ± 0.023	0.19 ± 0.03	1.9 ± 0.2	9.7 ± 0.9	-	-	-	-	-
3	3	N	R	20	2.07	1.882 ± 0.009	0.10 ± 0.02	1.7 ± 0.3	12.2 ± 1.9	-	-	-	-	-
3	3	N	R	0	2.30	2.368 ± 0.008	0.07 ± 0.02	1.7 ± 0.4	13.6 ± 2.6	-	-	-	-	-
3	3	N	R	-20	2.46	2.497 ± 0.013	0.07 ± 0.02	1.9 ± 0.4	12.6 ± 2.2	-	-	-	-	-
4	1	N	R	0	2.48	2.225 ± 0.003	0.08 ± 0.02	1.6 ± 0.4	14.9 ± 2.8	-	-	-	-	-
3	2	N	L	-20	2.84	2.599 ± 0.008	0.07 ± 0.02	2.7 ± 0.4	10.0 ± 1.2	-	-	-	-	-
2	1	Y	R	0	2.90	2.054 ± 0.013	0.11 ± 0.02	1.3 ± 0.6	19.0 ± 6.3	-	-	-	-	-
3	4	N	-	0	2.98	2.386 ± 0.005	0.06 ± 0.02	2.1 ± 0.5	13.6 ± 2.8	-	-	-	-	-
1	2	Y	R	30	3.04	-	0.08 ± 0.02	2.4 ± 0.4	12.2 ± 1.9	-	-	-	-	-
3	2	N	L	0	3.04	2.527 ± 0.005	0.08 ± 0.02	2.9 ± 0.4	10.3 ± 1.4	-	-	-	-	-
2	1	Y	R	-50	3.25	2.272 ± 0.010	0.17 ± 0.02	3.9 ± 0.3	7.5 ± 0.6	-	-	-	-	-
3	5	N	-	0	3.26	2.116 ± 0.006	0.04 ± 0.02	2.4 ± 0.6	13.2 ± 2.7	1.2	10.403 ± 0.003	-	-	-
3	2	N	L	20	3.35	2.593 ± 0.005	0.044 ± 0.009	2.7 ± 0.6	11.8 ± 2.2	-	-	-	-	-
1	2	Y	R	20	3.49	-	-	-	-	1.1	10.605 ± 0.010	-	-	-
3	1	N	-	0	3.54	2.868 ± 0.006	0.053 ± 0.014	2.9 ± 0.5	11.7 ± 1.8	2.9	14.5370 ± 0.0013	824 ± 3	0.723 ± 0.010	11.4 ± 0.6
1	2	Y	R	0	4.15	-	0.033 ± 0.014	2.4 ± 0.9	15.7 ± 4.3	-	-	-	-	-
1	3	Y	-	0	4.45	-	0.054 ± 0.013	3.3 ± 0.7	12.5 ± 2.4	1.6	12.31 ± 0.02	-	-	-
1	1	Y	-	0	4.89	-	0.104 ± 0.012	4.9 ± 0.6	9.1 ± 1.1	3.0	15.813 ± 0.007	-	-	-

Table 6.1: Overview of all measured states and the extracted parameters, shown errors represent the statistical error only and are not indicative of the physical measurement uncertainty.

In total we have performed successful magnetic field experiments on four samples in twelve different top gate states, a full overview of those states is presented in Table 6.1. For three samples the back gate was functional as well and this was used to measure four top gate states at three different back gate levels each. Two of our four samples (Samples 3 and 4) used the Si/SiO_2 wafer as the substrate directly. And for our other two samples (Samples 1 and 2) a hBN substrate was used as an intermediary as described in Section 5.2.

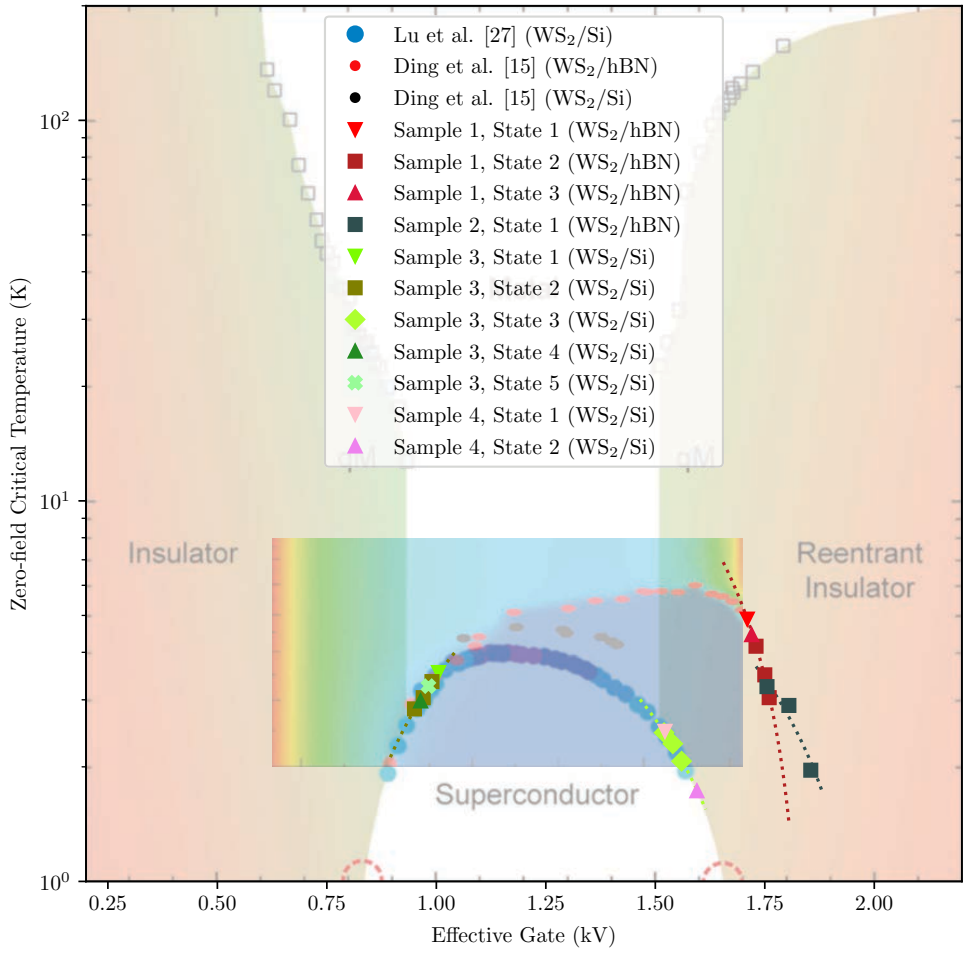

Figure 6.1.2: Overview of all measured states overlaid on top of the states measured previously by Lu et al. [27] and Ding et al. [15]. The points in the smaller inserted image with the rainbow colour map are from Ding et al. [15], here the red points are measured on a hBN substrate whereas the black points are measured on a Si/SiO_2 substrate. The bigger inserted image shows the points from Lu et al. [27] in blueish tints, all of these points are measured on a Si/SiO_2 substrate. From our samples, Samples 1 and 2 are WS_2 samples on hBN whereas Samples 3 and 4 are WS_2 samples on Si/SiO_2. The X-axis positioning is arbitrary and serves only an illustrative purpose. For ionic liquid top gate states that have been measured with multiple different back gates, dotted lines have been plotted as guides to the eye to visualise the trend. See also Table 6.1 and Appendix A for the complete overview of results from all measured states.

In Figure 6.1.2 we present an overview of all zero-field superconducting transition temperatures extracted for each measured state. We have plotted this against the "effective gate voltage" (V_{eff}) which represents the combined gating effect of the ionic-liquid top gate and the solid back gate, as was also done by Lu et al. [27] in Figure 4.1.2. This representation effectively makes the x-axis arbitrary but it does allow us to directly compare the slopes for sample devices that were measured at different back gate states (indicated by dashed lines) and gives a rough indication of where each state is in the superconducting dome. One thing to observe from this graph is that the slopes (as illustrated by dashed lines) belonging to the WS_2 samples that were stacked with hBN (Samples 1 and 2) is noticeably higher then the slopes belonging to the WS_2 samples that were in direct contact with the Si/SiO_2 wafer (Samples 3 and 4).

We have roughly overlaid our new points on top of the data points obtained in previous research. The points in the smaller inserted image with the rainbow colour map are from Ding et al. [15], here the red points are measured on a hBN substrate whereas the black points are measured on a Si/SiO_2 substrate. The bigger inserted image shows the points from Lu et al. [27] in blueish tints, all of these points are measured on a Si/SiO_2 substrate.

6.1.2 Critical current measurements

After having established and cooled down into a superconducting state we can now further characterise this state. To do this we perform critical current measurements at various temperatures which will allow us to extract several parameters describing the superconducting phase. The raw experimental data is shown in Figure 6.1.3 below. As the current is increased, initially the measured voltage remains zero but it then starts to gradually increase as the magnetic field associated with the applied current causes the sample to slowly return to the normal state. The sample therefore becomes more and more resistive and the voltage drop measured across the sample continues to increase. At a sufficiently high current

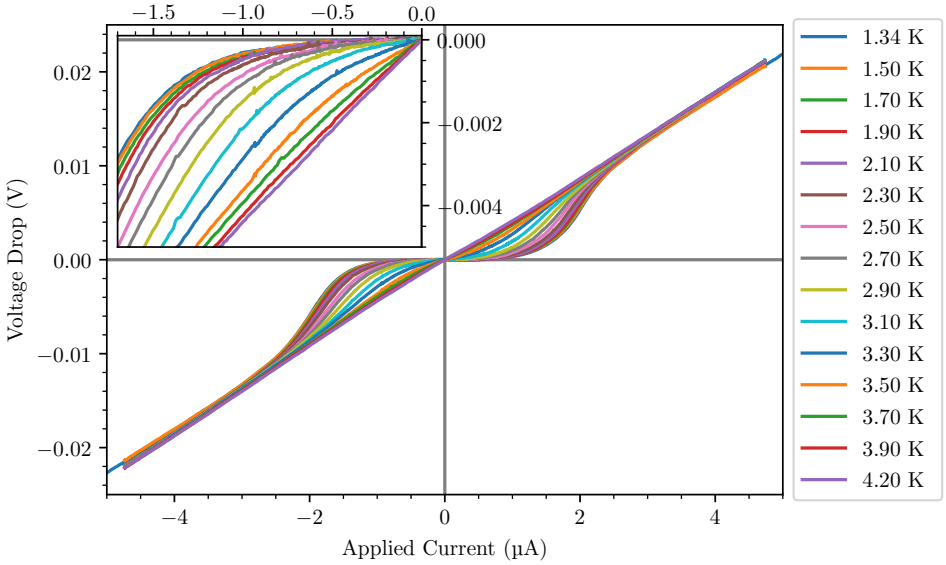

Figure 6.1.3: I-V graph for a WS_2 monolayer sample at various temperatures. The inset zooms in on the lower left quadrant.

the V-I characteristics return fully to the Ohmic behaviour of the normal state and the curve becomes linear. As one would expect, for higher temperatures the Ohmic behaviour is restored at lower currents. This makes sense since the superconducting critical magnetic field, and thus the superconducting critical current, must be lower at higher temperatures as discussed in Chapter 3.

Instead of looking at the raw V-I curve, let us define the differential resistance $\mathrm{d}V/\mathrm{d}I$ as the derivative of this curve and plot this again as a function of the applied current as shown in Figure 6.1.4. The resistance of the normal state we then define as the average of the resistance above 4 µA of applied current since we find that at this point the resistance curve has completely flattened out. Using this it is then possible to pinpoint the superconducting critical current using the criterion that this critical point occurs when the differential resistance reaches 50 % of the resistance of the normal state. These critical current points are represented in Figure 6.1.4 by black squares.

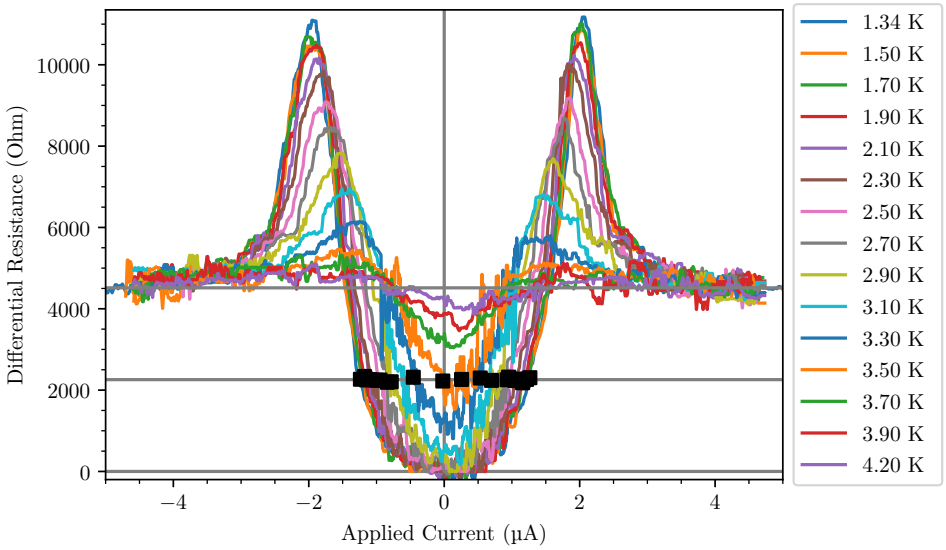

Figure 6.1.4: Differential resistance of a WS_2 monolayer sample versus the applied current at various temperatures, determined by taking the derivative of Figure 6.1.3. Since taking the derivative results in a rather noisy curve, rolling box averaging over 20 points has been applied to smoothen the curve. Black squares indicate the critical current, plotted again in Figure 6.1.5.

Next, we plot the determined superconducting critical current versus the sample temperature, this presents us with Figure 6.1.5. We see a steady decrease of the critical current until the superconductivity disappears just above 3.5 K. This plot now allows us to extract the parameters describing this superconducting phase by fitting the obtained J_c versus T_c data with Equation (3.3.2) [2, 28] as explained earlier in the theory Section 3.3. For this fitting, we use a value for the superconducting coherence length ξ_0 that will be extracted later in Section 6.3 from low-field measurements in a perpendicular magnetic field. The final result is a picture of the main parameters that describe the superconductivity of this state: the superconducting critical temperature at zero magnetic field and without any applied current T_{c_0}, the superconducting energy gap Δ_0, the superconducting coherence length of the Cooper pairs ξ_0, the penetration depth of externally applied magnetic fields λ_0 and the relative change in the specific heat at the superconducting transition $\Delta C/C$. The numerical values for these quantities, determined using

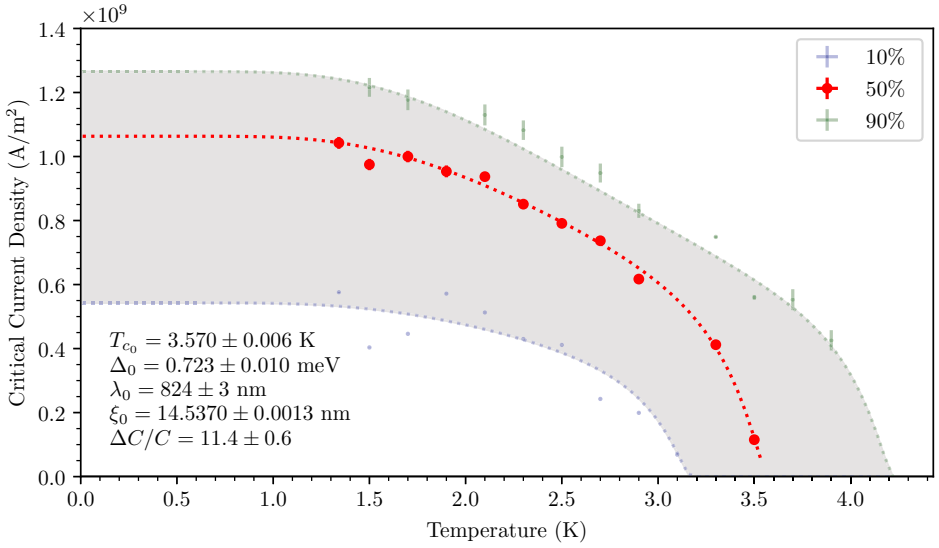

Figure 6.1.5: Critical current versus critical temperature of an ionic-liquid-gated WS_2 monolayer sample as determined from Figure 6.1.4 using 10 %, 50 %, and 90 % criteria as the definition for the transition point. The superconducting coherence length ξ_0 has been extracted by fitting Equation (3.2.3) (Ginzburg-Landau equation) to Figure 6.3.4. The remaining shown parameters, the zero-field superconducting transition temperature T_{c_0}, the superconducting energy gap Δ_0, the London penetration depth λ_0, and the relative shift in the specific heat at the superconducting transition temperature $\Delta C/C$, were extracted using Equation (3.3.2) [2, 28]. The shown errors represent only the statistical error returned from the fitting algorithm.

this fitting, are presented in Figure 6.1.5

Taking the ratio of the determined penetration depth and the coherence length, gives us the Ginzburg-Landau parameter $\kappa = \lambda_0/\xi_0 = 56.7 \pm 0.2$[1] which, according to the Ginzburg-Landau theory, indicates that this is a *Type-II* superconductor since $\kappa > 1/\sqrt{2}$ [48, 56]. Furthermore, taking the ratio of superconducting energy gap and the superconducting critical temperature at zero field, results in the gap ratio $2\Delta_0/k_B T_{c_0} = 4.70 \pm 0.07$. We find that this is well above the weak-coupling limit of 3.528 predicted by the *Bardeen–Cooper–Schrieffer theory* [55]. This suggests that the electron-phonon coupling in this superconductor could be rather strong [38]. Moreover, *Bardeen–Cooper–Schrieffer theory* also predicts that the relative shift in the specific heat at the superconducting transition temperature, $\Delta C/C$, is 1.42 [55]. Our fit finds instead a value of 11.4 ± 0.6, which is an order of magnitude larger. A larger value then predicted by *Bardeen–Cooper–Schrieffer theory* is again indicative for the potential presence of a rather strong electron-phonon coupling in this material [38]. That being said, our value for the relative shift in the specific heat at the superconducting transition temperature should be taken with a grain of salt. This is because, to the best of our knowledge, the accuracy of this model's prediction for the relative shift in the specific heat has not been verified by actual experiments, performing such experiments on two-dimensional systems is extremely challenging.

[1] As we shall see later (Figure 6.3.3), there is some variation of determined parameters such as the superconducting coherence length ξ_0 between different states. However, this variation is relatively small and therefore it is safe to assume that WS_2 remains a *Type-II* superconductor with strong electron-phonon coupling throughout the superconducting dome.

6.2 Hall effect measurements

By sweeping the magnetic field and measuring the resistance well above the superconducting critical temperature (10 K), we can extract from the slope the two dimensional charge carrier concentration (n_{2D}) using the relation:

$$R_H = \frac{1}{n_{2D}e} \tag{6.2.1}$$

With e being the electron charge, and R_H, the Hall coefficient, being equal to the Hall Resistance divided by the applied magnetic field, or in other words, the slope of the measured Hall voltage. Hence, applying linear regression to our data, shown in Figure 6.2.1, allows us to find a charge carrier concentration of $(2.868 \pm 0.006) \times 10^{13}\,\mathrm{cm}^{-2}$ for this state. Here once again the error represents the statistical error only, we estimate that the actual uncertainty is at least two orders of magnitude larger. Note that often when measuring the Hall effect there will be some offset at zero magnetic field, as also demonstrated in Figure 6.2.1. Such offsets are usually the result of inhomogeneities in the sample, or of an imperfect electrical contact alignment. We have performed similar Hall effect measurements on all samples where this was possible. The full overview of our results is presented in Table 6.2.

Sample	State	hBN	V_{BG} (V)	T_c (K)	n ($\times 10^{13}$/cm^2)
4	2	N	0	1.73	2.6
2	1	Y	50	1.96	2.5
3	3	N	20	2.07	1.9
3	3	N	0	2.30	2.4
3	3	N	−20	2.46	2.5
4	1	N	0	2.48	2.2
3	2	N	−20	2.84	2.6
2	1	Y	0	2.90	2.1
3	4	N	0	2.98	2.4
3	2	N	0	3.04	2.5
2	1	Y	−50	3.25	2.3
3	5	N	0	3.26	2.1
3	2	N	20	3.35	2.6
3	1	N	0	3.54	2.9

Table 6.2: Overview of all measured carrier concentrations. Statistical errors are omitted since these are two orders of magnitude lower than the estimated measurement uncertainty.

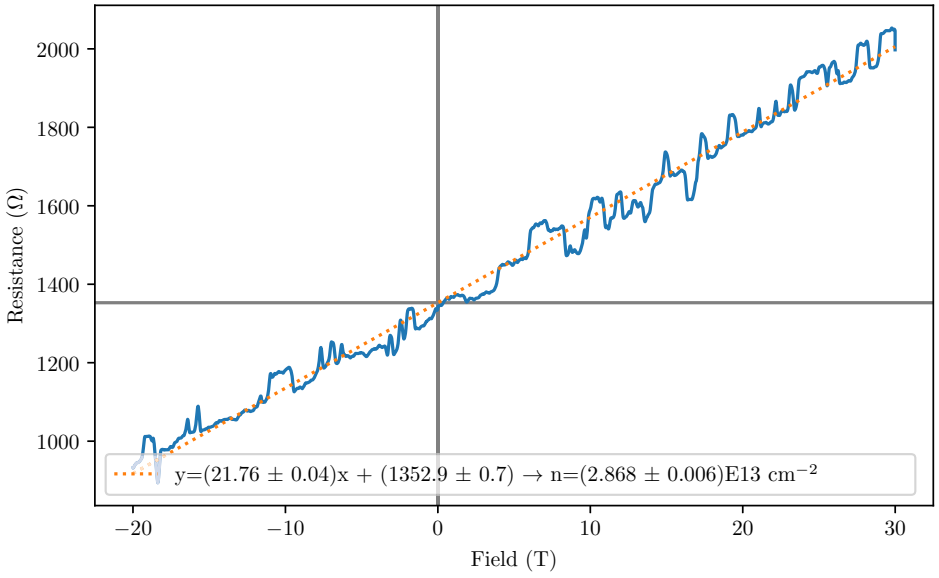

Figure 6.2.1: Resistance of a WS_2 monolayer sample versus the applied magnetic field at 10 K. Linear regression has been performed to obtain the charge carrier density from the Hall effect.

6.3 Suppression of T_c by perpendicular magnetic fields

Let us now look again at the same state that was characterised at zero-field in the previous Section 6.1 and determine its behaviour in a magnetic field perpendicular to the sample planes. As explained in Section 3.1, magnetic fields are usually detrimental to superconductivity. And since the superconducting critical temperature is around 3.5 K we expect that a relatively small magnetic field is already sufficient to destroy superconductivity in this material.

And indeed, as we can see from an example state shown in Figure 6.3.1, the critical magnetic field of the superconducting phase is rather low at about 0.6 T for this particular state. As the temperature is increased the critical magnetic field rapidly reduces, and at around 4.2 K all traces of superconductivity have disappeared. In Figure 6.3.2 the transition points have been extracted using 50 % of the normal state resistance as the transition criteria. Furthermore, we have also determined the 10 % and 90 % points to judge the width of the superconducting transition.

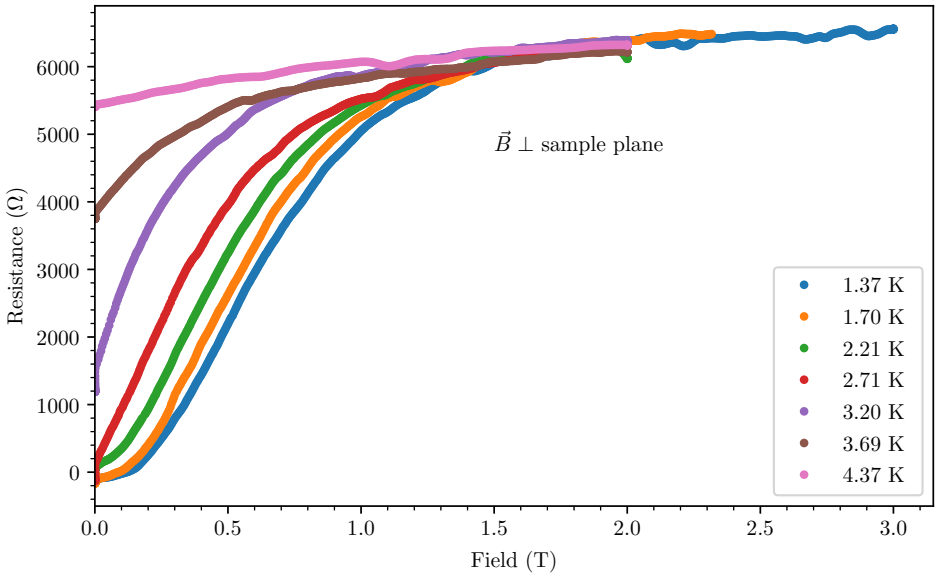

Figure 6.3.1: Superconducting transition of a state of WS_2 monolayer for different temperatures. The sample plane is perpendicular to the magnetic field direction.

In order to extract the diffusivity of the superconducting band D, fits have been made through the data points. Similar to what was done previously by Ding et al. [15], we use the one-band *Werthamer–Helfand–Hohenberg (WHH) model*, or *Maki-de Gennes* equation [19], given by Equation (3.2.5). The resulting fit extracts the band diffusivity ($D = 2.9\,\mathrm{cm^2\,s^{-1}}$) and is plotted in Figure 6.3.2 alongside our data.

Furthermore, we can also extract the superconducting coherence length ξ_0 by looking at the local slope of B_{c_2} versus T_c close to where the magnetic field is zero [43] (Equation (3.2.3)). For this state, performing such a fit results in a zero-field superconducting coherence length ξ_0 of $(14.5370 \pm 0.0013)\,\mathrm{nm}$. Where the error once again only represents the statistical error and not the physical measurement uncertainty.

In addition to these magnetic field sweeps, it is also possible to do the same experiment while keeping

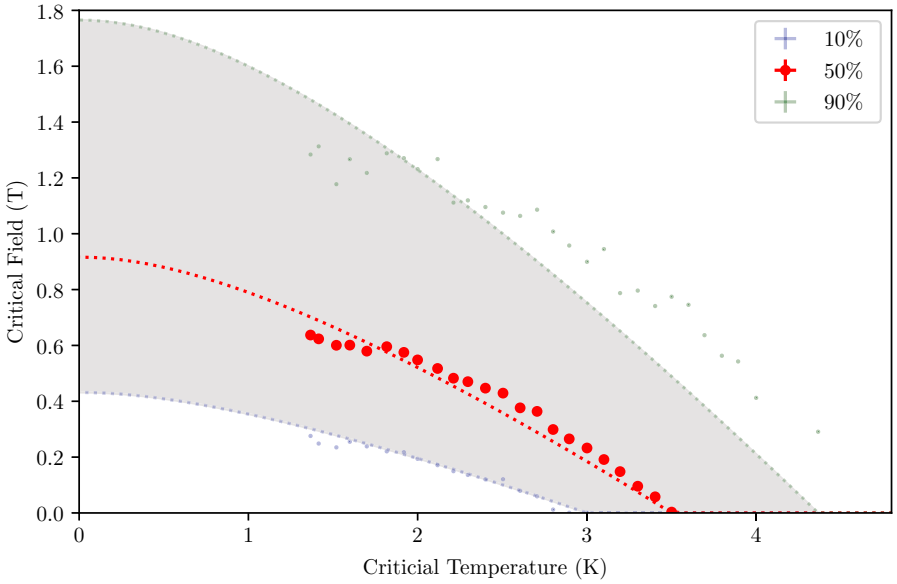

Figure 6.3.2: Superconducting transition points extracted from Figure 6.3.1 using 10 %, 50 %, and 90 % of the normal state resistance as the definition for the transition point. Fits are made through the points using the 1-band WHH model.

the magnetic field constant and varying the temperature instead. A full overview of all the different measurements done is presented in Appendix A. We summarise the results in Figure 6.3.4 where we

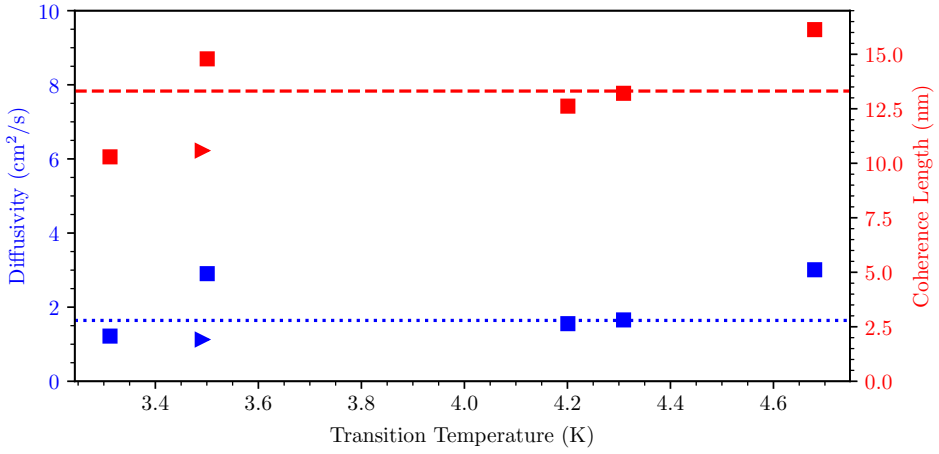

Figure 6.3.3: On the left axis in blue, diffusivity extracted from Figure 6.3.4 using the fitting Equation (3.2.5). And on the right axis in red, superconducting coherence length extracted from Figure 6.3.4 using the fitting Equation (3.2.3). Left pointing triangles indicate a state that is on the left side of the superconducting dome, right pointing triangles on the other hand indicate a state that is on the right side of the superconducting dome, squares indicate a state for which this information is not known.

plot the superconducting critical temperature versus the superconducting critical magnetic field for all the measured states. Moreover, in Figure 6.3.3 we show the diffusivity and superconducting coherence length resulting from the various fits. There does not appear to be any clear trend in our diffusivity or superconducting coherence length results. This suggests that these values are, within our measurement accuracy, constant throughout the superconducting dome. For the diffusivity we find a weighted average of $1.6\,\mathrm{cm^2\,s^{-1}}$ and for the superconducting coherence length we find a weighted average of 13.3 nm.

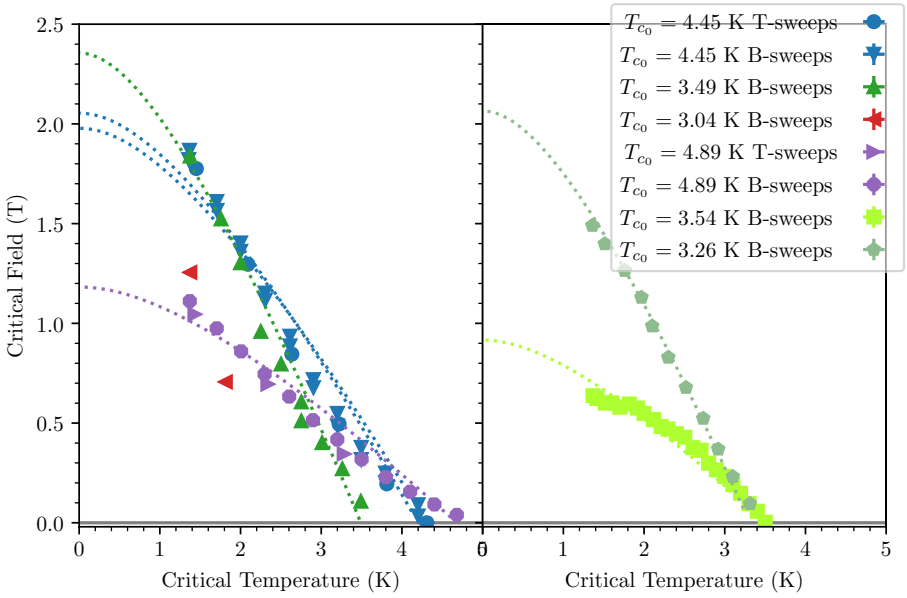

Figure 6.3.4: The superconducting critical field and critical temperatures for various WS_2 monolayer samples and states. Fits using the one-band WHH model are depicted with dashed lines. Curves on the left belong to Sample 1 (on a hBN substrate), and the curves on the right are measured on Sample 3 (on a Si/SiO_2 substrate). The sample plane is perpendicular to the magnetic field direction. Some points were measured at constant temperature, while sweeping the magnetic field (as in Figure 6.3.1), and some points were measured instead at constant magnetic field, while sweeping the temperature. The different measurement method changes the parameter to which the measurement lag is subject, in an ideal experimental scenario there is no observable difference.

6.3.1 The effect of the substrate

As already briefly mentioned before, Ding et al. [15] have found that using hBN as the substrate instead of having the WS_2 monolayers directly on the Si/SiO_2 wafer enhances the superconducting critical temperature. Ding et al. [15] theorise that the structurally more similar hBN substrate causes WS_2's Q valleys to participate in the electrical transport. We would therefore expect that the one-band *Werthamer–Helfand–Hohenberg (WHH) model* is not appropriate for TMD samples on a hBN substrate and a multi-band WHH model should be used instead. Unfortunately, the ratio of free parameters to the number of data points makes it unfeasible to fit this more complex model to our data. Nonetheless, if we take a look at the overview presented in Figure 6.3.4 we can already make some observations. In the order as shown in the legend, the first six curves are measured on a WS_2 sample with a hBN substrate whereas the final two are measured on a sample directly on the wafer. It is quite clear that only these two

final curves fit well with the one-band WHH model, the other six curves show strong deviations between the model and the data. This is of course no strong conclusive evidence that those first six curves do indeed follow two-band behaviour, it is however suggestive and in agreement with the theory proposed by Ding et al. [15].

6.4 Ising protection in parallel magnetic fields

In stark contrast to the perpendicular magnetic field measurements presented in the previous Section 6.3, are the parallel magnetic field measurements for which we shall again first look at the same state that was characterised without magnetic fields. These results are shown in Figure 6.4.1. Instead of the clear and steady decrease of the superconducting critical magnetic field that we see in Figure 6.3.1 as the temperature increases, in parallel magnetic field we barely see any change in the superconducting transition even for fields as high as 33 T. If we then zoom in on the superconducting transition in the inset of Figure 6.4.1 we see then that there is still a small but measurable shift in the superconducting transition temperature as more magnetic field is applied.

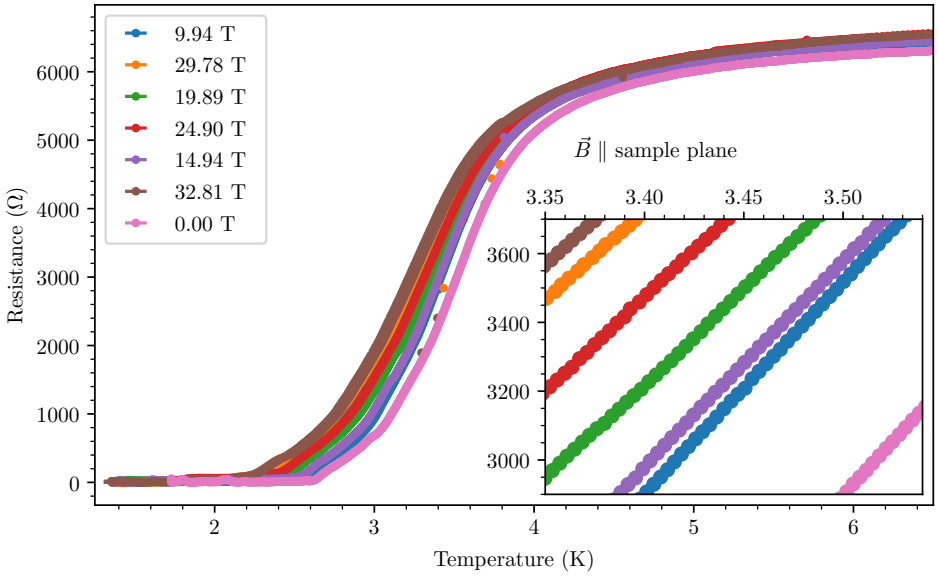

Figure 6.4.1: Superconducting transition of a state of WS_2 monolayer for different magnetic fields parallel to the sample planes, in order of measurement. The inset zooms in on the centre of the superconducting transition. A magneto-resistance correction for the temperature sensor has been performed as explained in Section 5.3.

In Figure 6.4.2 the transition points have been extracted using 50 % of the normal state resistance as the transition criteria. And the transition width is determined by extracting the 10 % and 90 % points as well.

In order to extract quantitive information from this data, fits have been made through the data points using a Mean-Field model accounting for *Rashba-type* ($\alpha_R k_F$) and *Zeeman-type* (β_{SO}) spin-orbit coupling [27], given by Equation (4.1.2). Since a two-parameter fit is tricky due to the relatively low

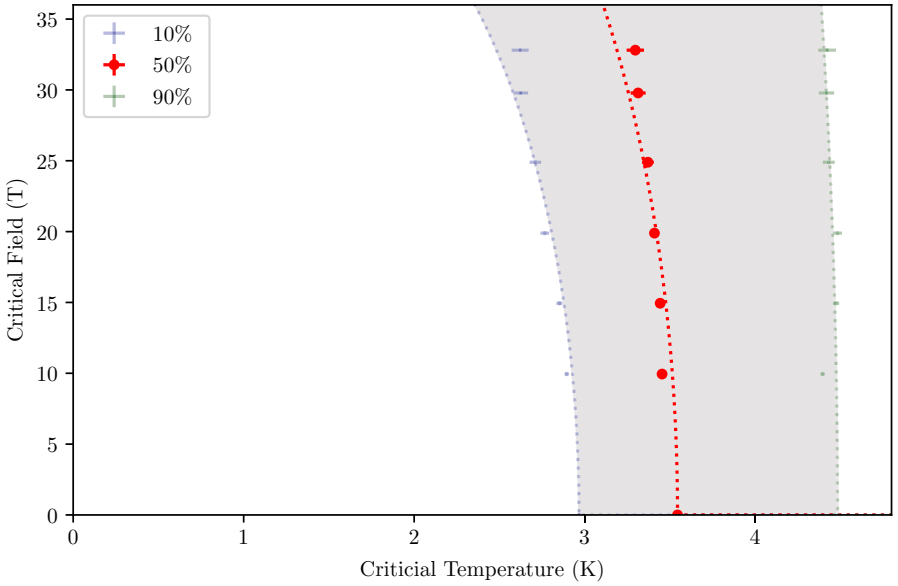

Figure 6.4.2: Superconducting transition points extracted from Figure 6.4.1 using 10 %, 50 %, and 90 % of the normal state resistance as the definition for the transition point. Dashed lines correspond to numerical fits (Equation (4.1.2)) as described in the main text.

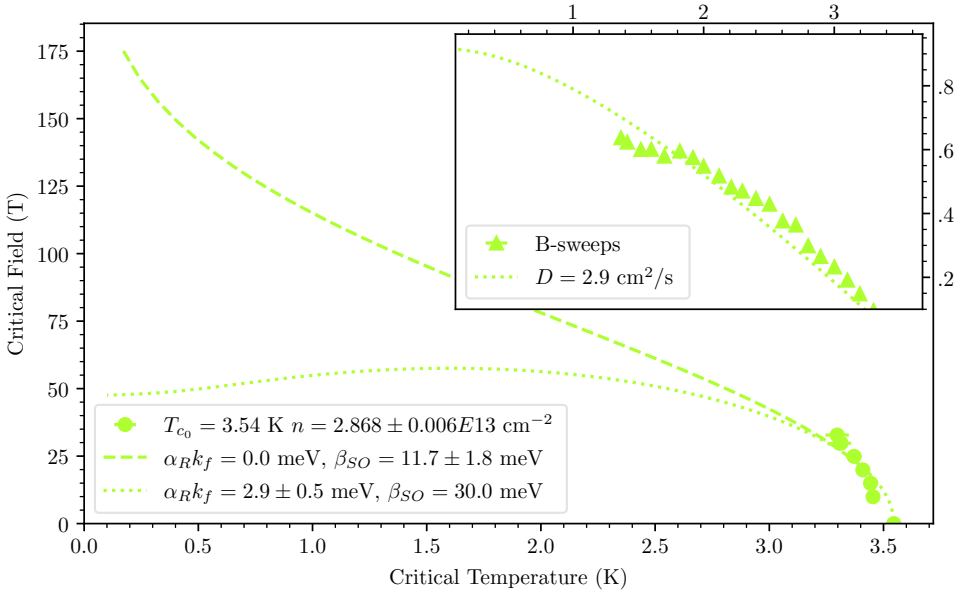

Figure 6.4.3: Parallel magnetic field data fit using Equation (4.1.2). The inset shows the same state measured in varying perpendicular fields at constant temperatures (Figure 6.3.2).

quantity of points per curve and the complexity of the equation, we instead perform two independent numerical one-parameter fits for both the Rashba and Zeeman energies similar to what was done by Lu et al. [27]. First, we fit the *Rashba-type* spin-orbit coupling energy while keeping the value for the *Zeeman-type* spin-orbit coupling energy fixed at the theoretical value of 30 meV [27]. Next we fit the *Zeeman-type* spin-orbit coupling energy while keeping the value for the *Rashba-type* spin-orbit coupling energy constant at 0 meV as a rough estimate. Effectively this means that the values we find are lower estimates for the *Rashba-type* and *Zeeman-type* spin-orbit coupling energies. Using this procedure we find a *Rashba-type* spin-orbit coupling energy of (2.9 ± 0.5) meV and a *Zeeman-type* spin-orbit coupling energy of (11.7 ± 1.8) meV for this particular state shown in Figure 6.4.3. Extrapolating both types of fits towards 0 K, as done in Figure 6.4.3, we find that while there is good agreement between the fits at relatively low magnetic fields, the two curves rapidly start diverging as the temperature reduces. The true values for the *Rashba-type* and *Zeeman-type* spin-orbit coupling energies should exist between these two extremes, more powerful magnets could narrow this range of possible values in the future.

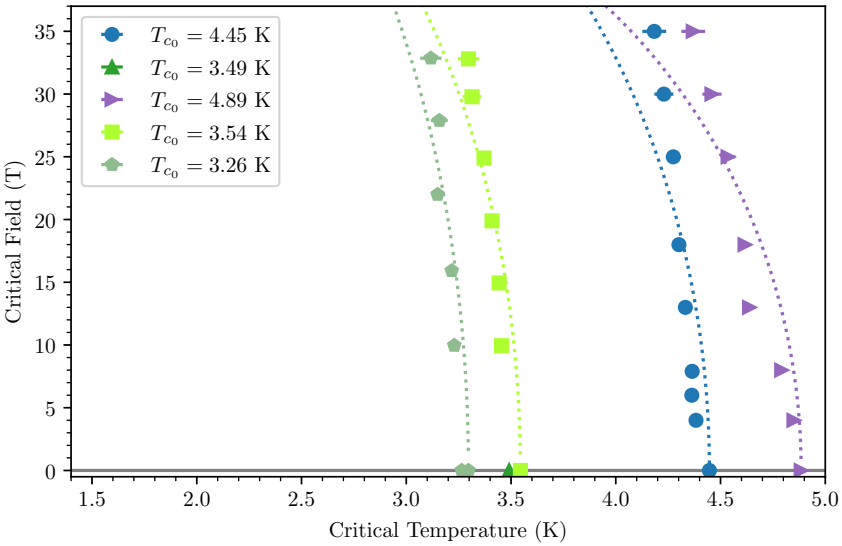

Figure 6.4.4: The superconducting critical field and critical temperatures for various WS_2 monolayer samples and states. The sample plane is parallel to the magnetic field direction. Dashed lines correspond to fits with the Mean-Field model accounting for *Rashba-type* ($\alpha_R k_F$) and *Zeeman-type* (β_{SO}) spin-orbit coupling. When performing this fit we have assumed that the *Zeeman-type* spin-orbit coupling energy is fixed at the theoretical value of 30 meV [27] as also described in the main text.

For completeness we present in Figure 6.4.4 the parallel magnetic field data belonging to all states for which we previously showed the perpendicular magnetic field data in Figure 6.3.4 in the previous Section 6.3. A full overview of all states measured in parallel magnetic fields is presented in Appendix A. All resulting *Rashba-type* and *Zeeman-type* spin-orbit coupling energies are plotted in Figure 6.4.5 against the zero-field superconducting critical temperatures of the various different states. Also plotted in this figure is the relative difference in critical temperature between zero magnetic field and the highest measured magnetic field.

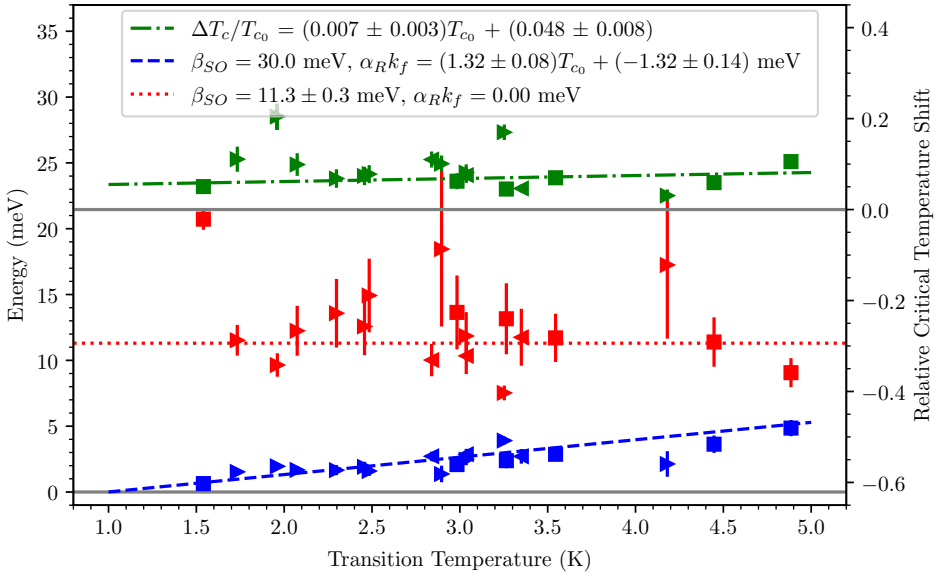

Figure 6.4.5: On the left axis, in blue: superconducting transition temperatures as a function of the determined *Rashba-type* ($\alpha_R k_f$) spin-orbit coupling energy, fitted while keeping the *Zeeman-type* (β_{SO}) spin-orbit coupling constant at 30 meV. And also on the left axis, in red: the superconducting transition temperatures as a function of the *Zeeman-type* (β_{SO}) spin-orbit coupling energy, fitted while keeping the *Rashba-type* ($\alpha_R k_f$) spin-orbit coupling constant at 0 meV. On the right axis, in green: the shift in superconducting critical temperature between zero-field and maximum field for different zero-field superconducting critical temperatures. Dotted lines are guides to the eye roughly indicating a possible trend. Left pointing triangles indicate a state that is on the left side of the superconducting dome, right pointing triangles on the other hand indicate a state that is on the right side of the superconducting dome, squares indicate a state for which this information is not known.

We find from Figure 6.4.5 that within the error bar the lower estimate for the *Zeeman-type* spin-orbit coupling energy (in red) is constant at a weighted average of (11.3 ± 0.3) meV. The lower bound for the *Rashba-type* spin-orbit coupling energy (in blue) on the other hand is slightly increasing as the superconducting critical temperature increases, a linear regression fit is shown as a guide to the eye. The increasing *Rashba-type* spin-orbit coupling energy suggest that the strength of the Ising protection is weakened towards the centre of the superconducting dome, while it is strongest at both edges of the superconducting dome. The relative shift in superconducting critical temperature (in green) remains near 10 % for all states.

6.5 Summary

In Table 6.1 all extracted parameters are summarised for each measured gating state in perpendicular and parallel magnetic fields. In Figures A.0.1 to A.0.11 of this Appendix A, we also provide magnetic field versus temperature plots of the superconducting transition for all gating states similar to Figure 6.3.2 and 6.4.2 shown above for our example state.

Combining the extracted parameters from each gating state, our main result becomes Figure 6.3.3 and

Figure 6.4.5, where we see an increasing trend for the Rashba energy towards the centre of the superconducting dome. The increasing *Rashba-type* spin-orbit coupling energy suggests that the relative strength of the Ising protection, though still very strong, might be weakening towards the centre of the superconducting dome. Moreover, we find no clear trend in the determined band diffusivity, charge carrier concentration or the *Zeeman-type* spin-orbit coupling energy. And finally, for all measured states we find that the superconducting critical temperature shifts by about 10 % between zero magnetic field and the maximum parallel magnetic field, independently of the states position in the superconducting dome.

Chapter 7

Conclusion and outlook

Our aim was to find if and how the Ising protection of the superconducting phase in ionic-liquid gated WS_2 changes as a function of the electron doping level. To that aim we have performed several experiments with and without magnetic fields in parallel and perpendicular directions. Furthermore, we have used theoretical models to fit to the data we have obtained in order to extract the parameters describing this superconducting phase.

From our experiments we can first of all conclude that WS_2 is a *Type-II* superconductor ($\kappa > 1/\sqrt{2}$) with strong electron-phonon coupling ($2\Delta_0/k_B T_{c_0} > 3.52$). Comparing our results to experiments done by Talantsev et al. [28] on bilayers of the very similar material, MoS_2, we find that the superconducting energy gap is smaller, $(0.723 \pm 0.010)\,\text{meV}$ in WS_2 compared to $(1.5 \pm 0.1)\,\text{meV}$ in MoS_2. The superconducting coherence length is a bit longer at $(14.5370 \pm 0.0013)\,\text{nm}$ compared to $(11.4 \pm 0.4)\,\text{nm}$. And finally, the superconducting penetration depth is also larger in WS_2 with $(824 \pm 3)\,\text{nm}$ compared to $(745 \pm 2)\,\text{nm}$ in MoS_2.

From perpendicular field measurements we find that neither the band diffusivity, nor the superconducting coherence length, vary strongly with the zero-field superconducting transition temperature. The diffusivity remains between 1 to $3\,\text{cm}^2\,\text{s}^{-1}$, and the superconducting coherence length also stays more or less constant between 10 to 16 nm, neither quantities show a very clear trend.

To the best of our knowledge, values for the superconducting energy gap and penetration depth in WS_2 have not been reported before. Zheliuk et al. [29] estimate the superconducting coherence length at 17.7 nm for WS_2 monolayers, which is longer than what we find for the state that was measured fully but does not fall very far outside of the spread that we observe when looking at all the states for which the superconducting coherence length was extracted.

Looking at Table 6.1 we find very roughly that the states measured with WS_2 on hBN have a higher zero-field superconducting transition temperature, when compared to the states where the WS_2 is directly on the Si/SiO_2 wafer. Though this correlation is not at all strong evidence to support a possible causation by itself, it does match with the experimental observations made by Ding et al. [15], who found that the addition of hBN in between the WS_2 sample and the Si/SiO_2 wafer may enhance the zero-field superconducting transition temperature by as much as 30 %. Ding et al. [15] theorise that this enhancement is the result of the Q valleys, in addition to the usual K/K' valleys, being populated and contributing to the superconductivity when the WS_2 sample is contacting the more structurally

similar hBN. Such multi-band superconductivity should be visible in the perpendicular magnetic field data (Figure 6.3.4) as a clear change in the slope of the curve where one band stops contributing to the superconductivity while the other band still remains superconducting, as illustrated by Ding et al. [15] in their Figure 4. Though we could not fit our perpendicular magnetic field data in Figure 6.3.4 to a two-band model (due to the ratio of data points versus the large number of free variables in this model), it is suggestive that the two curves belonging to devices without hBN (the final two in the order of the legend) fit noticeably better to the one-band model we used when compared to the curves belonging to devices with hBN (the first six in the order of the legend). Furthermore, Figure 6.1.2 shows us that the slope of the superconducting critical temperature versus applied gating voltage is significantly steeper for the samples on a hBN substrate (samples 1 and 2) than it is for the samples directly on the Si/SiO_2 wafer (samples 3 and 4), which is again suggestive of an enhanced Ising protection in these samples.

From parallel field measurements (Figure 6.4.5) we find on the one hand that the Rashba energy shows a clear increasing trend with increasing superconducting transition temperature. The Zeeman energy on the other hand remains constant at (11.3 ± 0.3) meV within the uncertainty level, which is significantly smaller then the value of 30 meV predicted by theory [27]. At the same time we find that the relative shift in the superconducting transition temperature between zero magnetic field and the highest measured magnetic field (34 T) also remains rather constant at about 10 %. This indicates that the relative strength of the Ising protection might be slightly weakening towards the centre of the superconducting dome, though overall the superconducting state remains well protected against the magnetic fields we are able to expose it to. There are a few outliers which show a stronger relative reduction of the superconducting transition temperature, these cases may be attributed to drifting of the alignment between the sample and the magnetic field throughout the measurement of that state. After all, if the angle drifts from the perfect alignment then there will be some component of the magnetic field perpendicular to the sample planes, this component is not subject to the Ising protection and therefore the superconductivity is suppressed sooner.

Our measurements of the charge carrier concentration proved unreliable. One would expect that there is a roughly linear trend of increasing charge carrier concentration with increasingly positive back gates until saturation [27]. We however find no trend at all. This indicates that the error bar in the charge carrier concentration measurements is a lot bigger than the error returned from the linear regression would suggest.

One of the biggest problems we ran into while performing ion gating experiments is getting the alignment of the sample right with respect to the magnetic field. That this was not always successful becomes evident from Figure 6.4.4. For these measurements in parallel magnetic field this problem manifests itself clearly in the 4.45 K curve, which starts off by going in the expected direction but then curves back such that the critical temperature at the highest magnetic field is actually almost equivalent to the zero-field critical temperature. This of course makes very little sense, and therefore the most likely explanation is that the alignment of the sample with respect to the magnetic field has changed throughout the measurement. Note that measurements in parallel magnetic field are not necessarily done in order of ascending magnetic field. In fact for these measurements we have intentionally alternated between measuring at high and measuring at low magnetic fields. Compared to measuring in order of highest magnetic fields first, this measurement sequence reduces the 15 min time averaged magnetic field value and thus reduces the associated 15 min averaged peak power consumption. The load the resistive magnets put on the power grid is thus reduced, which minimises the costs of the measurement run. A side-effect of this is that any drifting of the alignment will not necessarily be monotonically increasing with magnetic

field. This is good, because it creates some visible distinction between a misalignment problem (where the curve might locally be steeper then expected compared to the overall trend) and a real reduction of the Ising protection (where the curve as a whole will be steeper when compared to the other states).

No such alignment issue is present in our critical current measurements. There is, however, some small asymmetry between positive and negative currents. This is likely due to imperfections in the sample and contact fabrication, but it does not present a too big problem since we simply average the results for both current directions.

7.1 Suggestions for improvement

There are several areas where we could improve our experiment, which we will briefly list below:

- For starters, increasing sample longevity would increase the comparability of different gating states. It is inherent to the exfoliation-based method of sample fabrication that each sample is unique, therefore different samples can and do have differing critical temperatures and critical magnetic fields for the same charge carrier concentration. When attempting to compare the superconductivity at different places in the superconducting dome, it is therefore best to do so on the same sample. The main factors limiting the lifetime of a sample are:
  - Chemical reactions of the ionic liquid and the sample. This, of course, is a problem that scales inversely with the sample thickness and is therefore especially relevant for our monolayer samples. This problem is minimised by minimising the time a sample is stored before it is measured, and by always storing the sample at temperatures well below the glass transition temperature of the ionic liquid. Nonetheless, it cannot be avoided completely since every time the gating state of a sample is changed, the ionic liquid must be warmed up into the liquid state where it is also chemically reactive. The amount of times the state of the liquid gate has to be changed can be minimised by ensuring that the sample has a solid back gate that functions well.
  - Electrostatic discharge and electromagnetic spikes. Changing the state of the liquid gate requires lifting the probe out of the helium bath and into the heating element in the neck of the cryostat. Due to the design of the cryostats and size constraints imposed by the high field magnets, in this lifting process, the probe goes from a state where it is in electrical contact with the cryostat to one where it is not. And sometimes, along the way, the probe will touch the heat shields in the neck of the cryostat, briefly restoring electrical connectivity. This causes spikes and discharges which are detrimental to the sample and to the contacts between the sample and the chip-carrier. Additionally, in high magnetic fields, the cryostat and probe sometimes move and touch the magnet. If this happens, additional electrical and mechanical noise is transmitted to the sample which may also negatively effect the sample, the contacts, and the measured signals in general. A potential way to minimise this would be to redesign the probe such that it is always electrically isolated from the cryostat, using for example stycast, which is electrically isolating, yet still thermally conductive.
- Improving the accuracy and stability of the alignment of the sample with respect to the magnetic field would greatly improve the comparability of different experiments. Currently, the sample is mounted on a rotation platform which is controlled at the top of the probe. A Hall-sensor is used to align the sample perpendicular or parallel to the magnetic field. Getting the initial alignment

right is challenging and requires patience, the big issue however is that the alignment drifts ever so slightly during the experiment. This probably happens due to small thermal fluctuations causing contractions or expansions in the rods, wires, and cogwheels that comprise the rotation mechanism. To address this issue one could instead perform the experiment on a probe without a rotation head, this however comes with the drawback that one cannot measure the same state in both perpendicular and parallel magnetic fields. A better possible solution could be to design some mechanism to lock the rotation head in-place when it is not being rotated.

Part III

Critical current induced magnetisation of superconducting tapes measured using magnetometry techniques - Building the next generation of superconducting magnets

Chapter 8

Introduction

As we have seen also in the previous part, extreme conditions such as high magnetic fields are useful tools in the quest for better understanding the characteristics of complex and exotic materials. However, our resistive magnets are power hungry machines that require huge amounts of continuous cooling. Superconducting alternatives do exist, but they are limited to significantly lower maximum fields due to the superconducting critical magnetic field that is an inherent property of the material that the magnet is constructed with. Therefore, to continue to drive forward our understanding of science in high magnetic fields while keeping the electricity consumption manageable, it is essential to further push the boundaries of superconducting magnets and to further explore superconductivity. For this reason the European consortium of magnetic field laboratories (EMFL) has initiated the SuperEMFL project. This project aims to develop a 40 T or higher fully superconducting magnet. It is in this context of finding a suitable candidate material for these next-generation superconducting magnets, that we perform the experiments described in this Part III.

The most straightforward way to measure superconductivity is of course to measure resistance as we have also done in Part II. After all, at the onset of the superconducting phase one will find that the resistance quickly reduces to zero. This, however, is not the only type of experiment we can perform to determine the presence of a superconducting phase. After all, the superconducting phase has a characteristic magnetic response as we have discussed previously in Section 3.4. In this final part we will shift focus towards measuring superconductivity by means of measuring magnetisation using standard magnetometry techniques.

Magnetisation experiments on superconductors offer additional insights on the behaviour of the superconducting material in a magnetic field, specifically on how magnetic field lines penetrate and move through the material [41, 45, 46, 47]. This information is essential when one is considering using some material in the design of a new superconducting magnet since, as we have learned in Section 3.4, the behaviour of the magnetic field lines reflects strongly on the stability of the supercurrent and may introduce energy dissipation in the superconductor and therefore a pseudo-resistance.

Let us summarise what we can determine from the magnetisation curve of a superconductor. Firstly, the hysteresis in the magnetisation curve can be used to effectively measure the critical current of a *Type-II* superconductor with flux-pinning as a function of magnetic field. As we shall see in Figure 10.2.1, this magnetisation curve will look like an envelope and the width of this envelope at a given magnetic field value directly relates to the critical current. In the case of perfect flux pinning in the material, the width

of the magnetisation "envelope" does not depend on the sweeping rate. In practice, there will be some dependency on the sweep rate anyway since no flux pinning can be perfect. By measuring this sweep rate dependency we can gain some insight in the quality of the flux pinning and therefore on the energy dissipation of the superconductor. The final property we can extract from the magnetisation curve is the point where the hysteretic "envelope" closes. This point is called the *irreversibility field* (B_{irr}), and it represents either the break down of flux-pinning or the destruction of the superconducting phase itself (whichever occurs first).

Chapter 9

Experimental techniques: Magnetometry at HFML-FELIX

As specified in the previous Chapter 8, we would like to measure the magnetisation of superconductors in order to extract the properties describing the flux pinning as well as the superconducting critical current. Two standard and relatively simple techniques for measuring magnetisation are torque magnetometry and vibrating sample magnetometry (VSM). In addition to measuring magnetisation, torque magnetometry experiments can also extract the magnetic anisotropy of a sample. Furthermore, when comparing both setups at HFML-FELIX, torque magnetometry is usually more sensitive than vibrating sample magnetometry. However, torque magnetometry measurements are experimentally more challenging than vibrating sample magnetometry measurements, especially for samples with a relatively large magnetisation such as superconductors. We have used both techniques and will describe them in the following sections, starting with vibrating sample magnetometry in Section 9.1 before moving on to torque magnetometry in Section 9.2.

9.1 Vibrating sample magnetometry

9.1.1 Theoretical principle

The operation of a vibrating sample magnetometer (VSM) is based on *Faraday's law of induction*, which is a direct result of the *Maxwell-Faraday equation* (Equation (3.4.1)). To illustrate this, consider a magnetised sample moving through a coil. This movement creates an effective changing magnetic field which induces a voltage in each winding of the coil as described by Equation (9.1.1) below:

$$V = -\frac{\mathrm{d}\phi_B}{\mathrm{d}t} \tag{9.1.1}$$

Here V is the induced voltage, and ϕ_B is the magnetic flux through a winding of the coil which is given by:

$$\phi_B = \iint_{\Sigma} \vec{B}\left(\vec{r}, t\right) \cdot \mathrm{d}\vec{S} \tag{9.1.2}$$

Where Σ represents the surface enclosed by the windings of the coil and B is the magnetic field through each winding. When we assume that the changing magnetic field is purely perpendicular to the coils'

windings and homogeneous (which would be the case for a simple point-like isotropic and homogeneous sample) ($\vec{B}(\vec{r},t) = B_\perp(t)$), then Equation (9.1.2) simplifies to $\phi_B = B\Sigma$.

To then find the total induced voltage in the coil, we must sum over the induced voltage in each winding. Assuming that each winding is perfectly identical, this means Equation (9.1.1) becomes:

$$V(t) = -N\frac{\mathrm{d}\left(B\left(z\left(t\right)\right)\Sigma\right)}{\mathrm{d}t} \tag{9.1.3}$$

Which can be written as:

$$V(z,t) = -N\frac{\mathrm{d}B\left(z\right)}{\mathrm{d}z}\Sigma\frac{\mathrm{d}z}{\mathrm{d}t} \tag{9.1.4}$$

Here z represents the direction parallel to the vibrating motion. Ideally the vibrating motion of the sample is perfectly sinusoidal[1], i.e. $z(t) = a\cos\left(2\pi ft\right)$, and thus $\mathrm{d}z/\mathrm{d}t = -2\pi fa\sin\left(2\pi ft\right)$.

Since the sample is vibrating we wish to determine the sensitivity of our system as a function of the position z. In order to do so, let us look at the problem in reverse and find the magnetic field B, at a position z, produced by a perfect coil carrying current I (this we will call the magnetic field "profile" of the coil). This magnetic field profile is described by Equation (9.1.5) [35, 24], which is also applicable in reverse, meaning that if the strength of the magnetic field at a given position z is B, then a perfect coil will respond with current I.

$$\begin{aligned} B(z) = \frac{\mu_0 I}{2}\left(z-L\right)\left[\ln\left(r_2+\sqrt{r_2^2+\left(z-L\right)^2}\right)-\ln\left(r_1+\sqrt{r_1^2+\left(z-L\right)^2}\right)\right]+ \\ \frac{\mu_0 I}{2}z\left[\ln\left(r_1+\sqrt{r_1^2+z^2}\right)-\ln\left(r_2+\sqrt{r_2^2+z^2}\right)\right] \end{aligned} \tag{9.1.5}$$

Here r_1 and r_2 are the inner and outer radius of the coil respectively, and L is the length of the coil.

We now take the derivative of Equation (9.1.5) with respect to z and plug the result into Equation (9.1.4). We also use that our magnetised sample moves sinusoidally ($z\left(t\right) = a\cos\left(2\pi ft\right)$) and substitute this with $\mathrm{d}z/\mathrm{d}t$. The end result then becomes:

$$\begin{aligned} V(z,t) = Na\Sigma I\mu_0\pi f\sin\left(2\pi ft\right)\left[\ln\left(r_2+\sqrt{r_2^2+\left(z-L\right)^2}\right)-\ln\left(r_1+\sqrt{r_1^2+\left(z-L\right)^2}\right)+\right. \\ \left(z-L\right)^2\left(\frac{1}{r_2\sqrt{r_2^2+\left(z-L\right)^2}+r_2^2+\left(z-L\right)^2}-\frac{1}{r_1\sqrt{r_1^2+\left(z-L\right)^2}+r_1^2+\left(z-L\right)^2}\right)+ \\ \left.\ln\left(r_1+\sqrt{r_1^2+z^2}\right)-\ln\left(r_2+\sqrt{r_2^2+z^2}\right)+z^2\left(\frac{1}{r_1\sqrt{r_1^2+z^2}+r_1^2+z^2}-\frac{1}{r_2\sqrt{r_2^2+z^2}+r_2^2+z^2}\right)\right] \end{aligned} \tag{9.1.6}$$

Thus we find that the sinusoidal motion of a magnetised sample induces a (90° phase shifted) sinusoidal pickup voltage depending on the coils dimensions, as well as the amplitude and frequency of the oscillating motion.

In practice we will always measure the root mean square (RMS) of the AC impedance signal using lock-in amplifiers. Therefore, let us take the root mean square of Equation (9.1.6) and rewrite this in terms of

[1] In practice our motor can only set position, velocity and acceleration, and thus produces a second order (quadratic) Taylor expansion of a cosine wave

the impedance Z:

$$Z(z)_{RMS} = Na\Sigma\mu_0 \frac{f\pi}{\sqrt{2}} \left[\ln\left(r_2 + \sqrt{r_2^2 + (z-L)^2} \right) - \ln\left(r_1 + \sqrt{r_1^2 + (z-L)^2} \right) + (z-L)^2 \left(\frac{1}{r_2\sqrt{r_2^2 + (z-L)^2} + r_2^2 + (z-L)^2} - \frac{1}{r_1\sqrt{r_1^2 + (z-L)^2} + r_1^2 + (z-L)^2} \right) + \ln\left(r_1 + \sqrt{r_1^2 + z^2} \right) - \ln\left(r_2 + \sqrt{r_2^2 + z^2} \right) + z^2 \left(\frac{1}{r_1\sqrt{r_1^2 + z^2} + r_1^2 + z^2} - \frac{1}{r_2\sqrt{r_2^2 + z^2} + r_2^2 + z^2} \right) \right] \tag{9.1.7}$$

9.1.2 Setup and procedure for VSM experiments

Here we will describe the custom built vibrating sample magnetometry setup at HFML-FELIX and the usual procedure of performing measurements with it. We start with the heart of the vibrating sample magnetometer, the pickup coils. Next, we shift focus and describe how our setup is used in practice to perform a measurement. And finally we comment on how our setup may be calibrated to convert the raw data into useful units of magnetisation. A schematic overview of the full vibrating sample magnetometry setup and all its components is shown in Figure C.0.1 of Appendix C.

The author's direct contributions to the vibrating sample magnetometry setup involve simplifications and refinements of the measurement setup as well as a complete rewrite of the control software, integration with HFML's main data acquisition program, the creation of a manual, and the formalisation of measurement procedures.

Coils

Though one pickup coil can in principle measure the magnetisation of a vibrating sample as described by Equation (9.1.7), a single coil is insufficient for good experimental results for two reasons. The first reason is that we want to vibrate our sample at some position where the response curve of the coil (described by Equation (9.1.7)) is relatively flat. Otherwise the induced response will vary too much throughout the sinusoidal oscillation which increases errors when measuring the response with a lock-in

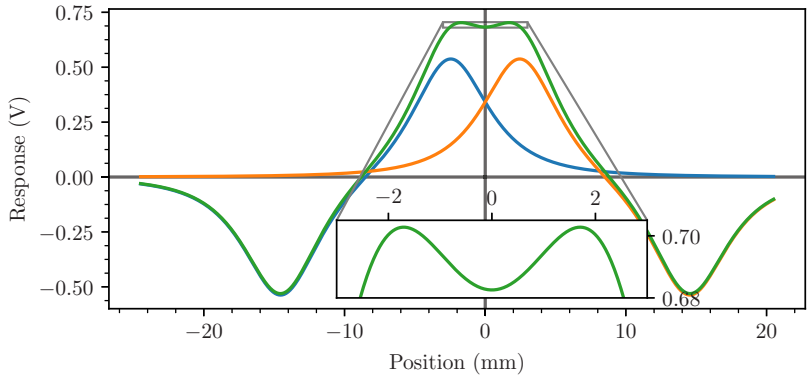

Figure 9.1.1: The simulated superposition (green) of the response of 2 pickup coils (blue and orange) separated from each other by a distance of 5 mm. Figure from Ammerlaan [24].

amplifier. For a single coil, such an area where the response (i.e. the sensitivity) is relatively independent of the position does not exist, as becomes evident when we look at Figure 9.1.1 where we have plotted the magnetic field profile of a single pickup coil in blue. At the peak, which is the area of the highest sensitivity, we also find that this sensitivity changes drastically if we move slightly above or below this maximum.

Let us now add a second pickup coil in orange and see what happens. For illustrative purposes the separation between the upper and lower coil set has been inflated to 5 mm, in reality it is 3 mm in our setup. We now wire these two pickup coils together in such a way that the response of one coil is exactly opposite to that of the other coil (hence the orange response curve is mirrored in the x-axis with respect to the blue response curve). When measuring the combined signal from both coils (in green) we will find that not only has the sensitivity increased when compared to the single coil but the area of the highest sensitivity is now also flatter. By centring the vibration of the sample on this flattened area we effectively ensure that the sensitivity of our combined system does not change throughout the motion of the vibrating sample. This helps eliminate distortions of the picked up sinusoidal signal, provided that

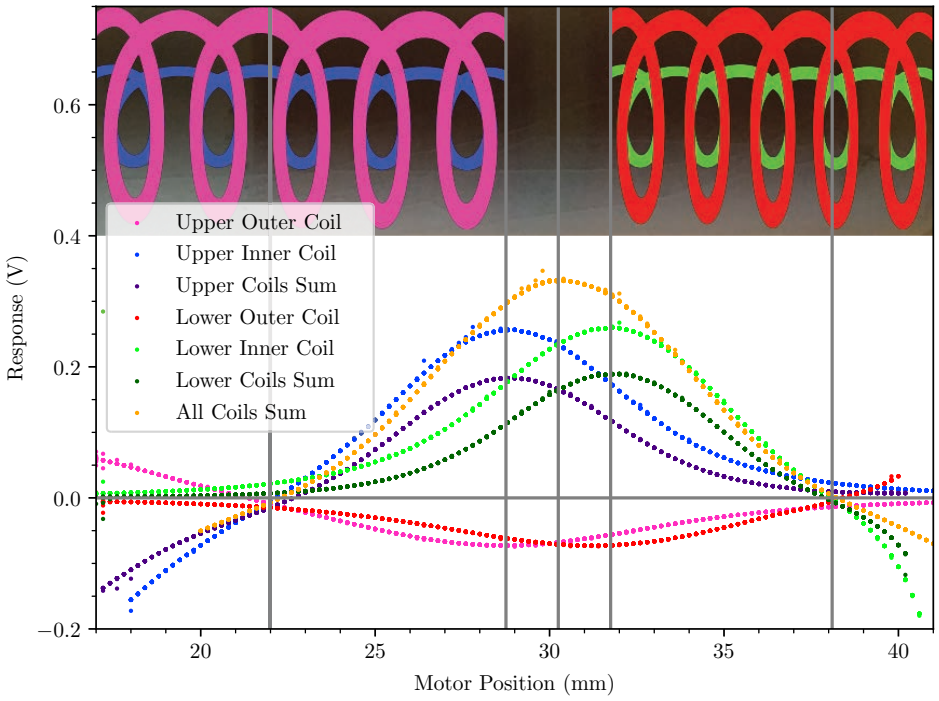

Figure 9.1.2: Response of each individual pickup coil, the combination of the upper coils, the combination of the lower coils, and the combination of all coils. The response curve has been corrected for vibration amplitude instability as described in the main text. Measured using a sample of 5 mg nickel. Vertical grey lines mark the centre of each coil, the end of the upper coil set, the start of the lower coil set, and the centre between the upper and lower coil sets. For illustrative purposes a photograph of the tip of the vibrating sample magnetometry probe is added showing the location of the pickup coils. For clarity, the photograph is overlaid with a schematic representation of each pickup coil in colours matching the ones used in the legend.

the vibration amplitude is not larger than the flattened area (i.e. not larger than the separation between the coils).

The second reason a set of multiple coils is required is because this allows us to effectively remove magnetic flux noise by compensating for the voltage induced by the changes in the external magnetic field itself. Consider for example a set of pickup coils that is correctly positioned exactly in the magnetic field centre. Changes in the external magnetic field will be symmetrical across the lower and upper set, i.e. $\mathrm{d}B/\mathrm{d}t$ will have the same sign in each coil. However, the changes caused by the vibrating sample will always be asymmetrical, i.e. $\mathrm{d}B/\mathrm{d}t$ will have the opposite sign in each coil. This is because if the sample is, for example, moving towards the upper set of coils, then it must be moving away from the lower set of coils and vice versa. Now since the upper and lower coils are wired together in opposing fashion, the symmetrically induced signals are nullified while the asymmetrically induced signals are enhanced. In this way we have effectively removed the background induction caused by the sweeping of the external magnetic field, as well as other magnetic flux noise, from our signal. In conclusion, instead of using just a single pickup coil, our vibrating sample magnetometer consists of four pickup coils, two sets of two, as shown schematically in Figure 9.1.2 on the previous page as well as in the full overview of the vibrating sample magnetometry setup in Figure C.0.1 in Appendix C.

To test the performance of our setup, we have measured the induced response curve of our full set of pickup coils, which we show in Figure 9.1.2. A nickel sample of 5 mg is used to find the response at different positions in the system. Due to mechanical constraints it is not possible to measure the complete profile from one end of each coil to the other end in one go. Instead only the immediate surroundings of the centre of the lower and upper coil set is shown. These centres are clearly identifiable by the intersection points with the x-axis. Furthermore, when summing all the coil profile curves together, we can identify the point exactly between the lower and upper set of coils by the maxima. A plot such as Figure 9.1.2 allows one to verify that the two inner coils, and the two outer coils, each respond the same (by comparing the peak height for each coil size) and to verify that the upper and lower coils are correctly spaced from the centre (by comparing the symmetry left and right from the centre marker)

Typical measurement

Since the vibrating sample magnetometer is a mechanical system, the resistance the driving motor experiences varies as a function of time, lubrication, alignment and other factors. Because this mechanical resistance varies from experiment to experiment it is important to not only record the input settings sent to the motor, but to also measure the actual output the motor is producing. For this purpose a potentiometer is part of the setup, as shown in Figure 9.1.3, the variable terminal of this potentiometer vibrates along with the motor and the sample stick. A second lock-in amplifier measures the AC component of the resistance over this potentiometer (henceforth, "the reference"), and a plain digital multimeter measures the DC component which may be used to record the position the vibration is driven at. The potentiometer is powered by two AA batteries (about 3 V for a fully charged set). The voltage applied by these batteries is

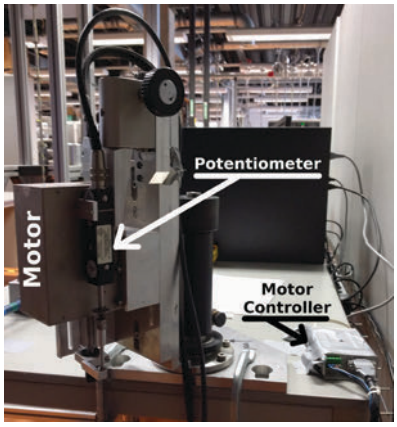

Figure 9.1.3: Photograph of the vibrating sample magnetometer motor, its controller and the potentiometer that is used to record the produced vibrations.

also recorded in order to compensate for depletion of the batteries over time, this can be done by simply dividing all voltages measured on the potentiometer by the voltage measured over the batteries.

The final invariant quantity that can be used to compare across measurements thus becomes:

$$\text{RelativeSignal(V)} = \frac{\text{Signal(V)}_y}{\text{Reference(V)}_x/\text{Battery(V)}} \tag{9.1.8}$$

Here the signal is measured across the full set of four coils using a lock-in amplifier (i.e. terminals 9-10 in Figure C.0.1), since this load is purely inductive we use the out-of-phase y-component measured by the lock-in amplifier. The reference is measured across the low and variable terminal of the potentiometer using a lock-in amplifier, since this load is purely resistive we use the in-phase x-component measured by the lock-in amplifier. Finally the battery charge is measured using a digital multimeter. Unless otherwise stated the corrected relative signal is always used to present data.

Calibration

The vibrating sample magnetometer may be calibrated with a sample of known magnetisation in order to obtain measurement results in more useful units of magnetisation (emu) instead of Volts. Nickel, for example, is a good candidate because it is a paramagnet that saturates at relatively low fields, it has a saturation magnetisation of $(58.57 \pm 0.03)\,\text{emu/g}$ ($1\,\text{emu/g} = 1\,\text{A}\,\text{m}^2\,\text{kg}^{-1}$) [39]. By simply measuring the response of the vibrating sample magnetometer to a sample of nickel with known mass, we can use the known mass and saturation magnetisation of nickel to determine a calibration parameter in units of emu per Volt. An example calibration measurement is shown in Figure 9.1.4. In the insets of Figure 9.1.4, we zoom in on the regime where the magnetisation of nickel saturates. Looking closely at this regime we see that there is a linear diamagnetic background present. This background originates from the sample holder and other components of the setup, it is therefore always present in vibrating

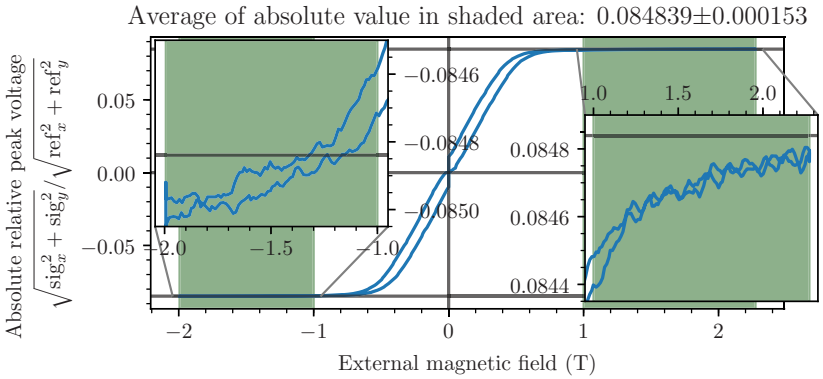

Figure 9.1.4: The response of the combination of all four pickup coils to 42.5 mg nickel vibrating at 18.1 Hz with an amplitude of 1.08 mm at room temperature while sweeping the magnetic field with $20\,\text{mT}\,\text{s}^{-1}$. Note this figure deviates from the established policy of only presenting data in the corrected relative signal format described by Equation (9.1.8) because it originates from before the potentiometer battery was introduced. Instead the data is presented as absolute signal divided by reference. The figure serves as an example on how the vibrating sample magnetometer may be calibrated. Each data set has its own accompanying calibration measurement when one is used. Figure from Ammerlaan [24]

sample magnetometry measurements For the best results, this linear diamagnetic background should be removed from the data by performing linear regression on the saturation regime and subtracting that result.

9.1.3 Example experiment

As an example of a typical experiment that can be performed with the vibrating sample magnetometer let us take a brief look at a tangential magnetometry experiment that the author was involved in. Lázpita et al. [16] have investigated the magnetic phase transition in Heusler alloys. These alloys structurally transform from a martensite phase to an austenite phase under the influence of temperature and magnetic field. This particular transition is fascinating as it shows a pronounced memory effect, meaning that the start and end points of this transition depend on the samples history. This is briefly illustrated in Figure 9.1.5, where we show the magnetisation of a Heusler alloy with composition $Ni_{100}Mn_{69}In_{31}$ as a function of applied magnetic field. There is a clear phase transition visible, here the lower magnetisation corresponds to the martensite phase and the higher magnetisation corresponds to the austenite phase. That there is a strong memory effect becomes evident when comparing the phase transitions of the sample when it was cooled down from room temperature without any magnetic field applied (ZFC), versus the same cool down with a magnetic field of 33 T applied (SFC). In this later case of cooling down in magnetic field we find that the martensite to austenite occurs at significantly lower magnetic fields. To learn all about this memory effect and the associated measurements we performed, we invite the reader to read Lázpita et al. [16].

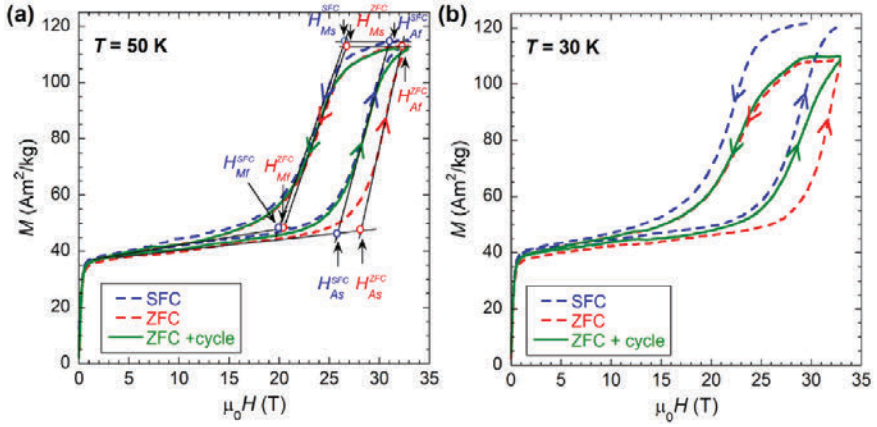

Figure 9.1.5: Magnetisation as a function of applied magnetic field for a Heusler alloy of composition $Ni_{100}Mn_{69}In_{31}$ at a) 50 K and b) 30 K. The zero-field cooling (ZFC) (red) curves were measured by cooling down the sample without any magnetic field applied. The strong-field cooling (SFC) (blue) curves on the other hand were obtained by cooling down the same sample in a magnetic field of 33 T. Finally the zero-field cooling plus cycle (ZFC+cycle) (green) curves represent the magnetisation of the same sample that was cooled down twice without any magnetic field applied. The starting and end points of the martensite to austenite transition, and the reverse transition, are indicated by arrows. Figure from Lázpita et al. [16].

9.2 Torque magnetometry

Another method to measure the magnetisation of some sample is torque magnetometry. Compared to the vibrating sample magnetometry setup at HFML-FELIX that was outlined in the previous section, torque magnetometry is more sensitive to small magnetisations. This may be an advantage but as we shall see later it may also be a disadvantage. Torque magnetometry has the additional benefit of being sensitive to magnetisations both parallel and perpendicular to the applied magnetic field and as such is capable of measuring magnetic anisotropy. In the subsections below we will explain in detail how this technique works, and how it is applied in practice.

9.2.1 Basic principle of capacitive torque magnetometry

Torque magnetometry measures magnetisation by measuring the torque a magnetised sample exerts on a cantilever. The induced deflection of the cantilever is often measured capacitively, but can also be measured using other techniques such as optically. Here we will focus on the capacitive option, since this is what was used for our measurements. Figure 9.2.1 shows schematically how a torque measurement works. A sample is placed on the end of a cantilever, this end of the cantilever hovers above a conducting base plate while the other end is fixed. As the external magnetic field is increased, and the sample is magnetised, the sample will exert torque on this cantilever causing the distance between the cantilever and the base plate to increase or decrease depending on the direction of the torque. This change can be measured as a change in capacitance using a capacitance bridge. As we shall see in the remainder of this section, the sensitivity of torque magnetometry is effectively controlled by the dimensions and the material properties of the cantilever. By making the cantilevers thinner and/or more flexible, we make the system more sensitive. For this reason, as a rule of thumb, torque magnetometry cam be more sensitive than vibrating sample magnetometry.

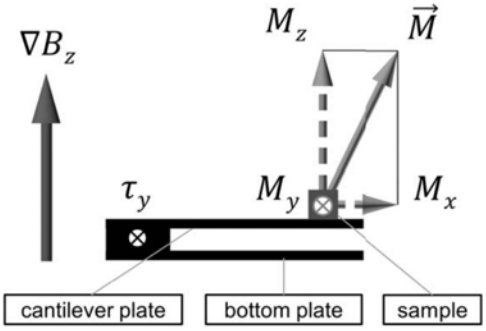

Figure 9.2.1: Basic principle of a torque magnetometry measurement. Figure from Peters [9].

In order to find how the magnetisation of a sample will affect the capacitance, let us first look at the component of the magnetic moment parallel to the external magnetic field. The energy of the magnetised sample in a magnetic field can be described as $U = -\vec{m} \cdot \vec{B}$ [9]. Therefore the force is given by:

$$\vec{F} = \vec{\nabla} \left(\vec{m} \cdot \vec{B} \right) \tag{9.2.1}$$

Using that the external magnetic field is purely in the z direction this reduces to:

$$\vec{F} = \vec{\nabla} \left(m_z B_z \right) = \vec{\nabla} \left(m_{\parallel} B \right) \tag{9.2.2}$$

Which gives us the force caused by the parallel component of the magnetic moment. Next, let us rewrite this force in terms of torque which will help us later to combine both directions of the magnetic moment into a single equation:

$$\vec{\tau} = \vec{x} \times \vec{F} = \vec{x} \times \vec{\nabla} \left(m_{\parallel} B \right) \tag{9.2.3}$$

Here we have defined $\vec{x}$ as the arm of the cantilever, the length of which will be $||\vec{x}|| \equiv L_c$. Assuming that the external magnetic field is radially homogeneous but has a gradient in the z direction, it becomes clear that both $m_{\parallel}$ and B can only depend on the z coordinate:

$$\tau_y = -L_c \frac{\partial \left(m_{\parallel} B \right)}{\partial z} \tag{9.2.4}$$

Now let us look at the perpendicular component of the magnetic moment. This expresses itself in the form of a torque on the cantilever given by:

$$\vec{\tau} = \vec{m} \times \vec{B} \tag{9.2.5}$$

Again assuming the dimensionality as shown in Figure 9.2.1, this reduces to:

$$\tau_y = -m_x B_z = -m_{\perp} B \tag{9.2.6}$$

Taking Equation (9.2.6) and Equation (9.2.4) together we obtain the total torque exerted on the cantilever:

$$\boxed{\tau = -m_{\perp} B - L_c \frac{\partial \left(m_{\parallel} B \right)}{\partial z} = - \left(m_{\perp} + L_c m_{\parallel} \frac{\partial}{\partial z} \right) B} \tag{9.2.7}$$

Where in the second step we have assumed that the change in the magnetic moment $m_{\parallel}$ with respect to the z direction is insignificant compared to the gradient of the external field.

Now let us focus on how this torque is going to effect the capacitance so we can directly relate the magnetic moment to capacitance. The area of the cantilever and bottom plate shall be A and the distance between them will be d. The capacitance of such a simple capacitor is given by:

$$C_0 = \frac{\epsilon_0 A}{d} \tag{9.2.8}$$

However once we start applying a torque to the cantilever Equation (9.2.8) no longer holds. The cantilever bends and this causes the distance between the cantilever and the ground plate to be non-uniform along the length of the cantilever. To obtain an equation that describes this non-uniform distance, we must first determine how the cantilever bends. Let us start with the Euler-Bernoulli equation, which describes the deflection of a beam upon applying a load to it:

$$\frac{d^2}{dx^2} \left(EI \frac{d^2 b}{dx^2} \right) = q = -F \delta \left(x - L_a \right) \tag{9.2.9}$$

Here, E is the elasticity of the cantilever, I is the second moment of area, $b(x)$ is the bending of the cantilever, and q is the distributed load (force per unit length). For simplicity we assume that all the

bending takes place in the arms of the cantilever, which is a reasonable approximation since the arms are much thinner compared to the cantilever platform (both are shown schematically in Figure 9.2.2 below).

We can therefore write $q = -F\delta(x - L_a)$ since the force that is bending the arms of the cantilever is only applied at the end of the arms. Where we have introduced L_a as the length of the cantilever's arms. Solving the differential Equation (9.2.9) leaves us with:

$$\frac{d}{dx}\left(EI\frac{d^2b}{dx^2}\right) = -F \implies EI\frac{d^2b}{dx^2} = -Fx + c_1$$

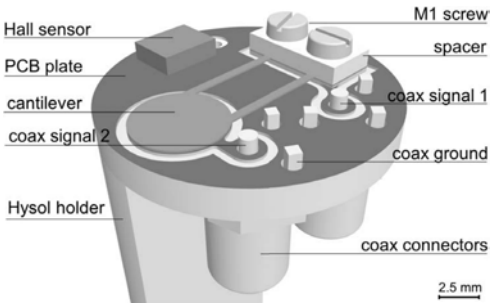

Figure 9.2.2: Schematic representation of the torque magnetometry measurement platform. Figure from Peters [9].

Bringing EI to the other side and integrating twice again gives:

$$\implies \frac{d^2b}{dx^2} = \frac{-Fx + c_1}{EI}$$

$$\implies \frac{db}{dx} = \frac{-Fx^2/2 + c_1x}{EI} + c_2$$

$$\implies b(x) = \frac{-Fx^3/6 + c_1x^2/2}{EI} + c_2x + c_3$$

Which leaves us with the constants c_1, c_2, c_3. The values for these constants we can find by looking at the boundary conditions. At $x = 0$ the bending b must also be 0 since this is where the cantilever is attached to the rest of the system and this point will never bend, for the very same reason the derivative of $b(x)$ must also be 0 at this point. Looking at the other end of the beam $x = L_a$, the second derivative of $b(x)$ should be 0 here since the slope of the bend can no longer change beyond this point.

$$b(0) = 0 \implies c_3 = 0$$

$$\left(\frac{db}{dx}\right)_{x=0} = 0 \implies c_2 = 0$$

$$\left(\frac{d^2b}{dx^2}\right)_{x=L_a} = 0 \implies c_1 = FL_a$$

Combining it all together we find that:

$$b(x) = \frac{-Fx^3/6 + FL_ax^2/2}{EI} = \frac{Fx^2}{6EI}(3L_a - x) \tag{9.2.10}$$

What we are mainly interested in, is the vertical position of the cantilevers main plate since this is where we will be measuring the capacitance. The main plate with our sample starts at the end of the arms therefore we want to know $b(L_a)$. Earlier we have assumed that the capacitive part of the cantilever does not bend significantly compared to the arms (Figure 9.2.2) and therefore we can describe the position of the cantilevers main plate with a simple linear equation. Let us therefore determine the position and slope of the arms at their end:

$$b\left(L_a\right) = b_{max} = \frac{FL_a^3}{3EI} \tag{9.2.11}$$

$$\left(\frac{db}{dx}\right)_{x=L_a} = a = \frac{FL_a^2}{2EI} \tag{9.2.12}$$

From this it follows that the distance between the capacitive plates can be described as follows:

$$d\left(x\right) = d_0 - \frac{FL_a^2}{2EI}x + b_{offset}$$

Where d_0 is the initial distance between the plates, or in other words, d_0 represents the rest position when no force is applied. b_{offset} we can determine by using that we know that $d\left(L_a\right) = d_0 - b_{max} = d_0 - \frac{FL_a^3}{3EI}$

$$d\left(L_a\right) = d_0 - \frac{FL_a^3}{3EI} = d_0 - \frac{FL_a^3}{2EI} + b_{offset} \implies b_{offset} = -\frac{FL_a^3}{3EI} + \frac{FL_a^3}{2EI} = \frac{FL_a^3}{6EI}$$

$$d\left(x\right) = d_0 - \frac{FL_a^2}{2EI}x + \frac{FL_a^3}{6EI} \tag{9.2.13}$$

Now that we know the distance between the plates as a function of x we can determine the capacitance by writing Equation (9.2.8) as an integral:

$$C_1 = \int_{L_c-r}^{L_c+r} \frac{\epsilon_0 w\left(x\right)}{d\left(x\right)} dx \tag{9.2.14}$$

Here L_c is the centre of the cantilever's capacitive plate. This coincides with L_c in Equation (9.2.4) because the point where the torque is applied should be the centre of the plate provided the sample is properly centred. Given that the main plate of the cantilever is circular, the width $w(x)$ is given by $2\sqrt{r^2 - \left(x - L_c\right)^2}$. This gives us:

$$C_1 = \int_{L_c-r}^{L_c+r} \frac{\epsilon_0 2\sqrt{r^2 - \left(x - L_c\right)^2}}{d_0 - \frac{FL_a^2}{2EI}x + \frac{FL_a^3}{6EI}} dx \tag{9.2.15}$$

An in-depth solution to Equation (9.2.15) is provided in Appendix B, the final result is:

$$C_1 = \frac{\epsilon_0 A}{d_0 - \frac{FL_a^3}{3EI}} \tag{9.2.16}$$

Note that Equation (9.2.16) reduces to Equation (9.2.8) if $F = 0$, as it should. The next step is to determine the second moment of area I. Because the cross-section of the cantilever arms lies in the y-z plane this is given by:

$$I = \int\int z^2 dydz = 2\int_{-t/2}^{t/2}\int_{\lambda/2-v/2}^{\lambda/2+v/2} z^2 dydz \tag{9.2.17}$$

Since we have two arms we multiply by 2. The separation between the centroid axis of both arms is represented by λ, v describes the width of the arms, and finally t is the arms thickness. The distance between the edges of the arms is thus equal to $\lambda - v$. And the solution to this integral is:

$$I = 2\left[y\right]_{\lambda/2-v/2}^{\lambda/2+v/2}\left[\frac{z^3}{3}\right]_{-t/2}^{t/2} = \frac{2}{3}\left(\frac{\lambda}{2}+\frac{v}{2}-\left(\frac{\lambda}{2}-\frac{v}{2}\right)\right)\left(\frac{t^3}{8}-\frac{(-t)^3}{8}\right) \tag{9.2.18}$$

$$\implies I = \frac{vt^3}{6} \tag{9.2.19}$$

Combining Equation (9.2.19) and Equation (9.2.16) results in:

$$C_1 = \frac{\epsilon_0 A}{d_0 - \frac{FL_a^3}{3E\frac{vt^3}{6}}}$$

$$\boxed{C_1 = \frac{\epsilon_0 A}{d_0 - \frac{2FL_a^3}{Evt^3}}} \tag{9.2.20}$$

Any bending of the cantilever (represented for convenience as Δd) must be small compared to d_0, else we risk deforming it permanently. Thus we can once again perform a Taylor expansions:

$$C_1 = \frac{\epsilon_0 A}{d_0 - \Delta d} \approx \frac{\epsilon_0 A}{d_0} + \frac{\epsilon_0 A}{d_0^2}\Delta d + \mathcal{O}\left(\left(\Delta d\right)^2\right)$$

$$C_1 = \frac{\epsilon_0 A}{d_0} + \frac{\epsilon_0 A}{d_0^2}\frac{2FL_a^3}{Evt^3} \tag{9.2.21}$$

This simplified form allows us to write the change in capacitance as a result of the induced magnetic moment as:

$$\Delta C = C_1 - C_0 = \frac{\epsilon_0 A}{d_0^2}\frac{2FL_a^3}{Evt^3}F \tag{9.2.22}$$

$$\implies F = \frac{d_0^2}{\epsilon_0 A}\frac{Evt^3}{2L_a^3}\Delta C$$

Or, when written in terms of torque instead:

$$\vec{\tau} = \vec{x}\times\vec{F} = \vec{x}\times\hat{z}\frac{d_0^2 Evt^3}{2\epsilon_0 AL_a^3}\Delta C \tag{9.2.23}$$

Where we have introduced $\hat{z}$ because the motion of the cantilever is restrained to the z-direction. This we can further simplify to:

$$\tau = \tau_y = -L_c\frac{d_0^2 Evt^3}{2\epsilon_0 AL_a^3}\Delta C \tag{9.2.24}$$

Finally, combing Equation (9.2.7) and Equation (9.2.24), and using that $L_c = L_a + r$, gives our end result:

$$\left(L_a + r\right)\frac{d_0^2 Evt^3}{2\epsilon_0 AL_a^3}\Delta C = m_\perp B + \left(L_a + r\right)\frac{\partial\left(m_\parallel B\right)}{\partial z} \tag{9.2.25}$$

$$\boxed{\implies \Delta C = \frac{2\epsilon_0 AL_a^3}{Evd_0^2 t^3}\left(\frac{m_\perp}{L_a + r} + m_\parallel\frac{\partial}{\partial z}\right)B} \tag{9.2.26}$$

Equation (9.2.26) thus shows us that we can measure both the parallel and perpendicular component of the magnetic moment by measuring both in a region where $\partial B/\partial z = 0$ and a region where it is not.

Calibration

As an alternative approach to calculating exactly how the change in capacitance relates to the magnetic moment, we can use the fact that we know there is some relation between these two quantities to calibrate the setup with a given cantilever and a sample with known magnetisation and known magnetic anisotropy. When looking at Equation (9.2.26) we find that we effectively have two calibration parameters, let us name them α and β. We also see that these two parameters describe fully the relation between the capacitance change and the magnetisation of some sample, as given by:

$$\Delta C = \alpha \left(\frac{m_\perp}{\beta} + m_\parallel \frac{\partial}{\partial z} \right) B \tag{9.2.27}$$

Where we know that theoretically α relates to the properties of the cantilever as:

$$\alpha = \frac{2\epsilon_0 A L_a^3}{E v d_0^2 t^3} \tag{9.2.28}$$

And β relates to these properties of the cantilever as:

$$\beta = L_a + r \tag{9.2.29}$$

Measuring then a sample of known magnetisation and known magnetic anisotropy allows us to find values for α and β which we can use to determine the magnetisation of some unknown sample.

9.2.2 Experimental setup and procedure

A typical torque measurement starts with selecting the right cantilever. Since we want the bending of the cantilever to stay within the elastic regime, we must make some estimate of the torque the sample will induce on the cantilever using Equation (9.2.7). When the cantilever will *yield* (i.e. exit the elastic regime) depends on the materials yield strength, but also on the dimensions of the arms, specifically the thickness and width of the arms. Depending on the amount of torque we estimate the sample will exert, we choose a cantilever which has appropriate arms. The used cantilevers are made from a Phosphor Bronze alloy[2] which has a yield strength of 300 to 690 MPa and elastic modules of 118 GPa or from a Copper Beryllium alloy[3] with a yield strength of 690 to 830 MPa and elastic modules of 138 GPa. The latter alloy is stronger but it is no longer feasible to procure cantilevers made from this alloy due to its toxicity, as such new batches are always made from the Phosphor Bronze alloy.

Once a suitable cantilever has been selected, the sample is glued to that cantilever. Then the cantilever is screwed onto the base plate of the torque magnetometry probe with a small separator in between at the mounting point to ensure that the cantilever does not touch the base plate, as illustrated in Figure 9.2.1. Next, the probe is inserted into the cryostat and the electronics are connected.

On the electronics side of the setup, there are two ways of measuring the capacitance change resulting from the magnetisation of the sample. The most straightforward method is to use a capacitance bridge.

[2] $CuSn_{5.5–7.0}P_{0.01–0.4}$
[3] C17410 HT $CuCo_{0.35–0.60}Be_{0.5}$

This device will actively try to balance the target capacitance with a series of known capacitors built into the device. From this, the device concludes what the target capacitance must be and returns this to the user. The alternative, approach is to instead wire the target capacitance into a plain Wien bridge configuration and to then measure the changing voltage resulting from the unbalance with a lock-in amplifier. With this approach the exact value of the capacitance is unknown, that is however not a problem since we are only interested in how the capacitance changes and not in its magnitude. This alternative method avoids the active balancing, switching and processing that a real capacitance bridge would do, and therefore is usually a bit faster and more accurate.

Chapter 10

Results: Magnetisation of superconducting tapes

As we have specified in Chapter 8, the experiments described here are part of the SuperEMFL project and our aim is to test the performance of a new material that is a candidate for the next generation of superconducting magnets. To that aim we wish to measure the magnetisation of this material as a function of applied magnetic field, in doing so we extract the *irreversibility field* of this material. We employ the techniques of vibrating sample magnetometry and torque magnetometry as described in sections 9.1 and 9.2 respectively. In this chapter we shall present the results of these magnetometry measurements.

10.1 Samples

The samples being measured consist of a proprietary high-T_c superconducting alloy produced by THEVA GmbH encapsulated in Kapton tape. They were assembled at the Institute of Electrical Engineering (IEE) of the Slovak Academy of Sciences. The samples were first measured using a commercial vibrating sample magnetometer in a (superconducting magnet) Physical Property Measurement System (PPMS) at the IEE. They were then transported to HFML-FELIX in order to be measured again in our custom built vibrating sample magnetometer (VSM), in both a superconducting and resistive magnet. We have also performed several measurements on these tapes using torque magnetometry in resistive magnets.

We already know that these THEVA tapes are a *Type-II* superconductor with strong flux pinning, this is after all the aim of the game when developing superconducting magnets as explained in Section 3.4. Therefore, we expect that the magnetic response of our tapes is strongly opposing the applied magnetic field and that it is almost fully proportional to the superconducting critical current density J_c as also explained in Section 3.4. Furthermore, we expect this critical current, and thus the magnetisation, to decrease as the strength of the applied magnetic field increases. Until the applied magnetic field reaches the superconducting critical magnetic field, where we expect the magnetisation to be reduced to the usual diamagnetic background levels.

10.2 VSM results in superconducting magnets

The initial results from the superconducting magnet VSM system at the IEE are shown in Figure 10.2.1. The dotted line shows the initial magnetic field sweep from 0 T into the loop and serves as an indication of the sweeping direction. After this initialisation we find that the magnetic moment decreases with increasingly (negative) magnetic field, this makes sense since the superconducting critical current J_c that is responsible for this magnetic moment is expected to decreases with increasing magnetic field strength. At around −3 T the magnetic field sweeping direction is inverted and as expected we find that the sign of the magnetic moment flips as the circular superconducting screening currents switch helicity. The magnetic moment then becomes increasingly (negative) for decreasingly (negative) magnetic fields until we reach 0 T again where we have the maximum magnetic moment. For the positive magnetic fields we find the exact mirror of the behaviour we found for negative magnetic fields. The magnetic moment decreases as the magnetic field increases until we switch the magnetic field sweeping direction again at the maximum magnetic field of 14 T for this system. The magnetic moment then increases until we close the loop just after crossing the 0 T threshold again from the other direction. Being a *Type-II* superconductor with a low B_{c_1} yet a very high B_{c_2}, this "envelope" shape is exactly what we would expect for these THEVA tapes as also explained in more detail in Section 3.4. However, with a maximum magnetic field of 14 T, this PPMS is not strong enough to reach the irreversibility field B_{irr} and destroy the flux pinning, nor is it strong enough to reach the critical magnetic field B_{c_2} to fully suppress the superconductivity. This is evident from the fact that the "envelope" does not close, instead we find a clear flip in the sign of the magnetic response as the sweeping direction of the magnetic field inverses.

In order to prove comparability between the PPMS VSM setup at the IEE and our home-built VSM

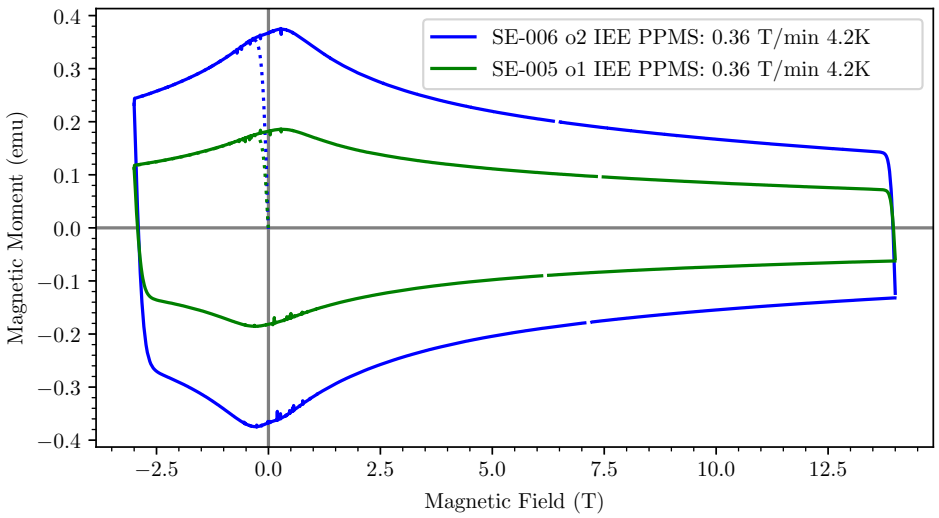

Figure 10.2.1: Isothermal magnetisation loops of two typical THEVA tapes as measured by the VSM PPMS at the IEE. The dotted line represents the initial magnetic field sweep from 0 T to −3 T, from there a full cycle is done up to the maximum field of 14 T and back. The field sweeping rate is 0.36 T min^{-1}. Experiments performed by Eugen Seiler at the Institute of Electrical Engineering (IEE).

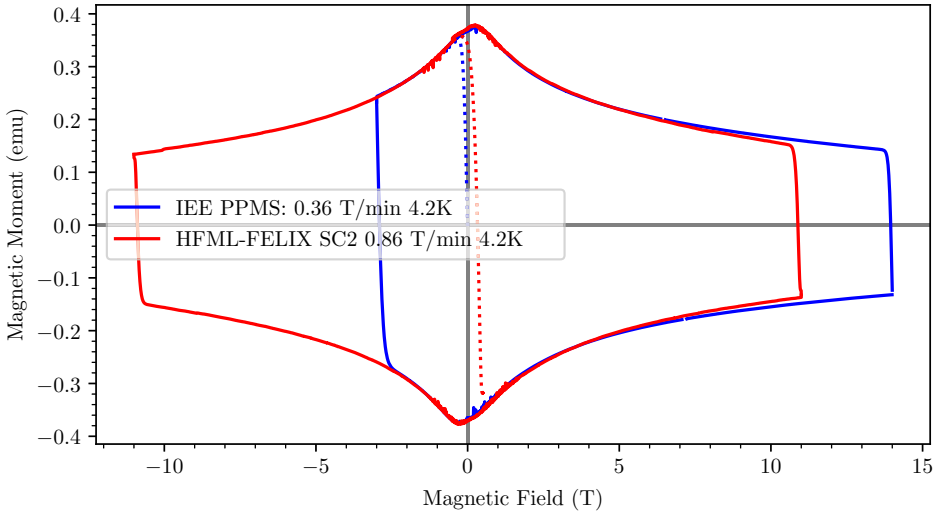

Figure 10.2.2: Comparison of the isothermal magnetisation loops of a THEVA tape as measured by the VSM PPMS at the IEE versus our home-built VSM system in Superconductor 2 at HFML-FELIX. The HFML-FELIX curve has been scaled so the peaks match with the data from the PPMS, and a correction for differing linear diamagnetic background magnetisation has been performed as described in the main text.

system at HFML-FELIX, one of the sample tapes has also been measured in Superconductor 2 at HFML-FELIX. The results from this comparative measurement are shown in Figure 10.2.2. Since our home-built VSM system produces magnetisation data in units of V, the HFML-FELIX data has been scaled so the peaks match with the data from the IEE. This scaling method usually produces better results compared to calibration with nickel, since calibration with nickel introduces an additional error source in the form of the mass determination of the calibration sample. Additionally, since the design of our home-built system is necessarily completely different when compared to the commercial PPMS setup, the diamagnetic background of both systems must be different as a result. We should therefore apply a correction for this differing diamagnetic background magnetisation. Since the diamagnetic background is always purely linear, comparability is restored by subtracting a linear slope from the HFML-FELIX data such that this “envelope” falls exactly in between the “envelope” as measured by the PPMS. Overall we find good agreement between both systems, this indicates that our home-built VSM system is performing as it should.

Having determined that the PPMS VSM setup and our HFML-FELIX VSM system produce comparable results, let us proceed and move the setup to the resistive magnets to obtain higher magnetic field data.

10.3 VSM results in the resistive magnet

Since we want to test these THEVA tapes for potential application in the next generation of superconducting magnets we need to characterise the tapes in higher magnetic fields than our Superconductor 2 can provide. So let us repeat the measurements from the previous section in the high-field resistive magnets, these results are shown in Figure 10.3.1. A first unexpected observation to make is that all "envelopes" measured in the resistive magnet are significantly smaller. To verify that this is not due to a difference in field sweeping rate, we performed the same measurement with both $4\,\mathrm{T\,min^{-1}}$ and $1\,\mathrm{T\,min^{-1}}$ field sweeping rates. As expected, the faster sweep has a slightly larger "envelope" compared to the slower sweep. However, this difference is clearly significantly smaller than the discrepancy we observe between the results from the superconducting magnets and the results measured in the resistive magnet. To eliminate the possibility of some temperature control inconsistencies, we also performed the same measurement at 2.2 K. We find that for this reduced temperature the peaks are slightly larger, the "envelope" is wider, and the closing point of the "envelope" occurs at higher magnetic field. This part of the result is expected. After all, at lower temperatures the superconducting critical magnetic field and therefore the superconducting critical current, will be higher and thus the magnetisation will be larger

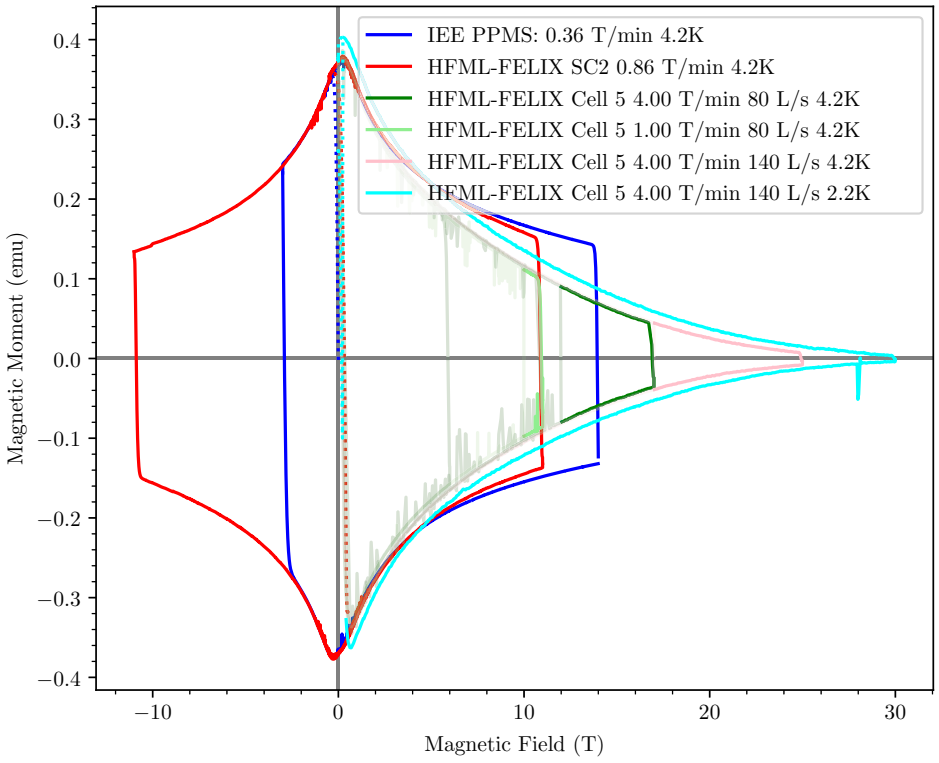

Figure 10.3.1: Comparison of the isothermal magnetisation loops of a THEVA tape as measured by the VSM PPMS at the IEE, Superconductor 2 and Cell 5 at HFML-FELIX. The HFML-FELIX curves have been scaled so the peaks match with the data from the PPMS, and a correction for differing linear diamagnetic background magnetisation has been performed.

as well. Nonetheless, the "envelope" we measure at this reduced temperature is still significantly smaller when compared to the results we obtained in the superconducting magnets. Clearly there is some issue with our measurements in the resistive magnets.

10.3.1 What is happening?

When attempting to replicate our results with other THEVA tape samples, and with several other superconducting samples, we consistently find that the measured "envelope" is smaller than expected in the resistive magnets. This would indicate that there is no problem with the sample itself and that somehow the obtained critical current J_c and the irreversibility field B_{irr} are actually lower when measured in a resistive magnet when compared to the same measurement in a superconducting magnet. How can this be? The specific sample shown in the figures here was measured first in the PPMS, then in Cell 5, then in Superconductor 2, and finally in Cell 5 again. This suggest that sample degradation is not the cause of the reduced superconductivity, after all Superconductor 2 agrees well with the PPMS. The setup in Superconductor 2 and Cell 5 is identical, apart of course from the type of magnet and its physical location[1].

As already noted before in Section 3.4, the hysteretic component (i.e the "envelope") of the magnetisation of a *Type-II* superconductor with flux pinning is a response not to magnetic field ($\vec{B}$) itself, but to change in magnetic field ($\mathrm{d}\vec{B}/\mathrm{d}t$) [44]. With this in mind, let us consider the effect of electromagnetic noise in a magnet on a superconducting sample. For example, if we are sweeping the magnetic field up, then the sample will respond with an opposing negative magnetisation proportional to J_c. However, if there are local short-lived moments where the change in magnetic field flips sign, then in these moments the samples magnetisation would also be driven to flip sign. If the timespan of this direction inversion is short-lived enough, then instead of observing a full flip in magnetisation from $\propto -J_c$ to $\propto +J_c$ one could observe this as a faster decay of the magnetisation. Time-averaged this could be described as:

$$\left|\vec{M}\right| \propto J_c - \alpha\left(B, T\right) J_c \tag{10.3.1}$$

With α being some factor relating to the frequency of sign flips occurring during the magnetic field sweep, possibly depending on the magnetic field strength and/or the temperature [44].

With the above in mind, let us consider how a superconducting magnet is different from a resistive magnet. Considering that a typical power supply for a superconducting magnet outputs a maximum of 100 A at 10 V and that the magnet itself is cooled by a stationary bath of liquid helium. And considering that our resistive magnets, on the other hand, operate on a maximum of 40 kA at 500 V and are cooled by a continues flow of up to $140\,\mathrm{L\,s^{-1}}$ of water. It is not surprising that a resistive magnet is audibly, mechanically and electromagnetically, more noisy when compared to a superconducting magnet. Since a Vibrating Sample Magnetometer consists of a series of pick-up coils, this higher electromagnetic noise level might effectively be further amplified by local (self-)induction in the pickup coils. This electromagnetic noise might then cause the superconducting screening currents on the surface of the sample to rapidly fluctuate, which could cause a local heating effect inside the sample [44].

In order to investigate the possible effect of mechanical noise on our measurement, we have performed the same measurement with a reduced cooling water flow of $80\,\mathrm{L\,s^{-1}}$. This is the minimum flow for which it is still safe to operate this resistive magnet. This reduced flow limits the maximum magnetic

[1] Meaning the stability of the electrical grounding could be different, which might negatively effect the measurement.

field that can be reached, but also significantly reduces the audible and mechanical noise in the system. The results from this measurement are included in Figure 10.3.1 for comparison. We did not observe any difference between the high water flow and low water flow curves, which would suggest that mechanical noise from the water flow is not responsible for the observed discrepancies. It is therefore likely that electromagnetic noise is the culprit instead. We therefore propose the following hypothesis to explain the discrepancy we observe between our measurements in a resistive magnet and our measurements in a superconducting magnet:

Proposed hypothesis

To explain the discrepancy we find between the measurements with resistive and superconducting magnets we postulate that the increased noise of the resistive magnet, combined with the inherent high sensitivity to electromagnetic noise of magnetisation experiments on *Type-II* superconductors with flux pinning, causes the measured magnetisation to decrease faster and therefore causes the "envelope" to close prematurely. One could treat our results has having a higher "effective temperature" which would restore some degree of comparability. Alternatively one could interpret our result as a lower boundary for the true superconducting critical magnetic field.

10.3.2 Sanity check with NbTi

As a sanity check, we repeated the VSM experiments in Superconductor 2 and Cell 5 with NbTi wires instead of the THEVA tapes. The results are shown in Figure 10.3.2. These wires have a significantly lower superconducting critical magnetic field, therefore the superconducting critical current J_c, and hence the magnetic moment is overall smaller. We find that the *irreversibility field* (B_{irr}) is around 7.8 T, which

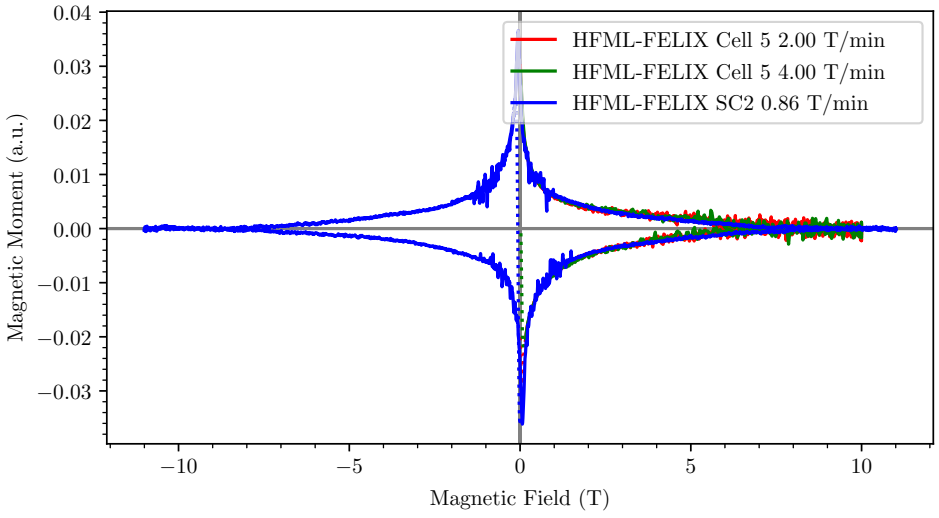

Figure 10.3.2: Comparison of the isothermal magnetisation loops of a NbTi wire as measured by Superconductor 2 and Cell 5 at HFML-FELIX. A correction for differing linear diamagnetic background magnetisation has been performed.

we have defined as the first data point where the up sweep and down sweep are not distinguishable within the noise level. Unfortunately, if there is any difference between the measurement in Superconductor 2 and Cell 5, it appears to be lost in the decreased signal to noise ratio in the resistive magnet.

As a rule of thumb, the electromagnetic noise as picked up by the vibrating sample magnetometer scales linearly with the magnetic field strength in our resistive magnets. Therefore, if our hypothesis is correct, then we would expect that samples with a larger superconducting phase (i.e. higher T_c, B_{irr}, B_{c_2}, J_c) are more affected by an apparent reduction in the size of the superconducting phase, when compared to samples that inherently already have a smaller superconducting phase. It is difficult to conclusively say whether there is no discrepancy in the measured magnetisation curves for NbTi, and our hypothesis needs revising. Or whether there actually is a discrepancy, but we lose it in the noise because the problem is less severe for the smaller superconducting phase of NbTi.

As this sanity check with NbTi is inconclusive, further investigation is required to prove or disprove our hypothesis. In order to test if our problem is specific to vibrating sample magnetometry, let us switch gears completely and try a different measurement technique: torque magnetometry

10.4 Torque magnetometry results

In order to cross-verify our vibrating sample magnetometry results with a completely different technique, we have measured the magnetisation of the THEVA tapes using Torque magnetometry. The capacitance between the base plate and the cantilever with the sample glued on top was measured in two different ways, as also described in more detail in Section 9.2.2. First using an Andeen-Hagerling capacitance bridge, which directly returns a value for the capacitance between the base plate and the cantilever. And second using a plain Wien bridge and lock-in amplifier. Here the Wien bridge was equilibrated at

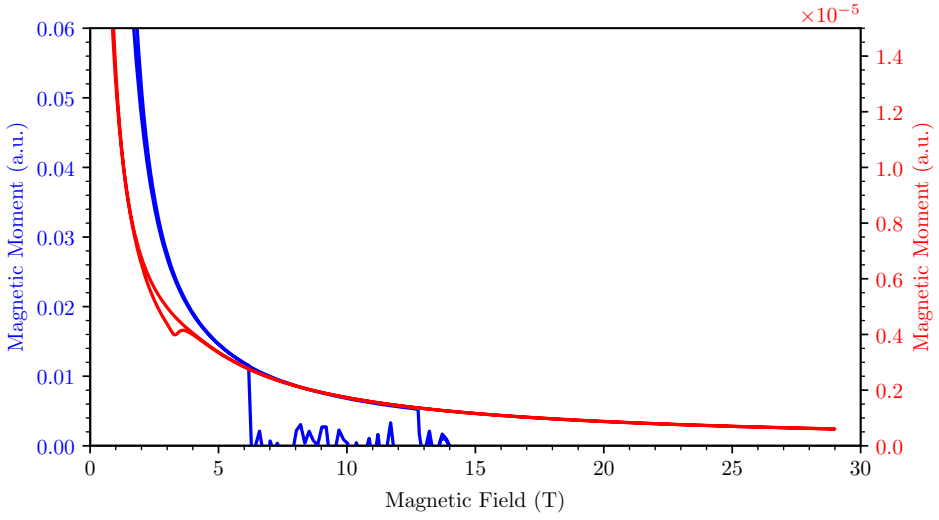

Figure 10.4.1: Magnetisation of THEVA tapes as measured with Torque magnetometry using two different methods. On the left axis, in blue, the change in capacitance is measured using an Andeen-Hagerling capacitance bridge. On the right, in red, the change in voltage is measured using a plain Wien bridge.

a magnetic field of 0 T. As the magnetic field changes, the capacitance changes and the Wien bridge is therefore no longer in equilibrium. A voltage corresponding to the change in capacitance was then measured on the lock-in amplifier. Our results are shown below in Figure 10.4.1.

Unfortunately, it proved difficult to get useful results using Torque magnetometry. The magnetic response from these tapes is rather large, which first of all created a challenge in keeping the samples glued tightly onto the cantilever. But this amount of magnetisation also proved to be too much for the cantilevers themselves as can be seen in Figure 10.4.1. At fields higher then 5 T we find that the deflection of the cantilever is already sufficiently large to cause the cantilever to touch the base plate and create an electrical short-circuit, as is evident from the blue line dropping to zero. When using the plain Wien bridge method instead (red line), this problem is less obvious since unlike the Andeen-Hagerling capacitance bridge, this setup does not directly measure the capacitance and does not feature short-circuit detection. Nonetheless, a visual inspection of the cantilevers after the measurement showed that they had been bent well beyond their elastic regime and that they were now permanently deformed. Consequently, the results from our torque magnetometry experiments are not completely trustworthy. Nonetheless, we do find in Figure 10.4.1 a non-zero magnetic moment at magnetic fields approaching 30 T, which might indicate that the superconductivity in the THEVA tapes is still present at these high fields.

10.5 Transport results

In addition to the magnetisation experiments performed at HFML-FELIX, the superconducting phase of the THEVA tapes has also been measured using transport techniques at the University of Geneva and at the LNCMI in Grenoble. We briefly show these results here as well in Figure 10.5.1 as a direct comparison with our results from magnetisation experiments. We find good agreement between the transport measurements and the VSM magnetisation measured as measured by the PPMS at the IEE, and reasonable agreement also with our home-built VSM setup in Superconductor 2. This result strengthens the credibility of the magnetisation data as it is measured in the superconducting magnets, and casts further doubt on the magnetisation data as it is measured in the resistive magnet. However, this unfortunately does not bring us closer to conclusively proving what is the cause of our problem.

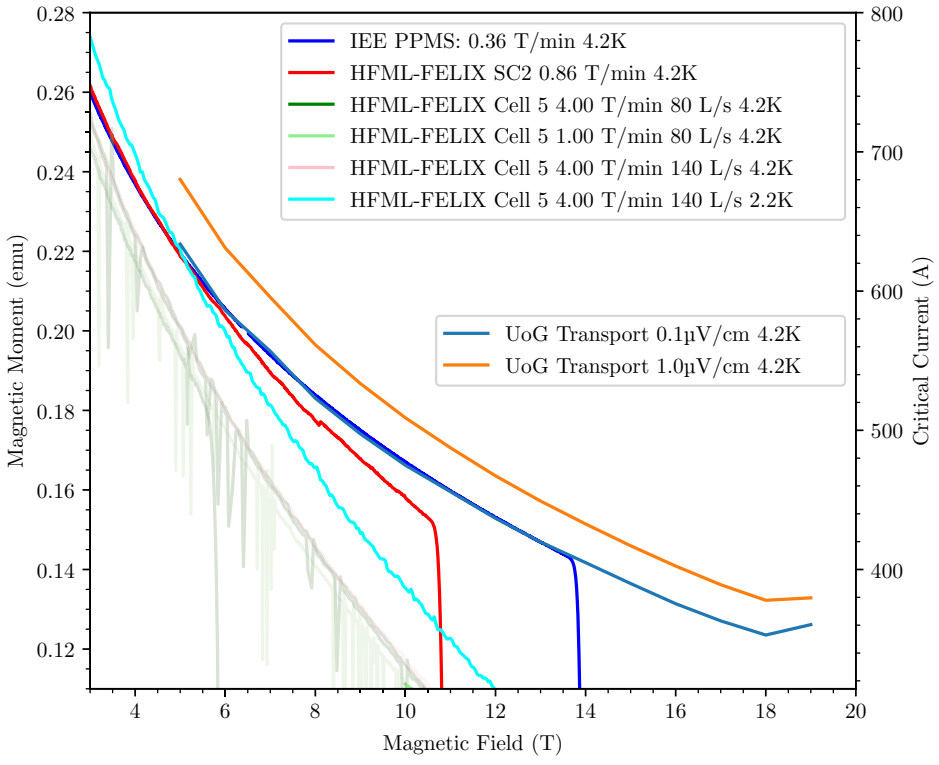

Figure 10.5.1: Comparison of isothermal magnetisation loops as measured by the VSMs at HFML-FELIX and the IEE with transport experiments performed at the University of Geneva by the group of Carmine Senatore.

Chapter 11

Conclusion and outlook

In this chapter we briefly summarise again our main findings and comment on further experiments that can be performed to debug and possibly resolve the problems we encountered. We start with our experiments using vibrating sample magnetometry experiments in Section 11.1 before moving on to our experiments using torque magnetometry in Section 11.2.

11.1 Vibrating sample magnetometry

Our results using vibrating sample magnetometry indicate some problem when measuring *Type-II* superconductors with flux pinning in our resistive magnets. We have proposed in Section 10.3 that this is due to the increased electromagnetic noise in a resistive magnet when compared to a superconducting magnet combined with the inherent sensitivity to noise in the magnetic field of this particular experiment. Several experiments can be performed to further investigate the problem and to verify or falsify this hypothesis:

- It is technically possible to drive more and bigger current oscillations (up to 50 Hz) into the resistive magnet. This way one could artificially introduce additional magnetic field noise. If our proposed hypothesis is correct, then the additional noise will make the "envelope" even smaller and close even faster. As such one could then conclusively prove the relation between noise and perceived reduced superconductivity in *Type-II* superconductors with flux pinning.

- Similar to the above, the possibility of introducing additional controlled magnetic field noise in the superconducting magnet could be investigated. This is possibly challenging due to the lower maximum field sweeping rate in a superconducting magnet, and the risk of quenching the magnet if the induced noise would exceed this limit.

- The amount of field noise the sample experiences while on the vibrating sample magnetometry probe could be better quantified by adding a Hall-sensor to the probe.

- Efforts could be made to better shield the sample from field noise by adding, for example, a cylinder of copper foil around the tip of the probe.

11.2 Torque magnetometry

When measuring the THEVA tapes with the torque magnetometry technique we found that the magnetisation is too large for the cantilevers we current have. Looking at Equation (9.2.26), there are several possible solutions to decrease the deflection of the cantilever $d(x)$:

- Increase the width of the arms v
- Increase the thickness of the arms and plate t
- Increase the elasticity E, or in other words, make the cantilevers from a different material
- Decrease the magnetisation $m_{\perp}$ and/or $m_{\parallel}$, or in other words, measure a smaller piece of sample.

Of these options, creating a new batch of cantilevers with thicker arms from the same sheet of metal is the easiest. Producing smaller samples from these tapes is challenging due to the layered nature of the tapes and the increased risk of delamination as the sample size is decreased.

If our hypothesis about the observed discrepancies between the magnetisation as measured with the vibrating sample magnetometer in the resistive magnet versus in the superconducting magnet is correct. Then we would expect to observe a similar reduction in width and slope of the magnetisation "envelope" when measuring the THEVA tapes with torque magnetometry. If this would indeed be the obtained result, then this could be another strong indicator that our hypothesis is correct.

Supplementary projects

Aside from my main projects as described in this dissertation thus far, I have been engaged in many side-quests, user-support projects, and other work during my time as a PhD candidate at HFML-FELIX. Lots of this work does not really fit into my PhD dissertation as a coherent story. Nonetheless, no overview of my PhD journey would be complete without at least briefly mentioning all this other work that has been keeping me busy during those times when progress on my main projects was temporarily halted. In fact, the whole contents of Part III started out as what should have been a relatively simple user-support project. However, as we have seen, unexpected difficulties turned that into a larger project requiring a significantly larger time investment than expected.

In addition to the THEVA tapes we have also done magnetisation experiments on Nb_3Sn superconducting wires with dr. Xingchen Xu and prof. dr. Michael Sumption from the Ohio state university, though we encountered the same difficulties as described in Part III. Additionally, we performed further vibrating sample magnetometry experiments on:

- the copper halide mineral atacamite in collaboration with dr. Leonie Heinze from the university of Braunschweig and dr. Tommy Reimann from the Helmholtz-zentrum Dresden-Rossendorf [4].
- the Heusler metamagnetic shape memory alloy Ni-Mn-In together with dr. Patricia Lázpita from the university of Basque Country and dr. Anabel Pérez-Checa from the Basque centre for materials [16].
- the halide double perovskite $Cs_2AgFeCl_6$ in collaboration with dr. Kingshuk Mukhuti, dr. Elvina Dilmieva, Maarten de Dreu, and Kilian Ramsamoedj from HFML-FELIX [6].
- the Heusler metamagnetic shape memory alloy Ni-Mn-In-B in a joint effort with dr. Elvina Dilmieva from HFML-FELIX.
- ErB_2 with Christoph Resch and André Deyerling from the technical university of München.

Furthermore, similar to our experiments on monolayer WS_2 described in Part II, we have also done additional ionic-liquid gating experiments on MoS_2 in order to measure the quantum oscillations in this material. This work was done in collaboration with dr. Xiaoli Peng from the university of Groningen and dr. Oleksandr Zheliuk and Davide Pizzirani from HFML-FELIX [8]. And finally, with the same group we have worked on measuring the quantum hall effect in Bi_2O_2Se [12].

Supplementing all this work on scientific research I have also been working as a (scientific) programmer. Mainly in the form of maintaining and improving the data acquisition software used at HFML-FELIX, as well as modernising and streamlining the control software for our vibrating sample magnetometer. In this role I feel that I have made a very positive contribution not just towards my own projects, and those user-support projects I have been directly involved in, but for all measurement projects at HFML-FELIX.

In addition to this software engineering work at HFML-FELIX, I have made further contributions to open source scientific software projects via the Gentoo Linux project. This flavour of the Linux operating system is unique due to its strong focus on tunability from the source up, while maintaining a coherent and smooth user experience. For this reason, Gentoo Linux and its package manager Portage are relatively popular choices in the (high energy) physics (HEP) and high performance computing (HPC) communities, especially in areas where those fields overlap [20].

Since December 2019 I have been actively involved in the Gentoo Linux project and in May 2021 I was accepted as an official developer. My main development focus has been on maintaining the Python ecosystem and a varied suite of scientific libraries and applications. A side project I rolled into in July 2023 is focussed on maintaining and automating the configuration, compilation, and deployment of the Linux kernel for numerous different systems. In this role I have extensively collaborated with fellow physicists and other scientists from various fields.

Summary

In Chapter 1 we briefly introduced the subject matter of this dissertation, superconductivity in high magnetic fields, and roughly explained the structure in which the reader will be guided through our research.

In Chapter 2 we showed the research infrastructure we have used in the remainder of this dissertation. Namely, the high field magnets at HFML-FELIX and the cryogenic equipment that was used in concert with these magnets.

In Chapter 3 we recapped and explained the theoretical framework of superconductivity that underlies our research. We encountered the Bardeen–Cooper–Schrieffer (BCS) and Ginzburg-Landau (GL) theory, as well as several concrete models for fitting and analysing various types of data obtained from experiments on superconductors.

In Chapter 4 we introduced a rather special form of superconductivity, Ising protected superconductivity, and the theoretical model we used to describe it. As we saw, this Ising protection is fascinating because it protects the superconducting phase from magnetic fields, which are usually detrimental to superconductivity as we explained in the preceding chapter. In this chapter we also introduce the Transition Metal Dichalcogenides (TMDs), and our material of interest: WS_2.

In Chapter 5 we presented the technique of ionic liquid gating. This technique was used in our experiments to reach electron doping levels well beyond what can be reached with traditional solid gates. We also show the methods we used to fabricate and characterise our WS_2 sample devices.

In Chapter 6 we showed the results from our experiments on the ionic liquid gating induced superconducting phase in WS_2. We performed characterisation experiments without magnetic field to extract the main parameters describing this superconducting phase. We then carried out experiments in parallel and perpendicular magnetic fields on several differently doped WS_2 sample devices and extracted the parameters describing the Ising protection.

In Chapter 7 we drew our conclusions based on the experiments described in the preceding chapter. We found that WS_2 is a *Type-II* superconductor with strong electron-phonon coupling, and we compared the parameters describing the superconducting phase in WS_2 with those obtained from similar experiments on MoS_2. We furthermore found a suggestive trend, that is in agreement with previous research, when comparing the superconducting transition temperature of sample devices with different substrates. In terms of Ising protection, we concluded that the *Rashba-type* spin-orbit coupling energy increases with an increasing superconducting transition temperature, while the *Zeeman-type* spin-orbit coupling energy remains constant within the uncertainty level of this experiment. Finally, we have given suggestions for improving our experiment in the future.

In Chapter 8 we introduced a second set of experiments focused on measuring the magnetisation of superconducting THEVA tapes, a candidate material for the next generation of superconducting magnets. Moreover, we briefly recapped the relevant details from the theoretical framework, and explained how we used magnetisation experiments in this context.

In Chapter 9 we explained the operating principle of vibrating sample magnetometry (VSM) and torque magnetometry. We compared both techniques and briefly described which technique is commonly used in which type of experiment.

In Chapter 10 we present the results from our magnetometry experiments. We start with results obtained using vibrating sample magnetometry in our superconducting magnet and compare these to measurements done on the same tapes in a physical property measurement system (PPMS) elsewhere. We then performed the same measurement in our high field resistive magnet and again compared the results. Finally we performed supplementing magnetisation measurements using torque magnetometry instead of vibrating sample magnetometry.

In Chapter 11 we drew our conclusions from our magnetisation experiments. We determined that there is a systemic inconsistency between the results for the magnetisation of superconducting samples as measured in superconducting magnets and resistive magnets. We hypothesised that this inconsistency is due to the additional electromagnetic noise that is present in a resistive magnet, which could prematurely destroy the supercurrents that form the basis of the magnetic response of *Type-II* superconductors. Finally, we provided suggestions for testing our hypothesis in future experiments, and to hopefully resolve the problem.

Samenvatting

In Hoofdstuk 1 hebben we kort het onderwerp van dit proefschrift geïntroduceerd, supergeleiding in hoge magneetvelden, en hebben we grofweg uitgelegd wat de structuur is waarmee de lezer door ons onderzoek wordt begeleidt.

In Hoofdstuk 2 hebben we de onderzoeksinfrastructuur gezien die we gebruiken in het resterende gedeelte van dit proefschrift. Namelijk de hoog veld magneten van HFML-FELIX en de cryogene apparatuur die bij deze magneten wordt gebruikt.

In Hoofdstuk 3 hebben we het theoretisch raamwerk van supergeleiding uitgelegd dat ten grondslag ligt aan ons onderzoek. We zijn de Bardeen–Cooper–Schrieffer (BCS) en Ginzburg-Landau (GL) theorie tegengekomen, evenals verscheidende concrete modellen voor het fitten en analyseren van de verschillende types data die verkregen kunnen worden door middel van experimenten op supergeleiders.

In Hoofdstuk 4 hebben we een bijzondere vorm van supergeleiding geïntroduceerd, Ising beschermde supergeleiding, en het theoretisch model dat we hebben gebruikt om dit te beschrijven. Zoals we hebben gezien, is deze Ising bescherming fascinerend omdat het de supergeleidende fase beschermt tegen magneetvelden, die normaal gesproken enorm schadelijk zijn voor supergeleiding zoals we hebben uitgelegd in het voorgaande hoofdstuk. In dit hoofdstuk introduceren we ook de overgangsmetaaldichalcogeniden (TMDs), en het materiaal waar onze nieuwsgierigheid op is gevestigd: WS_2.

In Hoofdstuk 5 hebben we de techniek van ionische vloeistofgating geïntroduceerd. Deze techniek hebben wij gebruikt om elektrondoping niveaus te bereiken ver voorbij wat bereikt kan worden met traditionele vaste gates. We hebben ook laten zien welke methodes wij hebben gebruikt om onze WS_2 voorbeeld apparaten te fabriceren en karakteriseren.

In Hoofdstuk 6 hebben we de resultaten laten zien van onze experimenten op de door ionische vloeistofgating geïnduceerde supergeleidende fase in WS_2. We hebben karakterisatie experimenten uitgevoerd zonder magneetveld om de hoofdparameters te vinden die deze supergeleidende fase beschrijven. Daarna hebben we experimenten gedaan in parallelle en loodrechte magneetvelden op verschillend gedopete WS_2 voorbeeld apparaten en de parameters die de Ising bescherming beschrijven geëxtraheerd.

In Hoofdstuk 7 hebben we onze conclusies getrokken uit ons onderzoek zoals beschreven in het voorgaande hoofdstuk. We hebben gevonden dat WS_2 een *Type-II* supergeleider is met sterke elektron-fonon koppeling, en we hebben de parameters die de supergeleidende fase in WS_2 beschrijven vergeleken met gelijksoortige experimenten op MoS_2. We hebben een suggestieve trend gevonden, die in overeenstemming is met voorgaand onderzoek, wanneer we de supergeleidende transitie temperatuur van voorbeeld apparaten vergelijken op verschillende substraten. In termen van de Ising bescherming, hebben we geconcludeerd dat de *Rashba-type* spin-baan koppelingsenergie stijgt met een stijgende supergeleidende

transitie temperatuur, terwijl de *Zeeman-type* spin-baan koppelingsenergie binnen het fouten marge van dit experiment constant blijft. Tot slot, hebben we suggesties gegeven voor verbetering van ons experiment in de toekomst.

In Hoofdstuk 8 hebben we een tweede set experimenten geïntroduceerd gefocust op het meten van de magnetisatie van supergeleidende THEVA tapes, een kandidaat materiaal voor de volgende generatie supergeleidende magneten. Daarnaast, hebben we kort de relevante details van ons theoretisch raamwerk samengevat, en in dit verband uitgelegd hoe wij magnetisatie experimenten hebben gebruikt.

In Hoofdstuk 9 hebben we de onderliggende principes van vibrerend monster magnetometrie (VSM) en draaimoment magnetometrie uitgelegd. We hebben beide technieken vergeleken en kort beschrijven welke techniek meestal wordt gebruikt voor welk type experiment.

In Hoofdstuk 10 presenteerde we de resultaten van onze magnetometrie experimenten. We starten met de resultaten behaald door middel van vibrerend monster magnetometrie in onze supergeleidende magneet en vergelijken deze met metingen gedaan elders op dezelfde tapes in een systeem voor het meten van fysieke eigenschappen (PPMS). Daarna, voerden we dezelfde metingen uit in onze hoogveld resistieve magneet en hebben we weer deze resultaten vergeleken. Tot slot, hebben we aanvullende metingen gedaan met behulp van draaimoment magnetometrie in plaats van vibrerend monster magnetometrie.

In Hoofdstuk 11 trokken we conclusies uit onze magnetometrie experimenten. We hebben vastgesteld dat er een systematische inconsistentie is tussen onze resultaten voor de magnetisatie van supergeleidende monsters zoals gemeten in supergeleidende magneten en resistieve magneten. We hypothetiseerde dat deze inconsistentie het gevolg is van de grotere elektromagnetische ruis die voorkomt in een resistieve magneet, dit zou ervoor kunnen zorgen dat de superstromen die de basis vormen van de magnetische respons van *Type-II* supergeleiders vroegtijdig worden vernietigd. Tot slot, gaven we suggesties voor het testen van deze hypothese in toekomstige experimenten, en om hopelijk het probleem op te lossen.

Data management

This research has been carried out in accordance with the research data management policy of the High Field Magnet Laboratory and FELIX Laboratory (HFML-FELIX), Radboud University, the Netherlands. Data sets for the results presented in this dissertation are deposited in the Radboud Data Repository as a data sharing collection with the unique digital object identifier (DOI) 10.34973/05et-t361. It can be accessed upon request to the promotor or the HFML-FELIX data steward.

Data, metadata and scripts are available for chapters 5, 6, 9 and 10.

Publications

Published

- P. Lázpita, A. Pérez-Checa, J. M. Barandiarán, E. L. Q. N. Ammerlaan, U. Zeitler, and V. Chernenko. "Suppression of martensitic transformation in Ni-Mn-In metamagnetic shape memory alloy under very strong magnetic field". In: *Journal of Alloys and Compounds* 874 (Sept. 5, 2021), p. 159814. ISSN: 0925-8388. DOI: 10.1016/j.jallcom.2021.159814
- O. Zheliuk, Y. Kreminska, Q. Fu, D. Pizzirani, E. L. Q. N. Ammerlaan, Y. Wang, S. Hameed, P. Wan, X. Peng, S. Wiedmann, Z. Liu, J. Ye, and U. Zeitler. "Quantum Hall effect in a CVD-grown oxide". In: *Nature Communications* 15.1 (Nov. 20, 2024). Publisher: Nature Publishing Group, p. 10052. ISSN: 2041-1723. DOI: 10.1038/s41467-024-54014-6
- K. Rubi, D. R. Candido, M. Dumen, S. Zeng, E. L. Q. N. Ammerlaan, F. Bangma, M. K. Chan, M. Goiran, A. Ariando, S. Chakraverty, W. Escoffier, U. Zeitler, and N. Harrison. "Unconventional quantum oscillations and evidence of nonparabolic electronic states in quasi-two-dimensional electron system at complex oxide interfaces". In: *Physical Review Research* 6.4 (Dec. 3, 2024). Publisher: American Physical Society, p. 043231. DOI: 10.1103/PhysRevResearch.6.043231
- L. Heinze, T. Kotte, R. Rausch, A. Demuer, S. Luther, R. Feyerherm, E. L. Q. N. Ammerlaan, U. Zeitler, D. I. Gorbunov, M. Uhlarz, K. C. Rule, A. U. B. Wolter, H. Kühne, J. Wosnitza, C. Karrasch, and S. Süllow. "Atacamite $Cu_2Cl(OH)_3$ in High Magnetic Fields: Quantum Criticality and Dimensional Reduction of a Sawtooth-Chain Compound". In: *Physical Review Letters* 134.21 (May 27, 2025). Publisher: American Physical Society, p. 216701. DOI: 10.1103/PhysRevLett.134.216701
- P. Lázpita, N. A. Río-López, D. Mérida, E. L. Q. N. Ammerlaan, U. Zeitler, V. Chernenko, and J. Gutiérrez. "Magnetic Field Suppression of the Martensitic Transformation in Mn-Based MnNi(Fe)Sn Metamagnetic Shape Memory Heusler Alloys". In: *Magnetism* 5.4 (Oct. 16, 2025). Publisher: Multidisciplinary Digital Publishing Institute. ISSN: 2673-8724. DOI: 10.3390/magnetism5040025

In preparation

- K. Mopoung, T. Quanzheng, M. Zhang, F. Orlandi, K. Mukhuti, M. de Dreu, E. Dilmieva, K. S. Ramsamoedj, E. L. Q. N. Ammerlaan, T. S. Ottenbros, S. R. Wiedmann, A. Boothroyd, P. C. M. Christianen, J. Rosén, F. Gao, I. A. Buyanova, W. M. Chen, and Puttisong. *Selective Antiferromagnetic Ordering Driven by Structural Phase Transition in Spin Frustrated Halide Double Perovskites.* 2025

- E. L. Q. N. Ammerlaan, O. Zheliuk, X. Peng, U. Zeitler, and J. Ye. *Ising protection in WS2 accross the superconducting dome.* 2026

Curriculum Vitae

1997	**Born**, Nijmegen
2001 - 2004	Montessorischool Dukenburg, Nijmegen
2005 - 2009	Rooms-Katholieke Basisschool De Geldershof, Nijmegen
2009 - 2015	**VWO**, Citadel College, Nijmegen
2015 - 2018	**Bachelor Physics and Astronomy**, Radboud University, Nijmegen
2018 - 2020	**Master Physics and Astronomy**, Radboud University, Nijmegen
2019 - present	**Gentoo Linux Developer**, python, science, GURU, and kernel distribution teams
2020 - 2025	**PhD and Scientific Software Engineer**, HFML-FELIX, Radboud University, Nijmegen
2025 - present	**System Engineer - Data Preservation**, SURF, Amsterdam

Acknowledgements

With the scientific part finally done, I find myself having to write what is in many ways the most difficult section. With the journey to get here being as grinding as it was, what on earth should I write here? I have thought long about whether I should write something here that will just "suffice", void of any real meaning. Or, whether I should actually write something from the heart, which undoubtedly would become very personal very quickly.

Recently I realised that this work, this book, does not just represent the completion of the PhD program. In many ways it marks the completion of my formal eduction as a whole. This book, everything that I have done during the PhD program, it builds on everything that came before. It builds on my master's in physics, which builds on my bachelor's in physics, which in turn builds on my secondary and primary education. To me, it feels very much like a continuous whole, which makes sense considering how I treated every level of it. For many years my only goal in education, or in life in general for that matter, was to advance to the next level. Always blindly pushing on, never stopping to think about what I was doing, never looking back, and certainly not looking ahead. Until, quite suddenly and with the finish line in sight, I could go no further...

No one, not even those closest to me, fully realise how close this bloody book came to never getting finished. If I have any superpower, it is the ability to obscure and hide whatever is going on in my head. It is an unhealthy skill I was forced to learn as a child, and have honed to near-perfection as a teen. With the result that the exact degree to which my mental state had declined continues to be severely underestimated, even by psychologists towards whom I try to be somewhat more open. It of course did not help that I never asked for help, how could I, not after the last time I received any kind of "help".

At time of writing, the Dutch organisation for the prevention of suicide (Stichting 113 Zelfmoordpreventie) reports that about 80 % of transgender people have had suicidal thoughts. That is seven times higher compared to the rest of the population. 90 % of those who try, do so before reaching the age of 25. Or, to put it more bluntly, anyone who does not fit into the made-up box that society forces upon them, is four times more likely to die.

I have found that this, raw statistics, is the way people prefer to engage with the subject of mental health and suicide. Anything else will make people uncomfortable. Those raw statistics are shocking for those unfamiliar with them, but dull, devoid of any meaning, reason, or lesson. And, most importantly, the statistics obfuscate agency; It reads as if it is some natural disaster without a man-made cause. Well tough luck for those people whom prefer the cold distance of statistical abstraction, because this is *my* book and I will write whatever the fuck I want. If I am going to write something from the heart to mark the end of 23 years of formal eduction, then I will write some hard and potentially shocking truths. So stop reading here if that is something you cannot handle.

A persons identity, or at least a pretty large part of it, is already set at birth. People can, and do, change but others cannot force them to change. Of course that never stopped people from trying, but trust me because I know, it does not work. What people are not at birth though, is depressed, anxious, insecure or suicidal about who or what they are. No that, that is something that society does to people, that is something people do to people. And once society breaks you down it treats your issues as personal failings. All context is suddenly removed, nothing is to blame and it is the failing of your own brain that is the reason for your suffering.

I have never fit in. It is only recently that I have not only found the words to describe how, but also the apathy and militancy to care next to nothing about what others think of that. People often mistake that for courage, it is not, at least not for me. It is desperation and stubbornness, a refusal to give in and nothing left to lose. It is a skill I gained after being pushed to the edge and beyond. As a child I first did not know those words, and when I learned the words I did not have the autonomy to act on it, nor the militancy to rebel.

When I was 7 my being different had reached the attention of the school and my parents. I was too timid, too quiet, too emotional, and worst of all, showed absolutely zero interest in playing football with the other boys. With the power of hindsight I now realise that what it really came down to was "not boyish enough". I do not remember ever perceiving it as a problem, but the adults clearly took issue with my personality. I had to see a psychologist who supposedly would find out what was wrong with me. I felt like a criminal on trial, I did not think that I had a problem but everyone else did, so clearly I must have done something terribly wrong? The psychologists conclusion: PDD-NOS.

Pervasive developmental disorder - not otherwise specified, that name speaks volumes. The diagnosis does not exist any more in the fifth version of the DSM. But at the time it was the catch-all for everyone that showed vaguely autism-like symptoms but did not really qualify for a "full" autism diagnosis. "Not otherwise specified", or in other words: you're weird but we also don't understand how or why. It is possibly the most unhelpful diagnosis in the whole DSM-IV-TR, which was the current version at the time. Just for fun I'll quote the definition here:

> This category should be used when there is a severe and pervasive impairment in the development of reciprocal social interaction associated with impairment in either verbal or nonverbal communication skills or with the presence of stereotyped behaviour, interests, and activities, but the criteria are not met for a specific Pervasive Developmental Disorder, Schizophrenia, Schizotypal Personality Disorder, or Avoidant Personality Disorder. For example, this category includes "atypical autism" - presentations that do not meet the criteria for Autistic Disorder because of late age at onset, atypical symptomatology, or subthreshold symptomatology, or all of these.

And that's it... Do you like trains? Or do you perhaps have any other "stereotypical behaviour, interests, or activities". Well, if so, then congratulations, you have a mental disorder according to the fourth version of the Diagnostic and Statistical Manual of Mental Disorder. And no that is not an exaggeration, the "manual" literally admits, instructs even, that the diagnosis is based on stereotypes and not on actual problems a child may or may not have. Words cannot express how much I hate this document, how damaging it was to me, and still is. And I have not even started about the batshit insane diagnostic criteria that this document states for what it calls "Gender Identity Disorder". That name is already disgusting, as if your identity can be a disorder, but we'll get to that later. Fuck the DSM!

With a fresh diagnosis I now suddenly had a problem. And when we moved to the other side of town me and my little brother were denied admittance to our school of choice. Supposedly the school, which branded itself as being progressive and inclusive, was not properly equipped to handle a kid with "special needs" such as myself. I did not perceive myself as needing special attention, nor did I request any, but of course none of that matters once a psychologist has put a big red autism warning sicker on your file. No, instead we had to go to the other school in the neighbourhood, which also did not offer any special facilities, but they did not have the luxury to say no since it was a public school.

And of course everyone at the new school was pre-informed about how supposedly problematic I was. Never before had I felt so alienated, not only was I the new kid, I was also the weird kid. The psychologists had put a name to how I was different, and now suddenly everything I did, my entire being, was viewed through the autism lens. Teachers never believed anything I said, and the smart bullies learned to exploit this. I will never forget the smirks on their faces as I was being punished for something they had done.

Of course, some empty diagnosis is not enough punishment for deviating from the expected norm. No, after diagnosis follows "treatment". I have lost count of how many different (psycho)therapists I saw those years. All of them undoubtedly well intentioned, none of them even remotely helpful. In fact quite the opposite, the more I saw them, the more I (stupidly) began to believe them when they said that something was wrong with me. They aimed to teach me "normal" social behaviour, or whatever view they held of that, but all they achieved was the complete erosion of my confidence. How was I supposed to have normal social interactions when everyone kept telling me that every instinct I had was wrong. I was discouraged from being friends with girls, who were in general nicer to me, and instead encouraged to befriend boys. With the obvious end result that I had no friends at all since the boys spat me out. Their supposed treatment left me socially isolated and afraid of expressing anything.

It is here that I learned to hide myself from everyone. Not physically, but psychologically. Even to a kid it is extremely obvious which answer some therapist or psychologist considers "correct" and which ones are "wrong". Supposedly there is no "right" or "wrong", that is what they say, but it is plain as day what earns a nod, and what earns a barely concealed frown and some squiggling in a notebook. I did what I can only describe as "a retreat into my mind", I either learned to lie and give the correct answer or just said nothing at all when I knew that the answer to a question would be the wrong answer. Which of course those therapists only saw as anti-social behaviour and thus as further confirmation of some autism-spectrum disorder. The whole ordeal was a wonderful demonstration of a toxic *confirmation bias* in clinical psychology, and it worked both ways. As the years progressed I more and more became convinced that I was indeed messed up and learned to just shut up. I was simultaneously under a microscope and on trial, everything I said could and would be used against me. But of course no therapy can be effective if the patient barely speaks, so at some point my parents finally gave up on it.

Years later I accidentally found the massive stack of notes left by all those psychologists and (psycho)therapists. In painful detail they described their interpretations of my behaviour and the meaning they had assigned to it. Never did they consider that what they were doing was actually making everything so much worse. I stopped reading when I got to a section that was describing how seriously unhealthy it was that the friends I did have were all girls. My social and emotional development would be severely impeded if I did not befriend more boys. That is when they started to describe how the school was supposed to manipulate, not just me, but the whole class, into making this happen. Something snapped in me that day. The feeling I felt, and still feel, transcends betrayal. Never again would I trust any kind of teacher, therapist, psychologist, or doctor with anything remotely personal.

That same evening I burned those notes, all of them, it was just too painful. Recently I asked my mum whether she thought that, had I been born a girl, would I still have had to go through that "therapy"? Would I still have received that diagnosis? Would I have even been in that psychologists office to receive it in the first place? Her answer? An immediate and resolute "No". No in that case my personality would have been seen as normal, in that case I would just have been shy. I already knew that, but I wanted the confirmation. I had already realised that what I have been put through is effectively just *conversion therapy* obfuscated in a convenient wrapper of "helping me manage my supposed autism" in order to make that toxic pill somewhat easier and more ethical to swallow.

Of course while giving up on the explicit social manipulation that they called "therapy", the school could not just stop there. No, of course they had to make it extremely difficult to get into secondary school at the level me and my parents wanted. Earning a more than sufficient score on the final exams is all well and good, but it says here in your file that you are a problem. An actual psychologist who you spoke to for a couple of afternoons said so, so it must be true. Ooh and remember all those things that others did but we blamed on you because we of course could not believe the "autistic child". And let's not forget that you have difficulty socialising in the "helpful" scenarios that we force upon you according to our view of how boys should socialise and with whom. No, you, you are much better off on the practical level, it does not matter what you want, nor does it matter that those classmates who treat you like shit are also going to that class. What's that? You want to force the issue and go over our heads and get a second opinion, well I guess that means you'll have to go see yet another fucking psychologist.

And so we did. I still have that report, it was just a single document, separate from that pile I would later burn. And of course it is the same old bullshit, you don't even have to read between the lines to find that the root of the issue is that I was shy, did not speak much (of course not, I did not trust you) and did not socialise with the other boys enough. Somehow that was again considered a mental disorder, even though it is considered perfectly normal for a kid that age to regard the boys as rough and icky if the kid is born with the other set of genitals. Funny how an obstetricians first examination of a newborn baby is crucial in determining which behaviour will later be considered normal, and which behaviour will be considered a mental disorder that needs close examination and correcting. Anyway, we got that psychologist to overrule the primary school and they recommended instead the class that I had originally wanted to register for.

With the secondary school registration drama handled, it was now time for what is in the Netherlands the traditional end of primary school: the "group 8 gala", or "final year gala". An event that quite literally would haunt my nightmares for years. You see, when I say traditional, I mean really traditional. Supposedly everyone in the liberal and free west is able to dress and express themselves however they want. Yet for some reason that I still cannot fathom, all of that goes out of the window when there is a party or other formal event (such as a PhD defence ceremony). Because the event is supposedly fun or official, it is now suddenly considered okay to force everyone to dress a certain way. Suddenly men and boys absolutely **must** wear a suit.

To this day no one has been able to explain to me why the morality of forcing your fashion sense on someone else, depends on how "official" or "fun" the event is. This was the first time it happened, but definitely not the last. Always the same unresolvable discussion, usually accompanied with threats about what would or would not happen if I did not conform. Of particular note is every graduation ceremony ever, including the traditional defence ceremony for this bloody book. Every single time I would be literally threatened with not receiving my diploma if I would not wear a fucking suit. Like, honestly,

really? Do you even hear what you are saying?? You would deny me a diploma based solely on how I want to dress??? I always called their bluff, because this is discrimination plain and simple, and in the supposedly free and liberal west we have laws against that. Usually I would say something like "the day you see me in a suit is the day you bury me", it would be taken as a joke but I meant this very literally.

I cannot explain why, after taking everything else, this was where I would take a stand. I would not, will not ever, wear a suit. The discussion went on for months, with my classmates, with the teachers, with my parents. I distinctly remember that there was a whole parent-teacher meeting about the matter. And with everyone it was just the same cyclic repetition of moves: It's a gala, you must wear a suit. Why? Because it is traditional for such an event. I don't want to wear a suit. You must, it is a rule at such an event. Okay fine, then I will not go. No, you must go, everyone is going. Fine, I will go, but I will not wear a suit. No, it's a gala, you must wear a suit. WHY?? And again, and again, and again.

Why? Why are you so stubborn about something so small?? At the time I could not answer the teachers question. I now understand that, to me, a suit is fashion-wise the ultimate expression of masculinity. The feeling I get at the thought of wearing one I can only describe as a sort of mental allergic reaction. Do this, don't do that, "else you'll be bullied" was something my parents often said in response to a choice of clothing, a haircut, or whatever. I always listened, or compromised, but not this time. I. Will. **Not**. Wear. A. Suit. I got bullied anyway, regardless of how much I tried to fit in, no matter how hard I was pushed to fit in that suffocatingly tight box.

I was twelve and this was the first time I toyed with the idea of killing myself. Mind you nothing serious, I did not actually want to die, not yet. But there was not really a way out, I was stuck between a requirement to attend, an unwritten law mandating what should be worn, and my stubborn refusal, my inability, to conform to that. In the end, whether or not I would attend that fucking party remained a subject of heavy debate and gossip up till the evening itself. I was fully prepared to stay at home and had committed to this. It was my mum who mere hours in advance, relented and decided I should go and that I would not have to wear a suit. "It's a one-time thing, and you'll regret it later if you do not go" is what she said. Well I went alright, and I wore a trusted hoodie, hated the whole evening, and regretted not staying at home. Though that evening was not nearly as bad as everything that led up to it.

Really, that whole ordeal should have been the trigger to re-evaluate the original assumption, the commandment, that I should and must be a boy and act accordingly. If not for everyone else, then at least for myself it should have been some hint. Alas, once again I found my actions interpreted through the all-explaining lens of autism. Just the weird autistic kid being weird and autistic again. Not that I could explain the matter any better myself, I did not know the words, and would not know them for several years to come.

And with that, perhaps a first round of some actual acknowledgements is overdue. To my primary school, the institution and the teachers, thanks for nothing and fuck you. Everything you did has ranged from passively unhelpful to actively damaging. I can only hope beyond reason that the school has improved since I left it. To all those psychologists and therapist I had to see. I recognise that you tried to help, I can only hope that at some point you'll realise that your misguided attempts at curing me from a vague supposed mental disorder were not just counter-productive, but also extremely unethical. For the love of all that is good and green on this earth, please just let kids be kids, please just let them grow and develop in their own way. Please stop medicalising their identities and personalities, please stop diagnosing kids based on their genitals.

The fascinating thing about being queer is that even if you don't know the words yourself. You'll somehow find yourself surrounded by other queer people without really trying. It's like magnetism. It is that same spark of otherness that causes the close-minded to push you away and bully you; that spark, even before it blossoms into concrete words, you can somehow recognise it in others. Folks sometimes call it *Gaydar* but the concept is more broadly applicable, and it works even if you don't realise that it works. It is sometimes thought of as being entirely based on stereotypes, however that is not quite accurate. At least that has been my experience in secondary school.

It is in my group of misfits that I first learned that there is more to humanity then the picture presented in the Disney movies. Sure, homosexuality was already part of the curriculum in secondary school. It was briefly mentioned that it was a thing that existed, in the same sense that you could notify a classroom about the existence of some far away planet. That fact by itself means very little if it is not fleshed out with further substance. Without anyone to personify the concept it is just an empty awareness. And that, is why representation is so crucial for young and confused queer kids. But I digress.

My parents divorced when I was 13. When they told me and my little brother, I was not surprised at all, I had felt it coming for weeks. It barely reached me on an emotional level, or any level at all for that matter. I had learned to hide deep inside my mind, very little reached me there. See the funny thing about suppressing every instinct, every impulse, every desire, is that this effectively amounts to suppressing personality itself. Do this long enough and you quite literally cease to be a person, still alive, still human, but somehow empty. Some folks who go through the same experience learn to present a facade. My acting skills are horrible so I could not do this, instead there was just nothingness. I think this is why I had so much trouble making and keeping close friends, there just was very little there to be friends with.

Indeed very little really reached, but even less came back out. If any form of expression or opinion was requested of me I felt a level of anxiety that effectively paralysed me. The question could be as trivial as "what's your favourite colour", and there it would be, pure terror. I could not think any more. I would evade the question or just provide whatever answer got my out of the situation the fastest. I always went clothing shopping with my mum, never alone, that was my worst nightmare. Yet even with my mum there; I would stand there in the shop, mind racing, barely able to move, not daring to look at any thing. I had learned that hard lesson, expression is weakness, everything you say or do can and will be used against you, and not just by bullies. So it should come as no surprise that when I discovered I was attracted to boys and not at all to girls, I told only my little brother and no one else. I knew my parents would not take it badly, I knew my friends would not care, yet hiding inside my mental fortress nothing could come out. Even when I actually really really wanted to speak, I could not. The moat around my mental fortress was too deep and the bridge had collapsed.

Puberty started late for me, I was almost 15. For years my classmates had talked to no end about relationships, sex and who was with with whom. I was not interested in any of it, nor was I bothered by being so far behind my classmates in this regard. I am sure those damned psychologists would have attributed this once again to some developmental disorder. But the real simple truth is that I did not look forward to puberty, on the contrary. Of course with the power of hindsight it becomes crystal clear why I dreaded the whole thing. Had I been able to, I would have somehow prevented it, stopped it. I would later learn that this is scientifically perfectly possible, and has been since the 1980s, but this forbidden knowledge was not yet available to me. My parents had shared a book with me explaining in fine detail what would happen. It's title? "Understanding the Facts of Life". What wonderful irony it

is that, somehow, the pivotal fact that there are other options available, should the 'facts of life' fill you with suicidal despair, did not make it to the final print. A pretty serious dereliction in what is otherwise a fine book.

I read that book cover to cover almost a dozen times looking for an escape. Deep down I knew the answerer was not in that book, it's not a particularly large piece of literature so after the first reading I kind of had already learnt all there was to learn from those pages. Still I kept picking that book up, could there maybe be a hint somewhere? Did the answer exist at all? I figured that if I just understood exactly what testosterone did and how, then I would somehow be able to mitigate its effects. But alas, reading that book only resulted in making me cry.

When I found the printed literature at hand wanting, I turned to the one place that I knew did have all the answers: the internet. Lots of gay boys looked and acted very feminine, what was their secret? How did they do it? Of course I was way to anxious for that level of self-expression, my parents' mantra would echo through my mind: "Are you sure? You'll get bullied". Would that really happen? I did not want secondary school to become a repetition of the hell of primary school. People actually treated me reasonably for once. Yet if others could do it, then why not me? My mental fortress was starting to feel more and more like a prison, I wanted out, but I did not understand how to conquer the fear.

I scourged the internet for everything from instructions for the most optimal shaving method to detailed descriptions on the workings of the pituitary gland. And that is when I found it, the secret reactionaries claim should be withheld from children to "protect" them from evil woke propaganda. That bloody book had lied to me, a boy did not have to become a man, nor was a girl required to become a women. The deception made all the more grievous once I discovered that the technical possibility to opt for an alternate puberty had existed for almost a full century.

The feeling I felt when I uncovered the hidden truth transcends description, a mysterious cocktail of intrigue, inexplicable desire, and a relaxing rightness. Perhaps the most descriptive word is something I can actually borrow from physics: Resonance. A deep, dark, overwhelming, and inexplicable resonance. That wondrous feeling unfortunately did not last long but it would come back to confuse me every now and then, usually alternating with soul-crushing envy. Once I regained some clarity, panic struck. What the fuck was that feeling, where did it come from, and what did it mean?? Nothing made sense, and so further literature research was required. And while illuminating, nothing I read provided definitive answers. Most stories I read contained elements of resonating relatability, but often there would also be elements that I did not recognise at all. Of course I now understand that the premise of finding a definitive answer on the internet was flawed. The answer is not there, it never was, it was inside, inside my mental fortress. Because despite what bureaucrats would have you believe, no person can diagnose another with what was then still called "Gender Identity Disorder". It does not matter how many degrees you have, the only expert on the matter of a persons identity is that person themselves. It would take me another decade to find the wisdom that the question is not "am I transgender?", but rather "do I want to be?". Technically this is the same question. After all, answering the second, automatically answers the first. Yet the implied distinction as a result of the different phrasing is huge and vital because of where the agency is placed, and thus the second question is infinity simpler to answer.

I did not understand this, I could not recognise that I was the subject of my examination, not the object. And so I continued my quest to find the objective answer, which occasionally would turn into an experiment. A carefully contained experiment of course, none of the preliminary findings could be shared with the public. The search continued to escalate, the further I went, the more I ached for more,

the more I longed to escape my mind-fortress. And before long I found myself researching the practical aspect of it all, not because I understood where I wanted to go and was ready to commit to it, but just in case. Of course the fact that I had reached this point, should have been a clear indication of what I wanted. Alas, I had become so well practised in ignoring what I wanted, that even now I could not act on this alone. I demanded evidence, actual answers, not vague feelings and confusing desires.

Despite that I could not find the objective proof I was looking for, I was well on my way to finding some sort of acceptance for what should have been plain as day. But that is when it all went sideways, when I tried to figure out the practical aspect. How does one actually obtain cross-sex hormones? It is not easy, and even less so if you're underage. General practitioners can and do prescribe estrogen, they'll explain how to use the medication correctly and ensure that you're aware of the risks. Next day you can visit the apothecary and odds are they'll have what you need in stock. That is, if you happen to have an "F" in your medical file and passport. If you do not then all of a sudden things are complicated, even though the use of the very same medication is not really more or less risky for you. It's discrimination pure and simple, yet saying so is somehow controversial.

No, of course it cannot be as simple as expressing your wishes and consenting to the effects. Instead of the live-saving medication you need, you'll get a referral letter to... you guessed it... yet another fucking psychologist. And of course, since this is supposedly super complicated, it cannot be just any psychologist. No, it must be a *special* psychologist, and naturally there's a waiting list. But okay, you wait, you talk to them, and then you go back to your general practitioner who will now give you what you need, right? right?? NO! Plot twist, not only do you yourself lack the autonomy to decided over your own body, the psychologist that you have been waiting for on that waiting list also does not have the authority to diagnose you. No, best they can do is send you up yet another level once they have decreed that you're not completely insane. And so you wait again until you find yourself in the office of a (special) psychiatrist, who will, spoiler alert, ask you the same questions all over again. Should you not have lost your mind by now, then you'll finally get an official "Gender Identity Disorder" diploma. Congratulations, you can now go back onto the waiting list for an appointment with a *special* endocrinologist; because of course, since you are completely alien, no regular endocrinologist could possibly hope to understand your biochemistry. And it is this special endocrinologist who will have the final say on whether or not you'll be allowed to live your life.

Naturally, 15 year old me considered this a bit of an obstacle. But I could do it, I could jump through all the silly hoops, I could go back to where I had promised myself I would never return, to the psychologists. This feeling of resonance was too big to just ignore. So okay, next step is to find out what kind of questions to expect, what is the measure that will be used to judge me? When I learned the absolutely batshit insane answer to this question, when I learned the criteria that are used to diagnose "Gender Identity Disorder", everything came to a grinding halt and I lost my mind.

In the list of criteria there are the things that make sense, such as a stated desire to become, or be perceived as, another gender. Then there's the sexist and stereotypical nonsense that unfortunately comes as no surprise, did you play with dolls or cars as a kid? And then there is the insane requirement to hate the genitals you were born with. A requirement that was, at the time, enshrined in law. In order to have the state recognise who I wanted to be, who I am, it was mandated that I must be not only sterilised but also "adjusted to the desired sex as far as medically and psychologically possible". Or, in other words, since genital surgery was medically possible, it was required. And therefore the desire to go through with surgery was also a diagnostic criteria.

And so there was my problem. I did not, and still do not, have any wish to undergo a vaginoplasty surgery. Yet, I hated what testosterone was doing to me, I could not stand it. Those two facts appeared to be in conflict since they were diagnostically, medically, and legally tied together. I once again felt trapped. I could of course lie to the general practitioner, a psychologist, a psychiatrist, and an endocrinologist. Not to mention that I would have to lie to my parents as well since they would have to sign-off on the whole thing. Yet even if I pulled that off convincingly then still, sooner or later, I would have to choose to either expose the lie or go through with a drastic surgery that I did not want. This realisation crushed my dream, my fantasy, my chance of escaping masculinity. It was the first time I almost killed myself.

Just like the incident with the suit about three and a half years prior, the whole ordeal is engraved in my memory. I distinctly remember how I was standing there, in the kitchen, with one of the knives. Not to slice a wrist or anything, no, that's how you get attention but not results. And I did not want attention, attention would just lead to questions and questions would inevitably lead to psychologists who would then start putting their noses into the very same thing that I was now running away from. No, instead I was going to stab myself upwards from the belly with that knife, samurai style. It would probably hurt, a lot, but it would be highly effective.

But wait a minute, should I now succeed, then would there not still be those questions? I would not be around to answer them, but nonetheless people will ask why and they will start digging, possibly in places where I did not want them to dig. I could invent some reason and write it down, possibly blame it on being gay, but then still, how could I be sure that my secrets would be protected if I was not around to protect them? And did I really want the last thing I would do on this earth to be a lie? So I stopped, too scared to continue life, but also too scared to end it. Scared of puberty, but also too scared to stop it. Stuck between nature and policy, either direction would take away my autonomy.

I had one trick up my sleeve, one masterful ploy to fool them all and get what I wanted without involving those nasty psychologists and their policies. You see I happened to have a little mole on my right testicle, now if I could convince everyone that this was a cancerous tumour then maybe I could get some doctor to do something about it. The doctor would have to give me the unfortunate "bad news" that they would have to remove the testicle, and I would pretend that I thought this was horrible. Then, after the operation, they would prescribe replacement testosterone, but this is the moment I would make my brilliant move. I would simply refuse to take those injections, checkmate psychologists! The doctors would undoubtedly complain that this is not healthy on the long term, so then I would take the cat out of the bag and demand estrogen instead. I now realise that this scheme was completely nuts, but I was just so fucking desperate, at this point I would reach and hold onto any straw. So I complained to my mum about the itchiness and the increasingly irregular size of the mole. We went to see the general practitioner who removed the mole for further inspection. The plan was foolproof if not for the one fatal flow that was now exposed, the mole was just a mole, benign. When the disappointment hit I finally realised that I had actually, genuinely, wished that I had cancer. But now I was defeated, my plans foiled. It should have ended that day, but my testicles were allowed to endure.

And thus began what I can only describe as slow torture. I no longer wished to come out and share how I felt because I was scared of the road I would be forced on, I did not want to live, nor could I die lest the whole can of worms be opened anyway. I was truly trapped, even more so then before. So instead I escaped where no one, not even myself, could bother me, in fantasy books, in computers, and in Minecraft. I focussed on school where I would abuse my endless curiosity to avoid thinking about the future and what was happening to me.

And that is how I graduated top of my class from secondary school. My classmates would ask how I did it: “do you not have a life??” Well, no, I did not, and I deeply regret that. I am sorry I could not be a better classmate, I am sorry I could not be a better friend, I am sorry I was such a weird wreck. You all were great, thank you for trying to include me. I also want to thank my teachers, specifically those teaching physics, chemistry, and mathematics, for engaging with my endless curiosity, for answering the barrages of questions I threw at you, and for encouraging me to start studying physics. You may not realise it, but you kept me going, along with my fantasy books. And finally I want to thank my biology teacher for going above and beyond the textbook and for never caring how weird my questions got. To my gymnastics teachers I would like to say, please ask the biology teachers to explain to you why you should ditch the fucking Cooper test.

I went to the university in my home town, partially because the government had cut the basic scholarship that students used to receive, and partially because I felt no need to move out of my parents’ houses. Houses, multiple, since they had divorced I was traversing the city every Sunday to live with the other parent for the next week. The weekly move was more taxing on me than I dared to admit. The odd thing about living in two houses is that sooner or later neither house will truly feel like home. Of course the only other alternative was picking one parent over the other, something I was at the time not willing to do. Perhaps I should have moved out sooner to avoid the problem entirely, but I did not, I did not feel restricted by my parents since I did nothing besides reading and playing Minecraft anyway.

I chose to study Physics, partially because I felt it was expected of me to aim high, but also because I was curious to go beyond the secondary school text book. I would later regret this decision, not because of the content, but because of the culture. I would find out the hard way that academic culture, and especially the academic culture in physics, is extremely toxic and even more so to anyone who deviates from the cisgender, heterosexual, white, male norm.

My mum convinced me to participate in the “introduction week” which is supposed to help you become acquainted with student life in the city and of course to meet your fellow students. It was another one of those “once in a lifetime” things that I would supposedly regret if I skipped out on it. And what an introduction it was. Between the expected excessive drinking I saw a degree of sexism and racism that I had never before seen so explicitly. Homosexuality was mostly accepted, but only insofar as it reproduced heterosexual sexist stereotypes. I had turned 18 two months prior and now found myself being sexually assaulted twice, once by a man, and once by a women. Though that turned out to be a fine representation of university life since it would happen four more times before I received my masters diploma five years later.

I had somewhat learned to avoid thinking about what puberty was still doing to my body. It was a conscious decision I had made after I had discovered that the road to womanhood was closed to me. Thinking about it just made me feel worse so I kept reminding myself that I was just an effeminate homosexual, that is how I managed the cognitive dissonance. Every now and then I would lose that control, which resulted in me being periodically suicidal. I could not escape my mental fortress, yet now I found that inside was no longer safe either. There is an aspect to puberty that very few people talk about, it certainly was not part of the education I received, and that is what sex-hormones do in the brain on a mental and emotional level. And it somewhat makes sense that it is not really talked about since it is near-impossible to quantify, research, or even describe. Yet those of us who have the lived experience of hormonally transitioning between genders know all to well how stark the mental and emotional difference can be.

Running your brain on the hormone that does not make you happy feels a lot like fuelling your petrol car with diesel. It might work for a very short while if you're going downhill, but sooner or later you end up by the side of the road crying for help and cursing the very moment that diesel went into your car. I now found that the water-well inside my mental fortress was poisoned. And there's no escaping, no mitigating, that. For the longest time I thought this was part of becoming an adult. I now know it was not, the poisoning of my mind was part of becoming a man, adulthood had little to do with it.

When I was 21 I joined the political youth organisation ROOD, which was then still the youth wing of the Socialist Party. I was, and still am, fed up with the injustice in the world, fed up with the pervasive sexism and queerphobia that infests the very fabric of society, and most importantly fed up with all those people who say "well that's just how the world works" as if the bulk of human suffering is not man-made. It is here that I learned to break my hell-bent focus on academic achievement. Here I found an environment that was not just accepting of being queer, no, they went beyond this by actually not giving a shit. And yes, there is a difference between accepting someone for who they are, and actually not caring that they are who they are. In many ways indifference is the ultimate form of acceptance. The culture, the ambiance, the comrades, at ROOD, were such a refreshing change compared to the hostile individualism of academia.

The role of ROOD in making me the person that I am today cannot be overstated. It is here that I finally dared to show some individuality, here I felt safe enough to casually mention that I was gay, and here I found my first partner. My comrades at ROOD kept me going during my dark periods, their fervour and drive is infectious. In so many different ways they gave, and continue to give, live purpose. Without them this book would not be here to read today. Dear comrades, thank you. Thank you for listening to my rants, for motivating me to fight for a better world, for not giving a shit about who or what I am, but most importantly, for being the wonderful people that you are.

With some social safety net in place I finally dared to be more open about being gay. Yet, despite that everyone knew and accepted this, I still felt trapped, incomplete. I somewhere deep down knew that the story was not complete. The suicidal and depressive episodes remained, the moments where I lost control and questioned everything still occurred, perhaps even more frequently then before. Always I would force myself to regain the reins of my own thoughts. I knew I could not be transgender, the experts had decreed that I did not meet the criteria and hence I must be just gay and effeminate. They're the experts, the specialist healthcare providers, the policymakers, they must know what they're talking about, right? right?? I now understand that, no, they don't know what they're talking about. There's only one expert when the subject matter is myself, and that is me. I now know that the bureaucrats making the policies do not understand that being forced through a wrong puberty is a level of psychological torture that even the CIA could not dream of. I now realise that, no, losing the ability to experience true joy is not a normal part of adulthood.

When the pandemic hit I was busy completing my masters thesis. It did not really affect me on the same level it affected so many others. I suppose I was used to staying inside, reading, or behind my computer. I had finally moved out and was living in a small attic room not far from campus. Being completely alone I found the freedom to experiment again. I had decided that even if I could not actually rid myself of testosterone completely, I could still experiment with some aspects of the femininity I so deeply longed for. That was not illegal, that was not a crime, it would be highly unlikely for a SWAT team of psychologists to drop down from the ceiling and arrest me for crimes against masculinity. It might feel as if that would happen, but I knew that it could not. No, I was relatively safe here.

Yet any experimentation usually just left me frustrated. Over the years I had to shave more and more, and by now I had to shave at least my face every day to maintain any degree of presentability. It all felt like one big uphill battle, no matter how well you shave, it just comes back again. Like Sisyphus's rock, an eternal punishment by some evil god. You cannot win, yet you cannot give up, lest you end up with a full fucking beard.

I had completed my bachelors and masters internships at the High Field Magnet Laboratory and was now offered a PhD position. I accepted because I liked working in the lab. Here I could not only dump my endless curiosity into some extremely complex problem, but also feel the satisfaction of solving it. I loved the small-scale, big-game atmosphere. And most importantly I enjoyed working with my supervisor Uli. It turned out to be the most difficult thing I had ever done. My ex-partner had warned me not to do it, warned me about how much work it is, and also warned me about the toxic culture of academia. I'm sorry Sara, I did not listen. Perhaps I should have, undoubtedly live would have been easier. But then again, the experience has now become a big part of who I am, and I undoubtedly learned a lot.

I think it is not controversial to say that everyone agrees the workload is too high. Yet there is little agreement on how it should be resolved, or if it even can be resolved. Endless arguing and complaining achieved next to nothing. And that is how I, a hardcore communist, ended up in a meeting with the Federation of Unions and a bunch of other PhD students. A meeting that should have been confidential, yet somehow ended up in the student newspaper. It was really not that big of a thing, but nonetheless it blew up into something huge. The leak evaporated the trust in the Union before it even had a chance to really materialise, we ended up with chaos and the "organisational coaches" instead.

The first, and only, time I spoke with the "organisational coaches" was in a group setting with the other PhD students. They made it abundantly and explicitly clear that they did not care about the challenges the PhD students faced, they were only there to fix the issues in upper management. Which is a fundamentally flawed approach, but then again the whole matter felt like a reaction to, and deflection from, the attempts by the Union to actually make some meaningful change.

About a year later the "coaches" were ready to present their conclusions and recommendations. We all were encouraged to participate and think about the road forward for the soon-to-be independent institution in smaller groups. And that is how I found myself being asked what I thought would be the best way to achieve the goals of the organisation. I replied with a, what I still think is entirely reasonable, "I don't know, I don't understand the obstacles on the road". Of course I could have said something snide like maybe start with actually listening to the complaints of the employees on the lowest levels. But I did not, no, now was not the place for that battle, so I just admitted I had no solutions to offer because I did not fully understand the problems at a higher level.

Yet somehow this was met with a relentless and ridiculous rant by the "coach". Supposedly I was seeking to dig up buried conflicts or something. Any attempts at explaining that, no, I just don't have an answer to your question, just pissed her off even more. She demanded an answer, and thoroughly rejected my position that, in order to make any meaningful contribution, I should understand the problem. I still think that asking for the opinion of the uninformed is just foolish. If you don't want to include me in the discussion that's fine. If you don't even want to listen to my point of view, that's your loss. But then don't bloody turn around and demand that I provide a solution when you are presenting your conclusions to a problem that you have taken it upon yourself to solve. Either involve me and then you will get my opinion, or leave me out of the mess completely.

I was fucking pissed, and that is quite an achievement, it used to be pretty difficult to get an emotional response out of me. I did not deserve that rant. She just went on and on, it took the entire breakout session. And my only crime was admitting ignorance! Here I was working my ass off for more than four years, working way longer than was reasonable or even legal. Prioritising my work above everything else, never even considering my wants or needs buried deep inside. Only to have someone yell at me for 20 minutes straight for absolutely no fucking reason. As if it is all somehow my fault?

The sheer ridiculousness of it broke me, it cracked the walls of my mental fortress. I called in sick the next day, not because I was physically sick but because I was too angry to work. I did not even know that was possible until it happened. Never again would I dedicate my life to work. I had done everything right, tried my hardest to somewhat fit into the box that society likes to force me in, never dared to even consider sticking a finger out of the box lest I kill my academic career even before it really started. I had sacrificed my youth and what was my reward? Continuous depression, long trips away from the safety of home, experiments that did not work, extremely long working hours with little to no recognition, and now some so-called "coach" screaming at me for no reason. Well no more! No more bullshit. No more fitting in tight boxes. No more listening to the dumb unwritten rules of gendered society.

Colleagues knew I was gay, but I never dared to really express myself out of fear for not being taken seriously. I knew the bar in physics is so much higher for women and queer people than it is for heterosexual men. Well now I knew for sure that I was not taken seriously anyway. It's just like primary school, even if you don't know how you're different, even if you try to hide it, they can somehow smell the difference on you and you end up suffering anyway. That same day I dyed my hair green, it was something I had always wanted, yet never dared, to do. Well now I was finally going to do it because I no longer gave a fuck. And so began a journey of unconstrained exploration where I finally dared to put my own wishes first.

Ironically the more I centred myself, the more I allowed my desires to lead me to where men are not permitted to go, the worse my depression got. Nothing would be enough, yet I needed more. It was like an echo of what had happened a decade before. The shaving had become obsessive, once per day had ceased to be effective for the face and twice per day was not always possible. I would shave my legs, and two days later it would be back with vengeance. I tried waxing which only hurt more but did not really last longer. The bloody hair was driving me insane. I had lost the capacity to see myself in the mirror years prior, now I became increasingly frustrated with this. And I don't mean that metaphorically, I mean it literally, I would stand there in front of the mirror and my eyes would just refuse to focus on the image. It's some sort of automatic mental self-protection I guess. The world did not feel real, nothing really reached me. I could look, but I did not feel as if I was seeing. I could eat, but did not really sense the taste. I could touch, but the feel of the object was damped. Life had started to feel like a television show and I was just the passive observer[1]. A side-effect of being stuck in that mental fortress for too long I suppose. Now that I once again wanted out, it became increasingly frustrating, unbearable even, that I could not. Something was still holding me back and I could not figure out what it was.

I had started to write down what I had been up to the past years in a first attempt to start this book. And it was after completing the first draft that shit really hit the fan. I had decided to skip the summer holidays in an effort to complete the bulk of this book before the new academic year. And I did, with about two weeks left to spare. But now I had a problem, I had nothing to do. It would be three more weeks before everyone would be back from holidays, my queue of open source programming work had

[1] Now is probably the perfect time to recommend the 2024 film "I Saw the TV Glow" it is an absolute masterpiece that perfectly captures this feeling.

dried up, and the political work was on pause. A racing and depressed mind with nothing left to occupy it, a dangerous combination. I accidentally thought about the future, what would happen after this book was completed? I did not have an answer. Not academia in any case, by now I had plenty of personal experience to know that I was not taken seriously in that world. I had always imagined myself to become a scientist, what would I do now that this was out of the question? I realised I did not see a future, and then I looked back at everything that had led me here. To the never ending uphill battle against my own body and that fucking hair fucking everywhere, did I really want to continue to fight that battle knowing there can be no victory? I thought about the permanent loss of youth, about *twink death*, about my distant childhood. When was the last time I was actually happy? I could not remember.

And that is when the casual apathy, the not caring whether I live or die, turned into a desperate need to die, turned into being unable to bear being alive any longer. It was so much worse than it had ever been before. I found myself reflecting on all that had happened, the core memories that really stuck with me, like that time in the kitchen when I was going to stab myself samurai style. A wound that I now dared to scratch a bit, it's not like I had anything to lose, it could not really get worse from this point onwards anyway. This went on for a whole week before I found myself, as so often, on the internet, ideally browsing. And that is when I found it. The missing puzzle piece that would make everything crystal clear. Why I had ended up here, why I felt the way I did, and why I now could not take another step even though the finish line was in sight.

"Cabinet apologises: 'Transgender law was dehumanising' " was the headline of the article on the website of the Dutch national state broadcaster. Published in November of 2021, now it was August 2024, I could only wish I had read it sooner, but then again I had my head thoroughly stuck in the sand so I was not looking for it. After realising it could not be, I had been so busy avoiding the topic that I had completely missed that the law was changed in 2014. And now here it was, the fucking state, fucking apologising. Not only that, but also offering financial compensation, not much but still. A bureaucrat giving you money to shut up is the ultimate sign that they know they seriously fucked up.

So there it was, the answer, the reason I had always felt something was missing, the reason why I was stuck in this decade long depression that I just could not climb out of, the reason why the world felt like an unreal murky mud, and the reason why I now wanted to die, again. Everything, everything, suddenly became crystal clear. I got screwed over, manipulated, deceived, and royally fucked. First "Understanding the Facts of Life" and everyone else lied to me, they hid from me that there is an opt-out for puberty. Then, once I discovered the truth, they erect a gazillion barriers and tell me that it is only for those special chosen people who check all their boxes, but certainly not for me. Now they removed one of their checkboxes and say sorry that it was ever there? What does this even say about the validity of the remaining checkboxes?? This entire time I had been right and the state, the bureaucrats, the psychologists, the policies, had been wrong. And of course they were wrong, is bodily autonomy not a human right anchored in the constitution?? So shouldn't I just be able to do whatever the fucking fuck I fucking want with my fucking body??? If I had only had the wisdom to see that, and the stubborn steadfastness to rebel against everyone, twelve years ago. It was all so obvious now.

And so I sat there between the pieces of my shattered mental fortress, feeling the full brunt of what I had been forced through and realising the pointless of it all. All I wanted was to go back, back to the first time I had been this serious about ending it, and to then choose a different path. To then choose to lie about not wanting the state-mandated surgeries. With the power of hindsight I now knew that the dreaded scenario of having to actually go through with it would never materialise anyway. I

had experienced regret before, but this was on a whole new level. The sheer desire to invent the time machine and punch my past self in the face, combined with the knowledge that this is an impossibility, was utterly unbearable. Thus began the hardest 8 weeks of my life.

All I wanted was for it all to stop, for the fucking torture to end. Where before shaving had been frustrating to the point of desperation, now I could not do it without collapsing. Where before I had just hated the name my parents gave me, now I could not hear it without mentally visualising shooting myself in the face then and there. Every day was a struggle against the urge to cycle to the nearest bridge and jump off. But I continued to struggle, because I had promised myself I would try. I would now actually try to do what I had always wanted to do but never even dared to think, let alone talk, about. I would now try to jump through all the damned hoops and transition. Instead of killing myself outright, I promised myself I would first try to kill the man I had been forced to become, and become something else. I really did not care who or what I would be in the future, as long as I did not have to be a man any longer. Should I fail, should I get rejected, should I be unable to find happiness, or should the results of hormone therapy be unsatisfactory because I was now too old, I could always kill myself later. But I owed it to that scared timid little kid I used to be to at least try.

And for that reason I tried. Every time I strayed I would remind myself that I had promised to try to live. I found a *genderteam* that did not do waiting lists. I might have promised to try, but I did not believe I had the strength to hold onto that straw for the three to six year waiting lists that the regular insurance-covered hospitals have nowadays. I really needed this **now** because the sheer desire to end everything was incapacitating, I could not work, I could barely sleep. Instead of a waiting list, this *genderteam* does a sort of first-come-first-serve registration that may, or may not, open up on the first Monday of the month. And that is how I found myself on the second day of September, 5 minutes before nine o'clock, preparing the answers to the questions that I knew would be asked in the form if it should appear today and configuring my browser to reload the website every 60 seconds. Nine o'clock came and went, still the same front page, 5 minutes passed and I began to believe that registration was not going to open up this month. But seven minutes after nine o'clock the front page changed, and there it was, the registration form. It took me two seconds to recover from the surprise, and the reality that this was really happening, before I copy-pasted my prepared answers into the form and hit enter. 'Submission received' the website said, never before had the submission of a form sparked so much feeling in me.

Of course I could not truly relax, not yet. First it took about 40 minutes before I received the confirmation email. And then I still had to get a referral letter from my general practitioner. So I called them and asked for an appointment, I did not feel like breaking down on the phone so I did not tell them why I wanted to see the general practitioner, just that I wanted an appointment. Three fucking weeks, that was how far away the first option for an appointment was. But it's not like I had a choice, so I accepted that spot. I then broke down anyway, I could not wait three weeks to get the referral, I knew that the sooner you get a valid referral the sooner you get an appointment with a psychologist. But really any physician's referral will do, so I decided to make an appointment with the universities occupational physician. I wanted to work part-time so I had to see the occupational physician sooner or later anyway. But guess what? Another impossible phone-robot and another minimum three weeks of waiting time.

The next morning I went to the local general practice centre and did the only thing that I now could do, have my daily mental breakdown in the receptionists' office. That I could go do this now, while not too long ago my social anxiety made even the most basic expression of emotion impossible, shows how low I had sunk. I quite literally felt like I had nothing left to lose, and that is in a sense weirdly freeing.

Letting all that out in the receptionists' office was very helpful, suddenly I could have my appointment tomorrow afternoon.

I got that referral letter from that general practitioner whom I had never seen before. And now all I had to do was wait for an invitation from the psychologist, it sounds so easy, but it's not when every day feels like torment. Most days I just stayed in bed, staying in bed is a pretty safe and easy way to avoid the overwhelming urge to die, you can't really kill yourself without getting out of bed. Of course I still had that appointment planned with the universities occupational physician, which was the most useless thing ever and perfectly demonstrated exactly what is wrong with transgender healthcare. It took a whole hour and the physician kept telling me that it was "such a complicated problem", it really is not. It's super simple, I hate what testosterone does to me, I want to die, please give me estrogen, end of story. The requirement for a diagnosis makes it complicated, the never-ending hoops make it complicated, the constant barriers and the incessant delaying make it complicated, the fact that someone must oh so graciously *grant* me the bodily autonomy that should be a human right makes it complicated.

One thing the universities occupational physician said really stuck with me: "I am surprised you lasted this long". It is something I still regularly think about, now that I know how live can be, how it should be, I too am surprised I did not collapse sooner. But then I remember that I did not know better, that everything and everyone had me convinced that my desires were wrong. Then I remember the criteria they used to uphold, and the barriers they still set. And then, then I just get fucking pissed all over again, because it is not just something that happened to me. I knew what I wanted and instead of simply allowing me to be I was, and still am, presented with hoops to jump through, barriers to surmount, insane psychoanalysis, and criteria that I can not meet. Nature may have caused me to be born "a boy", but it was the state and those bloody psychologists that forced me to be a man and in doing so drove me to a hair's breadth away from the grave. The physician may be surprised I managed to survive testosterone-poisoning for a dozen of years, well I am surprised society still insists on structuring everyone and everything around a collection of genital-based stereotypes and insists on policing the boundaries of those made-up stereotype boxes, even when this has been proven to cost lives.

So far no one had been particularly helpful, yet navigating the path of the bureaucracy at least made me feel like I was doing something. Those moments helped me keep my eyes on the ball, helped me keep my promise. But then there were the other moments where the lack of progress left me alone with my thoughts. That roller-coaster continued until one of my best friends showed me in which dark corners of the internet one can just buy estrogen. It's so easy once you know where to look. And it's the real deal, the stuff that you'd also get from a more reputable pharmacy albeit more expensive. Delivered right to my doorstep, no questions asked, just a signature required, it was almost anti-climactic. By now I had completed the first introductory meeting with the psychologists which was quite the opposite experience, many questions asked, no solutions provided. I unpacked the box and hesitated just long enough to read the German package insert, not that there was anything in there that I didn't already know: Beware, long term exposure might magically turn you into a women! And then it really hit me that this was now actually happening. With the arrival of that box, the choice that was stolen from me before had now been returned to me, for the first time in my life *I* held the power to end male puberty. I could choose to proceed and rub that gel on my leg, or I could decide not to, the choice was mine and mine alone. The moment was magical for many reasons, but most of all because of the choice. I delayed for a couple of minutes, not because I was hesitating, but because I was savouring the moment, the ability to choose. I still cherish that memory, it would not have been the same had it been "sanctioned" estrogen pre-approved by a psychologist, a psychiatrist, and an endocrinologist.

What surprised me was how fast it works, not physically, but mentally and emotionally. About four hours in I became convinced I was experiencing some placebo effect until I read on Wikipedia that the biological half-life of sex hormones is actually measured in just several hours and therefore it actually is conceivable to feel different before the day is over. It was truly magical, it felt like someone had grabbed my eyes from the back of my mind and pushed them into the sockets where they should have been all along. The next week I was sitting in the break room at work, staring outside of the window as if I was high. I swear, somehow, the trees looked greener, the little lake was bluer, the clouds more fluffy. Suddenly there was a whole new dimension of colours and sensations that I had been too numb to see. Then it hit me that, no, this actually was not new. This was old, this was how it used to be way back, before testosterone poisoned my mind. Back then I used to be able to enjoy trees, lakes, and clouds in full-colour. I had thought that losing the child-like wonder was part of becoming an adult, but no, here it was, back again. That evening I cried for hours, another thing I had not been able to do even when I had really wanted to, another thing I thought I had lost to adulthood but was now returned to me. I cried for everything that had been taken from me, for the cruelty of the world, and for all those times I had been unable to cry.

So that's the story of how this book almost never progressed beyond that first draft. Having finally started *Hormone Replacement Therapy* I very rapidly started to feel better. The world feels more real, I feel more grounded, I can look at my reflection again, and best of all is the self-confidence that I gained. Of course this is not the end of the tale, lots more has happened. The whole "diagnostic" procedure was still ongoing and the so-called experts weren't done pushing me around in their emotional roller-coaster of bureaucracy. The psychologist had made it crystal clear that it was highly unlikely for me to progress to the endocrinological level unless I had completed the "social transition" first, whatever that may mean. Of course I had already started using hormones unofficially, but it would be lots cheaper if they would be prescribed to me officially since the insurance would then cover them. Concretely the psychologist demanded that I tell everyone I knew what I was doing, and that I always dress accordingly (whatever that may mean). I remind the reader that I was acutely suicidal, and challenge the reader to think of any other situation where a medical professional may threaten to withhold treatment unless the patient tells all their colleagues, friends, and family exactly what is wrong with them. Clearly the Hippocratic oath and the transgender patient's life are subordinate to the confusion a cisgender person might experience when someone suddenly starts to grow boobs.

I had wanted to just finish the remaining months on my employment contract, and to then start fresh. But silly me, I should have known that what I wanted was irrelevant in the face of their omniscient god called: the policy. You'd think I would have learned that lesson by now. They claim their policies protect the patient, but they do not, they protect the dichotomisation of the society we live in. They claim you have to get a diagnosis from a psychologist to make sure you're not making a mistake you'll regret later. But the reality is that they are the border-patrol protecting the invisible boundary in society between "man" and "woman", controlling who can cross and how. Even if the regret-rate for gender-affirming care would not be astronomically low, then still it is my body, my choice, and my mistake to make.

That was the last time I would give the honest answer when I knew the honest answer was not the correct answer they were looking for. Anyway, that cat was now out of the bag, so I did the only thing I could do, have a mental breakdown on the department mailing-list. I then told the psychologist they could now check the "social transition complete" box. After that it took only a couple of sessions before I could advance to the next level, the psychiatrist, for a second opinion. I will never forget what that psychiatrist said to me.

He had the audacity to tell me outright: “I see in your file that you have ‘PDD-NOS’. Have you considered that the body and facial hair that you have been complaining about so fiercely, might just be overstimulating to you?”. He was well on his way towards denying me to progress to the endocrinological level on the basis of “comorbidity”. I should be pissed, and I was, but I hit him with the ultimate trump card. The panicked foraging through my files that followed was deeply satisfying. You see, when you cheat the system and take matters into your own hands, lights tend to become green a lot faster: “I think it would be a good idea if you continued that under the care of an endocrinologist”. And just like that I had won the battle and received my “gender dysphoria” diploma. Now I can finally say to that psychiatrist: Fuck You in particular, how dare you dig that out from the bottom of my file and use it as a weapon against me. Again!

So why write all this here? Well as I already said at the beginning, it either was something true and from the heart or something empty. And physics is a toxically masculine world where the human behind the science is usually forgotten. Everyone always asks ‘how’s your dissertation?’, no one asks ‘how are you?’. I got inspired by others to break that silence and to write my true experience down in this acknowledgements section. I became inspired to not only write about people and things that helped, but also about those that did not. Moreover this book carries quite a bit of emotional luggage for me because of how close it came to never being finished. Writing that down here has been extremely therapeutic. The process of finishing my dissertation could not be complete without also addressing the emotional aspects of the journey, allowing me to close that chapter of my life.

Then now, without further ado, the final part of acknowledgements. Words cannot express my gratitude towards the unnamed friend who showed me those dark corners of the internet where money can buy any medication. You gave me back what had been stolen from me, you gifted me with the autonomy to make my own choice. You, more than anyone else, are the reason this book is here today. I owe you a debt I can never repay, thank you.

Next, to my supervisor Uli. I know that the pandemic and the years following have not been easy for you. Your dedication and commitment to the lab knows no bounds and your tireless effort kept the lab running during difficult times. You have guided me through my bachelors internship, my masters internship, and now through the PhD program. Not to mention the courses in experimental techniques and electromagnetism, during one of which I remember that you demonstrated live to the class that touching a charged Van de Graaff generator hurts, a lot. And though that moment might not have been the best illustration of it, you have been a great source of wisdom and knowledge to me. I know I was not the easiest student or employee, I love science but I integrated badly with academia because of aforementioned reasons. I thank you for your patience and for your support. I thank you for being understanding when everything was more difficult then it should have been. But most importantly I thank you for being the wonderful person that you are. You may not always express it but you have the biggest heart. I hope that you can find some quiet-time and relaxation, far away from stress, now that you have decided to leave the lab.

I thank Sasha, Xiaoli, Justin and everyone else from the team in Groningen. I may not have liked to travel far from home for work, but your kindness made it worthwhile. Thank you for showing me around the nanolab and for teaching me how to use all the cool stuff you have there. Thank you for including me in the adventure that is the transition metal dichalcogenides. The research we did is far from finished and I hope you’ll continue without me to find the answers we were looking for now that I work in a different sector.

I thank Eugen and Enric for working with me on the superconducting THEVA tapes. We never managed to solve our experimental problem, but I do feel we understand it a bit better now. Superconducting tapes were never supposed to be part of my dissertation, it should have been a simple experiment. Practice turned out to be more complex then theory here and we ended up spending so much time on debugging that it is now more then justifiable that the superconducting tapes make up about half of this book. I hope you'll succeed in obtaining useful results in the future, perhaps in a new magnet.

I thank Elvina for adopting the vibrating sample magnetometer. For many years it was my baby and I have put a great deal of effort into perfecting it and making it easier to use. We have done many interesting experiments together and I now leave the vibrating sample magnetometer in your capable hands.

And a big thank you to everyone else works or has worked in the lab. HFML brands itself as being unique due to its connection with Felix, and that is of course very much so. But what also makes HFML unique is the drive and passion of the people working there. So much work is done with such a small workforce, it is truly remarkable. I know that not everyone always feels like their effort is seen, recognised, and acknowledged, so I will do so now. You move mountains, I saw that and continue to see it.

I want to thank my partner Ties for your unending support even when I worked too much, for sticking with me even when I was no fun to be around, and for tolerating my insanity. You are a treasure and I don't say so often enough. I want to thank my little brother for supporting me through everything, the world may suck but I know we can always count on each other. And then finally I want to thank my parents. You may not always have understood me but you did try to support me. I have heard you say things that sound suspiciously like blaming yourselves for what happened, but none of it is your fault. It is not your fault that society is the way it is, it is not your fault that clinical psychology as a field is rotten to the core, and it is not your fault that the government denied me my bodily autonomy. You have only ever had my best interests at heart and I know that.

In loving memory of those that did not survive the gender-bureaucracy, murdered by the state that claimed to protect them.

Bibliography

[1] *Magnet specifications*. High Field Magnet Laboratory (HFML). Last Modified: 2021-09-06. URL: https://www.ru.nl/hfml/use-our-facility/magnet-specifications/ (visited on 02/14/2024).

[2] E. F. Talantsev and W. P. Crump. *WayneCrump/BCS-theory-critical-current-fit: Contains a program for fitting critical currents using thermodynamic parameters from the paper*. URL: https://github.com/WayneCrump/BCS-theory-critical-current-fit (visited on 09/05/2024).

[3] E. L. Q. N. Ammerlaan, O. Zheliuk, X. Peng, U. Zeitler, and J. Ye. *Ising protection in WS2 across the superconducting dome*. 2026.

[4] L. Heinze, T. Kotte, R. Rausch, A. Demuer, S. Luther, R. Feyerherm, E. L. Q. N. Ammerlaan, U. Zeitler, D. I. Gorbunov, M. Uhlarz, K. C. Rule, A. U. B. Wolter, H. Kühne, J. Wosnitza, C. Karrasch, and S. Süllow. "Atacamite $Cu_2Cl(OH)_3$ in High Magnetic Fields: Quantum Criticality and Dimensional Reduction of a Sawtooth-Chain Compound". In: *Physical Review Letters* 134.21 (May 27, 2025). Publisher: American Physical Society, p. 216701. DOI: 10.1103/PhysRevLett.134.216701.

[5] P. Lázpita, N. A. Río-López, D. Mérida, E. L. Q. N. Ammerlaan, U. Zeitler, V. Chernenko, and J. Gutiérrez. "Magnetic Field Suppression of the Martensitic Transformation in Mn-Based MnNi(Fe)Sn Metamagnetic Shape Memory Heusler Alloys". In: *Magnetism* 5.4 (Oct. 16, 2025). Publisher: Multidisciplinary Digital Publishing Institute. ISSN: 2673-8724. DOI: 10.3390/magnetism5040025.

[6] K. Mopoung, T. Quanzheng, M. Zhang, F. Orlandi, K. Mukhuti, M. de Dreu, E. Dilmieva, K. S. Ramsamoedj, E. L. Q. N. Ammerlaan, T. S. Ottenbros, S. R. Wiedmann, A. Boothroyd, P. C. M. Christianen, J. Rosén, F. Gao, I. A. Buyanova, W. M. Chen, and Puttisong. *Selective Antiferromagnetic Ordering Driven by Structural Phase Transition in Spin Frustrated Halide Double Perovskites*. 2025.

[7] E. L. Q. N. Ammerlaan. *MagnetoResistance-tool: Tool to create calibration matrix allowing to correct for magneto-resistance in resisitive sensors*. Version 0.0.4. 2024.

[8] X. Peng. "Ion-gated high mobility 2D transition metal dichalcogenides transistors". PhD thesis. Groningen: University of Groningen, 2024. DOI: 10.33612/diss.892806873.

[9] L. Peters. "Probing the spin interactions of molecular magnets through high field cantilever magnetometry". PhD thesis. Nijmegen: Radboud University, Feb. 21, 2024.

[10] D. Pizzirani, T. Ottenbros, M. van Rijssel, O. Zheliuk, Y. Kreminska, M. Rösner, J. F. Linnartz, A. de Visser, N. E. Hussey, J. Ye, S. Wiedmann, and M. R. van Delft. "From orbital to paramagnetic pair breaking in layered superconductor 2H-NbS2". In: *Physical Review Re-*

search 6.4 (Oct. 7, 2024). Publisher: American Physical Society, p. L042006. DOI: 10.1103/PhysRevResearch.6.L042006.

[11] K. Rubi, D. R. Candido, M. Dumen, S. Zeng, E. L. Q. N. Ammerlaan, F. Bangma, M. K. Chan, M. Goiran, A. Ariando, S. Chakraverty, W. Escoffier, U. Zeitler, and N. Harrison. "Unconventional quantum oscillations and evidence of nonparabolic electronic states in quasi-two-dimensional electron system at complex oxide interfaces". In: *Physical Review Research* 6.4 (Dec. 3, 2024). Publisher: American Physical Society, p. 043231. DOI: 10.1103/PhysRevResearch.6.043231.

[12] O. Zheliuk, Y. Kreminska, Q. Fu, D. Pizzirani, E. L. Q. N. Ammerlaan, Y. Wang, S. Hameed, P. Wan, X. Peng, S. Wiedmann, Z. Liu, J. Ye, and U. Zeitler. "Quantum Hall effect in a CVD-grown oxide". In: *Nature Communications* 15.1 (Nov. 20, 2024). Publisher: Nature Publishing Group, p. 10052. ISSN: 2041-1723. DOI: 10.1038/s41467-024-54014-6.

[13] P. Wan. "Quantum Phase Transitions in Clean Ising Superconductors". PhD thesis. Groningen: University of Groningen, 2023. DOI: 10.33612/diss.561223255.

[14] P. Wan, O. Zheliuk, N. F. Q. Yuan, X. Peng, L. Zhang, M. Liang, U. Zeitler, S. Wiedmann, N. E. Hussey, T. T. M. Palstra, and J. Ye. "Orbital Fulde–Ferrell–Larkin–Ovchinnikov state in an Ising superconductor". In: *Nature* 619.7968 (July 2023). Publisher: Nature Publishing Group, pp. 46–51. ISSN: 1476-4687. DOI: 10.1038/s41586-023-05967-z.

[15] D. Ding, Z. Qu, X. Han, C. Han, Q. Zhuang, X.-L. Yu, R. Niu, Z. Wang, Z. Li, Z. Gan, J. Wu, and J. Lu. "Multivalley Superconductivity in Monolayer Transition Metal Dichalcogenides". In: *Nano Letters* (Sept. 29, 2022). Publisher: American Chemical Society. ISSN: 1530-6984. DOI: 10.1021/acs.nanolett.2c02947.

[16] P. Lázpita, A. Pérez-Checa, J. M. Barandiarán, E. L. Q. N. Ammerlaan, U. Zeitler, and V. Chernenko. "Suppression of martensitic transformation in Ni-Mn-In metamagnetic shape memory alloy under very strong magnetic field". In: *Journal of Alloys and Compounds* 874 (Sept. 5, 2021), p. 159814. ISSN: 0925-8388. DOI: 10.1016/j.jallcom.2021.159814.

[17] P. Wan, Q. Chen, O. Zheliuk, L. Zhang, M. Liang, X. Peng, and J. Ye. *Dual Universality and Unconventional Phase Diagram of a Clean 2D Superconductor with Tunable Disorders*. Apr. 9, 2021. DOI: 10.48550/arXiv.2104.03872. arXiv: 2104.03872[cond-mat].

[18] D. Shen, C. N. Kuo, T. W. Yang, I. N. Chen, C. S. Lue, and L. M. Wang. "Two-dimensional superconductivity and magnetotransport from topological surface states in AuSn4 semimetal". In: *Communications Materials* 1.1 (Aug. 12, 2020). Publisher: Nature Publishing Group, pp. 1–11. ISSN: 2662-4443. DOI: 10.1038/s43246-020-00060-8.

[19] A. Ślebarski and M. M. Maśka. "Enhancing Superconductivity of the Nonmagnetic Quasiskutterudites by Atomic Disorder". In: *Materials* 13.24 (Jan. 2020). Number: 24 Publisher: Multidisciplinary Digital Publishing Institute, p. 5830. ISSN: 1996-1944. DOI: 10.3390/ma13245830.

[20] B. Xu, G. Amadio, F. Groffen, and M. Haubenwallner. "Gentoo Prefix as a Physics Software Manager". In: *EPJ Web of Conferences* 245 (2020). Publisher: EDP Sciences, p. 05036. ISSN: 2100-014X. DOI: 10.1051/epjconf/202024505036.

[21] O. Zheliuk. "Magnetotransport of Ising superconductors". PhD thesis. Groningen: University of Groningen, 2020. 122 pp. DOI: 10.33612/diss.113195218.

[22] S. Schlör. *Sketch of a wet helium dilution refrigerator*. Feb. 14, 2019.

[23] O. Zheliuk, J. M. Lu, Q. H. Chen, A. A. E. Yumin, S. Golightly, and J. T. Ye. "Josephson coupled Ising pairing induced in suspended MoS2 bilayers by double-side ionic gating". In: *Nature*

Nanotechnology 14.12 (Dec. 2019). Number: 12 Publisher: Nature Publishing Group, pp. 1123–1128. ISSN: 1748-3395. DOI: 10.1038/s41565-019-0564-1.

[24] E. L. Q. N. Ammerlaan. "Vibrating Sample Magnetometry". Bachelor. Nijmegen: Radboud University, Dec. 5, 2018. 30 pp.

[25] M. Liao, Y. Zang, Z. Guan, H. Li, Y. Gong, K. Zhu, X.-P. Hu, D. Zhang, Y. Xu, Y.-Y. Wang, K. He, X.-C. Ma, S.-C. Zhang, and Q.-K. Xue. "Superconductivity in few-layer stanene". In: *Nature Physics* 14.4 (Apr. 2018). Publisher: Nature Publishing Group, pp. 344–348. ISSN: 1745-2481. DOI: 10.1038/s41567-017-0031-6.

[26] C. Liu, C.-S. Lian, M.-H. Liao, Y. Wang, Y. Zhong, C. Ding, W. Li, C.-L. Song, K. He, X.-C. Ma, W. Duan, D. Zhang, Y. Xu, L. Wang, and Q.-K. Xue. "Two-dimensional superconductivity and topological states in ${\mathrm{PdTe}}_{2}$ thin films". In: *Physical Review Materials* 2.9 (Sept. 4, 2018). Publisher: American Physical Society, p. 094001. DOI: 10.1103/PhysRevMaterials.2.094001.

[27] J. Lu, O. Zheliuk, Q. Chen, I. Leermakers, N. E. Hussey, U. Zeitler, and J. Ye. "Full superconducting dome of strong Ising protection in gated monolayer WS2". In: *Proceedings of the National Academy of Sciences* 115.14 (Apr. 3, 2018). Publisher: National Academy of Sciences Section: Physical Sciences, pp. 3551–3556. ISSN: 0027-8424, 1091-6490. DOI: 10.1073/pnas.1716781115.

[28] E. F. Talantsev, W. P. Crump, J. O. Island, Y. Xing, Y. Sun, J. Wang, and J. L. Tallon. "On the origin of critical temperature enhancement in atomically thin superconductors". In: *2D Materials* 4.2 (Apr. 2017). Publisher: IOP Publishing, p. 025072. ISSN: 2053-1583. DOI: 10.1088/2053-1583/aa6917.

[29] O. Zheliuk, J. Lu, J. Yang, and J. Ye. "Monolayer Superconductivity in WS2". In: *physica status solidi (RRL) – Rapid Research Letters* 11.9 (2017), p. 1700245. ISSN: 1862-6270. DOI: 10.1002/pssr.201700245.

[30] A. den Ouden, C. A. Wulffers, N. E. Hussey, G. Laureijs, F. J. P. Wijnen, G. F. A. J. Wulterkens, M. D. Bird, I. R. Dixon, and J. A. A. J. Perenboom. "Progress in the Development of the HFML 45 T Hybrid Magnet". In: *IEEE Transactions on Applied Superconductivity* 26.4 (June 2016), pp. 1–7. ISSN: 1558-2515. DOI: 10.1109/TASC.2016.2524544.

[31] F. J. P. Wijnen, S. A. J. Wiegers, J. M. H. van Velsen, J. Rook, A. den Ouden, J. A. A. J. Perenboom, and N. E. Hussey. "Construction and Performance of a 38-T Resistive Magnet at the Nijmegen High Field Magnet Laboratory". In: *IEEE Transactions on Applied Superconductivity* 26.4 (June 2016), pp. 1–5. ISSN: 1558-2515. DOI: 10.1109/TASC.2016.2537141.

[32] S. Jo, D. Costanzo, H. Berger, and A. F. Morpurgo. "Electrostatically Induced Superconductivity at the Surface of WS2". In: *Nano Letters* 15.2 (Feb. 11, 2015). Publisher: American Chemical Society, pp. 1197–1202. ISSN: 1530-6984. DOI: 10.1021/nl504314c.

[33] J. M. Lu, O. Zheliuk, I. Leermakers, N. F. Q. Yuan, U. Zeitler, K. T. Law, and J. T. Ye. "Evidence for two-dimensional Ising superconductivity in gated MoS2". In: *Science* 350.6266 (Dec. 11, 2015). Publisher: American Association for the Advancement of Science, pp. 1353–1357. DOI: 10.1126/science.aab2277.

[34] H. R. Gutiérrez, N. Perea-López, A. L. Elías, A. Berkdemir, B. Wang, R. Lv, F. López-Urías, V. H. Crespi, H. Terrones, and M. Terrones. "Extraordinary Room-Temperature Photoluminescence in Triangular WS2 Monolayers". In: *Nano Letters* 13.8 (Aug. 14, 2013). Publisher: American Chemical Society, pp. 3447–3454. ISSN: 1530-6984. DOI: 10.1021/nl3026357.

[35] W. A. G. Kampert. “Magnetic properties of organometallic compounds in high magnetic fields”. PhD thesis. Nijmegen: Radboud University, Apr. 17, 2012. 117 pp.

[36] M. Kim, Y. Kozuka, C. Bell, Y. Hikita, and H. Y. Hwang. “Intrinsic spin-orbit coupling in superconducting $\ensuremath{\delta}$-doped SrTiO${}_{3}$ heterostructures”. In: *Physical Review B* 86.8 (Aug. 15, 2012). Publisher: American Physical Society, p. 085121. DOI: 10.1103/PhysRevB.86.085121.

[37] J. Bobroff, F. Bouquet, and A. Rorheim. *This is my (Adrian Rorheim) own adaptation of a diagram by Frederic Bouquet and Julien Bobroff of the Laboratoire de physique des solides (LPS). My diagram is simply a cleaned-up digital version of theirs, and I take no credit for the information it conveys, nor the general presentation thereof.* Dec. 2011.

[38] D. S. Inosov, J. T. Park, A. Charnukha, Y. Li, A. V. Boris, B. Keimer, and V. Hinkov. “Crossover from weak to strong pairing in unconventional superconductors”. In: *Physical Review B* 83.21 (June 29, 2011). Publisher: American Physical Society, p. 214520. DOI: 10.1103/PhysRevB.83.214520.

[39] H. Danan, A. Herr, and A. J. P. Meyer. “New Determinations of the Saturation Magnetization of Nickel and Iron”. In: *Journal of Applied Physics* 39.2 (Dec. 30, 2008), pp. 669–670. ISSN: 0021-8979. DOI: 10.1063/1.2163571.

[40] Eynar. *Magnetisation in superconductors depends on the external magnetic field. The value of the Ginzburg-Landau parameter will tell us if the superconductor is a Type I or a Type II, as Abrikosov showed in 1957.* May 22, 2008.

[41] H. Ullmaier. *Irreversible Properties of Type II Superconductors*. Google-Books-ID: EJl0DgAAQBAJ. Springer, Apr. 11, 2006. 177 pp. ISBN: 978-3-540-37963-8.

[42] J. A. A. J. Perenboom, S. A. J. Wiegers, P. C. M. Christianen, U. Zeitler, and J. C. Maan. “The new installation at the Nijmegen High Field Magnet Laboratory”. In: *Physica B: Condensed Matter*. Proceedings of the 7th International Symposium on Research in High Magnetic Fields 346-347 (Apr. 30, 2004), pp. 659–662. ISSN: 0921-4526. DOI: 10.1016/j.physb.2004.01.078.

[43] J. F. Annett. *Superconductivity, Superfluids and Condensates*. Oxford University Press, May 2003. 140 pp.

[44] E. H. Brandt and G. P. Mikitik. “Why an ac Magnetic Field Shifts the Irreversibility Line in Type-II Superconductors”. In: *Physical Review Letters* 89.2 (June 20, 2002). Publisher: American Physical Society, p. 027002. DOI: 10.1103/PhysRevLett.89.027002.

[45] C. B. Eom, M. K. Lee, J. H. Choi, L. J. Belenky, X. Song, L. D. Cooley, M. T. Naus, S. Patnaik, J. Jiang, M. Rikel, A. Polyanskii, A. Gurevich, X. Y. Cai, S. D. Bu, S. E. Babcock, E. E. Hellstrom, D. C. Larbalestier, N. Rogado, K. A. Regan, M. A. Hayward, T. He, J. S. Slusky, K. Inumaru, M. K. Haas, and R. J. Cava. “High critical current density and enhanced irreversibility field in superconducting MgB2 thin films”. In: *Nature* 411.6837 (May 2001). Publisher: Nature Publishing Group, pp. 558–560. ISSN: 1476-4687. DOI: 10.1038/35079018.

[46] G. Fuchs, K. .-. Müller, A. Handstein, K. Nenkov, V. N. Narozhnyi, D. Eckert, M. Wolf, and L. Schultz. “Upper critical field and irreversibility line in superconducting MgB2”. In: *Solid State Communications* 118.10 (June 5, 2001), pp. 497–501. ISSN: 0038-1098. DOI: 10.1016/S0038-1098(01)00157-0.

[47] J. L. MacManus-Driscoll. “Recent developments in conductor processing of high irreversibility field superconductors”. In: *Annual Review of Materials Research* 28 (Volume 28, 1998 Aug. 1, 1998). Publisher: Annual Reviews, pp. 421–462. ISSN: 1531-7331, 1545-4118. DOI: 10.1146/annurev.matsci.28.1.421.

[48] V. L. Ginzburg. “Superconductivity and superfluidity (what was done and what was not)”. In: *Physics-Uspekhi* 40.4 (Apr. 30, 1997). Publisher: IOP Publishing, p. 407. ISSN: 1063-7869. DOI: 10.1070/PU1997v040n04ABEH000230.

[49] H. K. Onnes. “Further experiments with Liquid Helium. G. On the Electrical Resistance of Pure Metals, etc. VI. On the Sudden Change in the Rate at which the Resistance of Mercury Disappears.” In: *Through Measurement to Knowledge: The Selected Papers of Heike Kamerlingh Onnes 1853–1926*. Ed. by K. Gavroglu and Y. Goudaroulis. Dordrecht: Springer Netherlands, 1991, pp. 267–272. ISBN: 978-94-009-2079-8. DOI: 10.1007/978-94-009-2079-8_17.

[50] K. von Klitzing. “The quantized Hall effect”. In: *Reviews of Modern Physics* 58.3 (July 1, 1986). Publisher: American Physical Society, pp. 519–531. DOI: 10.1103/RevModPhys.58.519.

[51] P. Fulde. “High field superconductivity in thin films”. In: *Advances in Physics* 22.6 (Nov. 1, 1973). Publisher: Taylor & Francis _eprint: https://doi.org/10.1080/00018737300101369, pp. 667–719. ISSN: 0001-8732. DOI: 10.1080/00018737300101369.

[52] N. R. Werthamer, E. Helfand, and P. C. Hohenberg. “Temperature and Purity Dependence of the Superconducting Critical Field, ${H}_{c2}$. III. Electron Spin and Spin-Orbit Effects”. In: *Physical Review* 147.1 (July 8, 1966). Publisher: American Physical Society, pp. 295–302. DOI: 10.1103/PhysRev.147.295.

[53] B. S. Chandrasekhar. “A note on the maximum critical field of high-field superconductors”. In: *Applied Physics Letters* 1.1 (Sept. 1, 1962), pp. 7–8. ISSN: 0003-6951. DOI: 10.1063/1.1777362.

[54] A. M. Clogston. “Upper Limit for the Critical Field in Hard Superconductors”. In: *Physical Review Letters* 9.6 (Sept. 15, 1962). Publisher: American Physical Society, pp. 266–267. DOI: 10.1103/PhysRevLett.9.266.

[55] J. Bardeen, L. N. Cooper, and J. R. Schrieffer. “Theory of Superconductivity”. In: *Physical Review* 108.5 (Dec. 1, 1957). Publisher: American Physical Society, pp. 1175–1204. DOI: 10.1103/PhysRev.108.1175.

[56] V. L. Ginzburg and L. D. Landau. “To the theory of superconductivity”. In: *Zhurnal Éksperimental'noĭ i Teoreticheskoĭ Fiziki* 20.1064 (1950).

[57] W. J. de Haas and P. M. van Alphen. “The dependence of the susceptibility of diamagnetic metals upon the field”. In: *Proceedings of the Amsterdam Academy of Sciences* 33 (Dec. 20, 1930), pp. 1106–1118.

[58] L. Landau. “Diamagnetismus der Metalle”. In: *Zeitschrift für Physik* 64.9 (Sept. 1, 1930), pp. 629–637. ISSN: 0044-3328. DOI: 10.1007/BF01397213.

[59] L. Schubnikow and W. J. de Haas. “Die Widerstandsänderung von Wismuthkristallen im Magnetfeld bei der Temperatur von flüssigem Stickstoff”. In: *Proceedings of the Royal Netherlands Academy of Arts and Science* 33 (May 31, 1930), pp. 433–439.

[60] N. Bohr. “I. On the constitution of atoms and molecules”. In: *The London, Edinburgh, and Dublin Philosophical Magazine and Journal of Science* 26.151 (July 1, 1913). Publisher: Taylor & Francis _eprint: https://doi.org/10.1080/14786441308634955, pp. 1–25. ISSN: 1941-5982. DOI: 10.1080/14786441308634955.

[61] N. Bohr. “LXXIII. On the constitution of atoms and molecules”. In: *The London, Edinburgh, and Dublin Philosophical Magazine and Journal of Science* 26.155 (Nov. 1, 1913). Publisher: Taylor & Francis _eprint: https://doi.org/10.1080/14786441308635031, pp. 857–875. ISSN: 1941-5982. DOI: 10.1080/14786441308635031.

[62] N. Bohr. “XXXVII. On the constitution of atoms and molecules”. In: *The London, Edinburgh, and Dublin Philosophical Magazine and Journal of Science* 26.153 (Sept. 1, 1913). Publisher:

Taylor & Francis _eprint: https://doi.org/10.1080/14786441308634993, pp. 476–502. ISSN: 1941-5982. DOI: 10.1080/14786441308634993.

[63] R. A. Millikan. "The Isolation of an Ion, a Precision Measurement of Its Charge, and the Correction of Stokes's Law". In: *Science* 32.822 (Sept. 30, 1910). Publisher: American Association for the Advancement of Science, pp. 436–448. DOI: 10.1126/science.32.822.436.

[64] P. Drude. "Zur Elektronentheorie der Metalle". In: *Annalen der Physik* 306.3 (1900). _eprint: https://onlinelibrary.wiley.com/doi/pdf/10.1002/andp.19003060312, pp. 566–613. ISSN: 1521-3889. DOI: 10.1002/andp.19003060312.

[65] H. A. Lorentz. *Versuch eine Theorie der electrischen und optischen Erscheinungen in bewegten Körpern*. Leiden, 1895.

[66] E. H. Hall. "On a New Action of the Magnet on Electric Currents". In: *American Journal of Mathematics* 2.3 (1879). Publisher: Johns Hopkins University Press, pp. 287–292. ISSN: 0002-9327. DOI: 10.2307/2369245.

Appendix A

Overview of all measured WS_2 states

In this appendix we present a full overview of all measured states. Figures A.0.1 to A.0.11 plot all data in parallel magnetic fields, with in the insets the accompanying data in perpendicular magnetic fields if it exists. Fits and the extracted parameters are shown in the legend. Several top-gate states have been measured at various back-gate voltages, these are shown together in the same figure using different colours. The colour map used in each of these figures corresponds to the colours used in the summarising plots of Figures 6.3.4 and 6.4.4. Finally, in Table 6.1 we summarise all extracted parameters for every measured gating state.

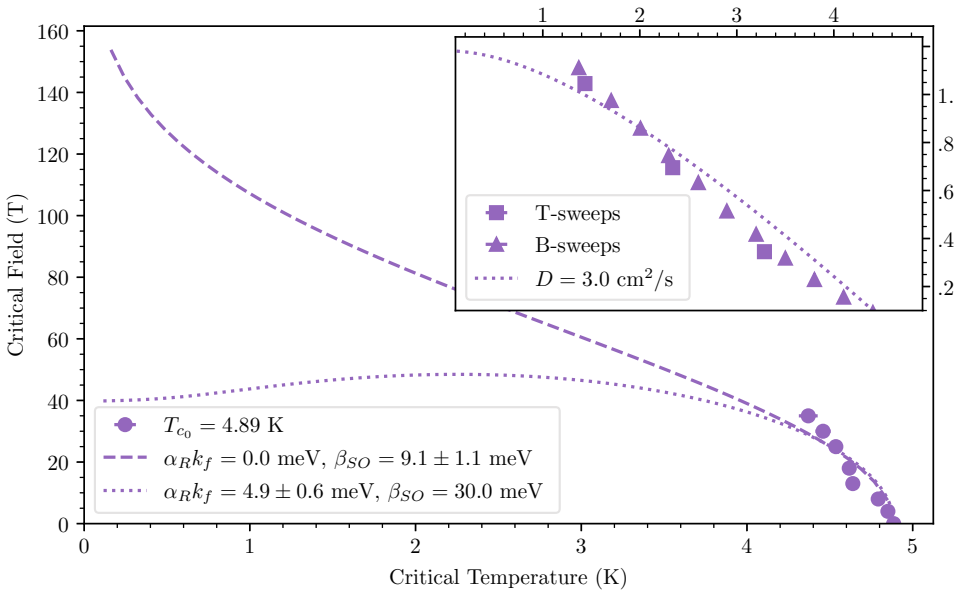

Figure A.0.1: Sample 1, State 1: Parallel magnetic field data fit using Equation (4.1.2). The inset shows the same state measured in perpendicular field. Squares indicate points measured at constant magnetic field while varying the temperature, and triangles indicate points measured at constant temperature while varying the magnetic field. Data has been fit using Equation (3.2.5).

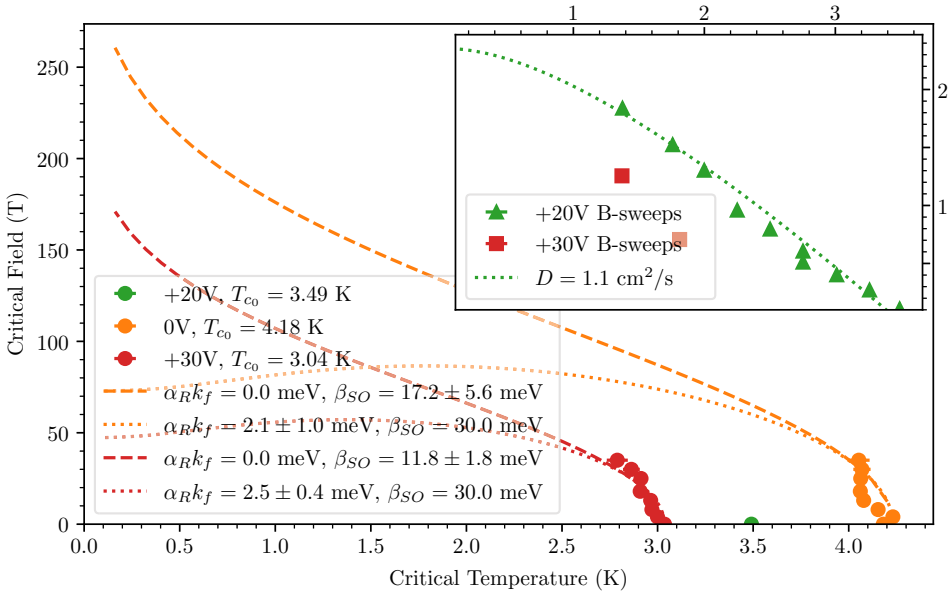

Figure A.0.2: Sample 1, State 2: Parallel magnetic field data of two back gate states, fit using Equation (4.1.2). The inset shows the same states measured in perpendicular field. Squares indicate points measured at constant magnetic field while varying the temperature, and triangles indicate points measured at constant temperature while varying the magnetic field. Data has been fit using Equation (3.2.5).

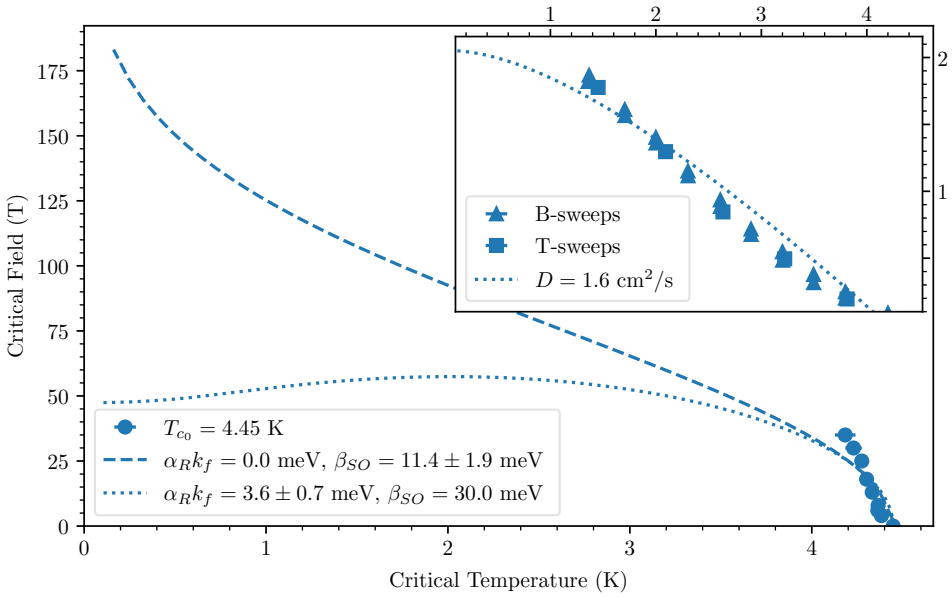

Figure A.0.3: Sample 1, State 3: Parallel magnetic field data fit using Equation (4.1.2). The inset shows the same state measured in perpendicular field. Squares indicate points measured at constant magnetic field while varying the temperature, and triangles indicate points measured at constant temperature while varying the magnetic field. Data has been fit using Equation (3.2.5).

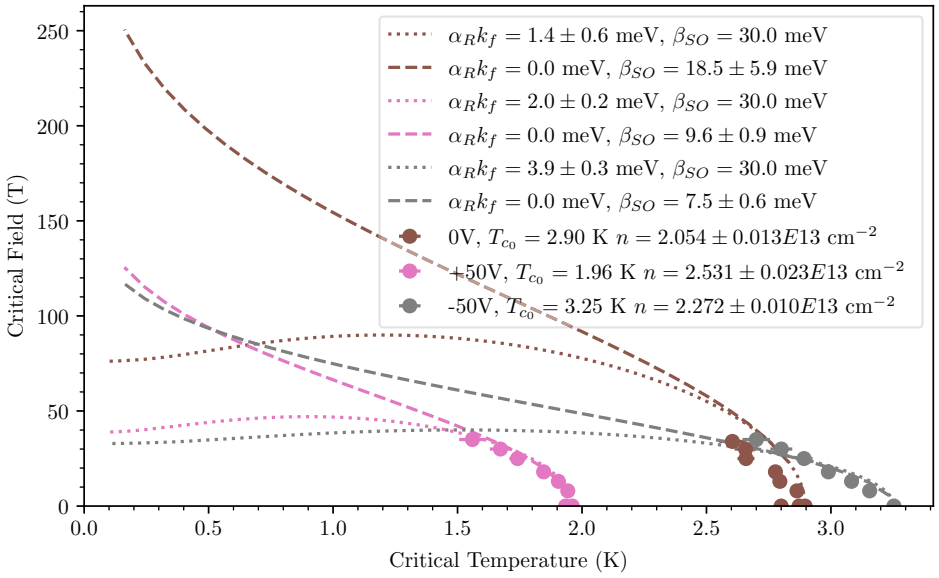

Figure A.0.4: Sample 2, State 1: Parallel magnetic field data of three different solid back gate states, fit using Equation (4.1.2). The charge carrier density of each state has been determined by measuring the Hall effect.

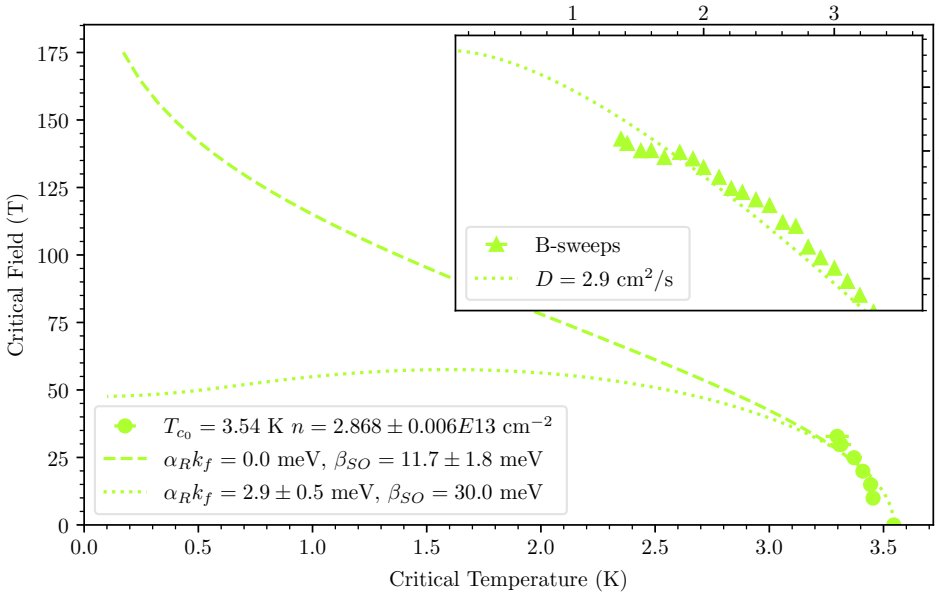

Figure A.0.5: Sample 3, State 1: Parallel magnetic field data fit using Equation (4.1.2). The inset shows the same state measured in varying perpendicular fields at constant temperatures. Data has been fit using Equation (3.2.5).

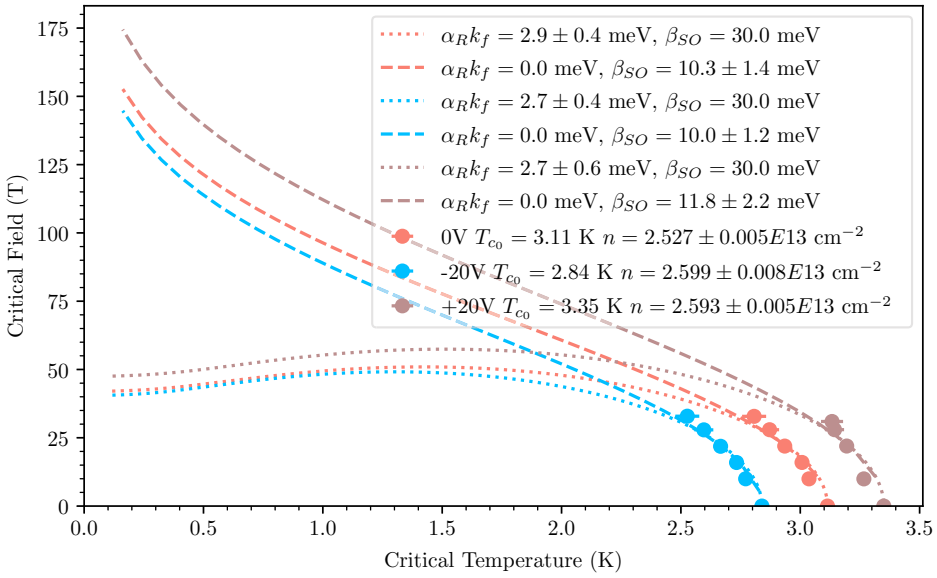

Figure A.0.6: Sample 3, State 2: Parallel magnetic field data of three different solid back gate states, fit using Equation (4.1.2). The charge carrier density of each state has been determined by measuring the Hall effect.

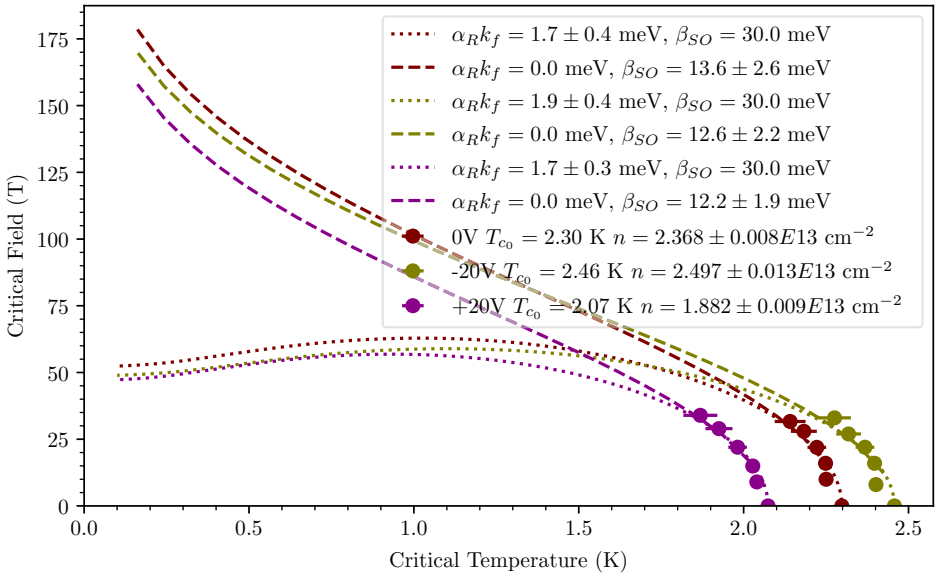

Figure A.0.7: Sample 3, State 3: Parallel magnetic field data of three different solid back gate states, fit using Equation (4.1.2). The charge carrier density of each state has been determined by measuring the Hall effect.

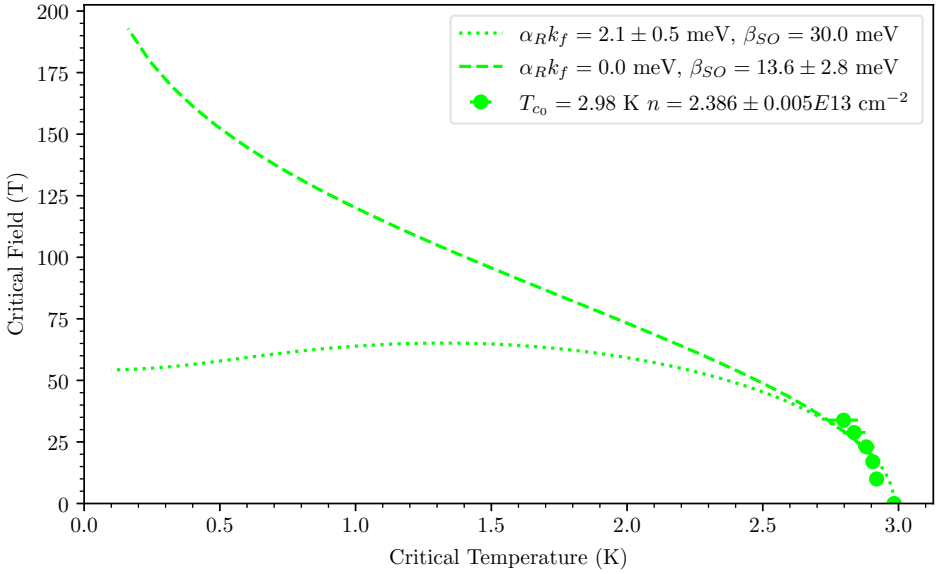

Figure A.0.8: Sample 3, State 4: Parallel magnetic field data fit using Equation (4.1.2). The charge carrier density of this state has been determined by measuring the Hall effect.

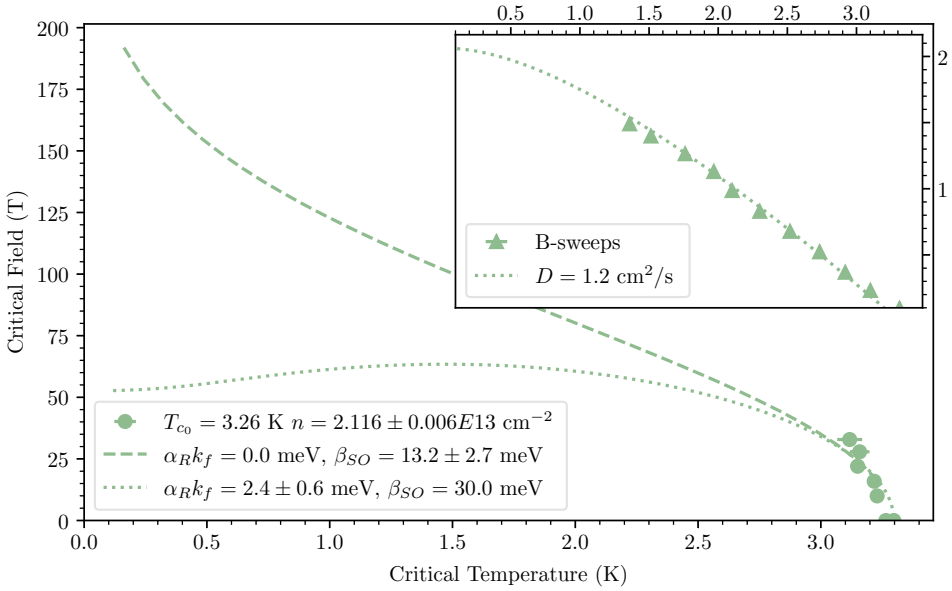

Figure A.0.9: Sample 3, State 5: Parallel magnetic field data fit using Equation (4.1.2). The inset shows the same state measured in varying perpendicular fields at constant temperatures. The data has been fit using Equation (3.2.5).

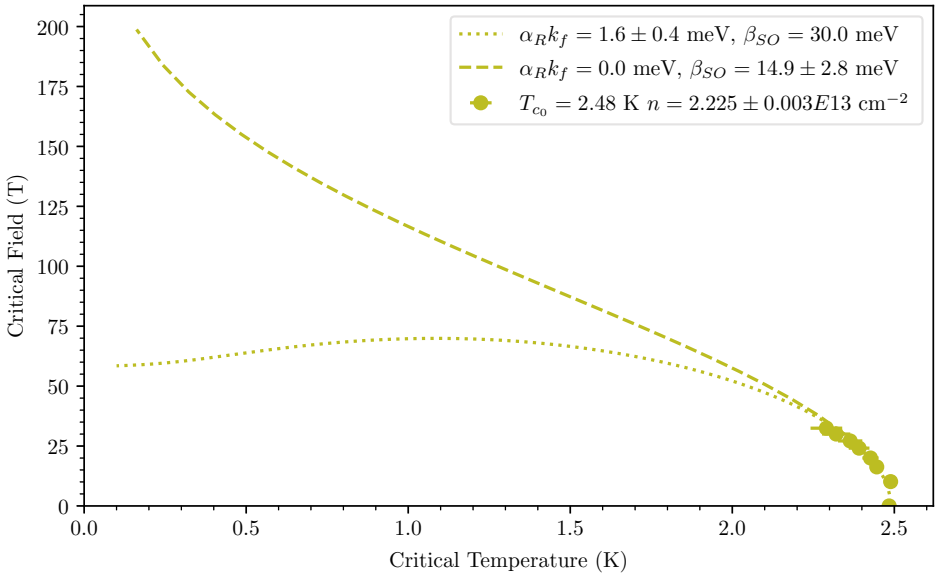

Figure A.0.10: Sample 4, State 1: Parallel magnetic field data fit using Equation (4.1.2). The charge carrier density of this state has been determined by measuring the Hall effect.

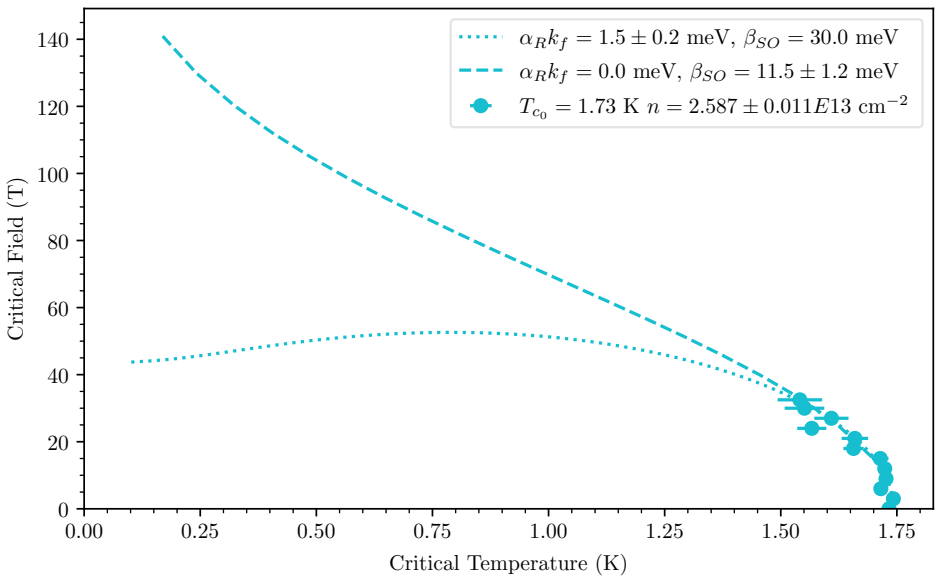

Figure A.0.11: Sample 4, State 2: Parallel magnetic field data fit using Equation (4.1.2). The charge carrier density of this state has been determined by measuring the Hall effect.

Appendix B

The capacitance change of a bending cantilever

Here we will solve:

$$C_1 = \int_{L_c - r}^{L_c + r} \frac{\epsilon_0 2\sqrt{r^2 - (x - L_c)^2}}{d_0 - \frac{FL_a^2}{2EI}x + \frac{FL_a^3}{6EI}} dx$$

We start by doing a coordinate transformation $\alpha = x - L_c$ to the centre of the capacitive plate:

$$C_1 = \int_{-r}^{r} \frac{2\epsilon_0\sqrt{r^2 - \alpha^2}}{d_0 - \frac{FL_a^2}{2EI}(\alpha + L_c) + \frac{FL_a^3}{6EI}} d\alpha$$
$$\implies \int_{-r}^{r} \frac{2\epsilon_0\sqrt{r^2 - \alpha^2}}{d_0 - \frac{FL_a^2}{2EI}\alpha + \frac{FL_a^2}{6EI}(L_a - 3L_c)} d\alpha$$

We use that $L_c = L_a + r$ to reduce the amount of variables:

$$C_1 = \int_{-r}^{r} \frac{2\epsilon_0\sqrt{r^2 - \alpha^2}}{d_0 - \frac{FL_a^2}{2EI}\alpha + \frac{FL_a^2}{6EI}(-2L_a - 3r)} d\alpha$$
$$\implies \int_{-r}^{r} \frac{2\epsilon_0\sqrt{r^2 - \alpha^2}}{d_0 - \frac{FL_a^2}{2EI}\alpha - \frac{FL_a^3}{3EI} - \frac{FL_a^2 r}{2EI}} d\alpha$$
$$\implies \frac{2\epsilon_0 EI}{FL_a^2} \int_{-r}^{r} \frac{\sqrt{r^2 - \alpha^2}}{\frac{d_0 EI}{FL_a^2} - \alpha/2 - L_a/3 - r/2} d\alpha$$
$$\implies \frac{12\epsilon_0 EI}{FL_a^2} \int_{-r}^{r} \frac{\sqrt{r^2 - \alpha^2}}{\frac{6d_0 EI}{FL_a^2} - 3\alpha - 2L_a - 3r} d\alpha$$
$$\implies \frac{12\epsilon_0 EI}{FL_a^2} \int_{-r}^{r} \frac{\sqrt{r^2 - \alpha^2}}{\frac{6d_0 EI}{FL_a^2} - 3(r + \alpha) - 2L_a} d\alpha$$

Now we switch to polar coordinates $\alpha = r\cos(\phi)$, $d\alpha = -r\sin(\phi)d\phi$, $\sqrt{r^2 - \alpha^2} = r\sin(\phi)$:

$$C_1 = \frac{-12\epsilon_0 EI}{FL_a^2}\int_\pi^0 \frac{r\sin(\phi)}{\frac{6d_0EI}{FL_a^2} - 3r(1+\cos(\phi)) - 2L_a} r\sin(\phi)d\phi$$

$$\implies \frac{12\epsilon_0 EI}{FL_a^2}\int_0^\pi \frac{r^2\sin(\phi)^2}{\frac{6d_0EI}{FL_a^2} - 3r(1+\cos(\phi)) - 2L_a} d\phi$$

Next we do a transformation that might not be completely obvious but it will prove helpful: $u = \tan(\phi/2)$, $du = 1/\left(2\cos(\phi/2)^2\right)d\phi$

$$u = \tan(\phi/2) = \frac{\sin(\phi/2)}{\cos(\phi/2)} = \frac{\sin(\phi)}{2\cos(\phi/2)^2} = \frac{\sin(\phi)}{1+\cos(\phi)}$$

$$\implies \sin(\phi) = u2\cos(\phi/2)^2 = \frac{2u\cos(\phi/2)^2}{\sin(\phi/2)^2+\cos(\phi/2)^2} = \frac{2u}{\frac{\sin(\phi/2)^2}{\cos(\phi/2)^2}+1} = \frac{2u}{\tan(\phi/2)^2+1} = \frac{2u}{u^2+1}$$

$$\implies 1+\cos(\phi) = \frac{\sin(\phi)}{u} = \frac{2}{u^2+1}$$

$$\implies \cos(\phi) = \frac{2}{u^2+1} - 1 = \frac{2}{u^2+1} - \frac{u^2+1}{u^2+1} = \frac{1-u^2}{1+u^2}$$

$$\implies d\phi = 2du\cos(\phi/2)^2 = 2du\frac{\sin(\phi)}{2u} = \frac{2du}{1+u^2}$$

Plugging all this in gives:

$$C_1 = \frac{12\epsilon_0 EI}{FL_a^2}\int_0^\infty \frac{r^2\frac{4u^2}{(1+u^2)^2}}{\frac{6d_0EI}{FL_a^2} - 3r\left(\frac{2}{1+u^2}\right) - 2L_a}\frac{2du}{1+u^2}$$

$$\implies \frac{12\epsilon_0 EI}{FL_a^2}\int_0^\infty \frac{8r^2u^2}{\frac{6d_0EI}{FL_a^2} - \frac{6r}{1+u^2} - 2L_a}\frac{du}{(1+u^2)^3}$$

$$\implies \frac{12\epsilon_0 EI}{FL_a^2}\int_0^\infty \frac{8r^2u^2}{\left(\frac{6d_0EI}{FL_a^2} - 2L_a\right)(1+u^2) - 6r}\frac{du}{(1+u^2)^2}$$

$$\implies \frac{16\epsilon_0 EIr}{FL_a^2}\int_0^\infty \underbrace{\frac{u^2}{\left(\frac{d_0EI}{rFL_a^2} - \frac{L_a}{3r}\right)(1+u^2)^3 - (1+u^2)^2}}_{c} du$$

$$\implies \frac{16\epsilon_0 EIr}{FL_a^2}\int_0^\infty \frac{1}{(1+u^2)^2}\frac{u^2}{c(1+u^2)-1}du$$

$$\implies \frac{16\epsilon_0 EIr}{FL_a^2}\int_0^\infty \frac{1}{(1+u^2)^2}\frac{u^2}{cu^2+c-1}du$$

$$\implies \frac{16\epsilon_0 EIr}{FL_a^2}\int_0^\infty \frac{c-1}{u^2+1} - \frac{c(c-1)}{cu^2+c-1} + \frac{1}{(1+u^2)^2}du$$

$$\implies \frac{16\epsilon_0 EIr}{FL_a^2}\left((c-1)\left[\arctan(u)\right]_0^\infty - \int_0^\infty \frac{c(c-1)}{(c-1)\left(\frac{cu^2}{c-1}+1\right)}du + \int_0^\infty \frac{1}{(1+u^2)^2}du\right)$$

In the last integral we substitute $u = \tan(s)$, $du = 1/\cos(s)^2 ds$:

$$C_1 = \frac{16\epsilon_0 EIr}{FL_a^2}\left((c-1)\frac{\pi}{2} - \int_0^\infty \frac{c}{\frac{cu^2}{c-1}+1}du + \int_0^{\pi/2}\frac{1}{\left(1+\tan(s)^2\right)^2}\frac{ds}{\cos(s)^2}\right)$$

In the middle term we substitute $t = \sqrt{\frac{c}{c-1}}u$, $dt = \sqrt{\frac{c}{c-1}}du$

$$C_1 = \frac{16\epsilon_0 EIr}{FL_a^2}\left((c-1)\frac{\pi}{2} - c\sqrt{\frac{c-1}{c}}\int_0^\infty \frac{1}{t^2+1}dt + \int_0^{\pi/2}\frac{1}{\left(\frac{\cos(s)^2}{\cos(s)^2}+\frac{\sin(s)^2}{\cos(s)^2}\right)^2}\frac{ds}{\cos(s)^2}\right)$$

$$\implies \frac{16\epsilon_0 EIr}{FL_a^2}\left((c-1)\frac{\pi}{2} - \sqrt{c(c-1)}\left[\arctan(t)\right]_0^\infty + \int_0^{\pi/2}\cos(s)^2 ds\right)$$

$$\implies \frac{16\epsilon_0 EIr}{FL_a^2}\left((c-1)\frac{\pi}{2} - \sqrt{c(c-1)}\frac{\pi}{2} + \int_0^{\pi/2}\frac{1}{2}+\frac{\cos(2s)}{2}ds\right)$$

$$\implies \frac{16\epsilon_0 EIr}{FL_a^2}\left((c-1)\frac{\pi}{2} - \sqrt{c(c-1)}\frac{\pi}{2} + \frac{\pi}{4} + \left[\frac{\sin(2s)}{2}\right]_0^{\pi/2}\right)$$

$$\implies \frac{8\pi\epsilon_0 EIr}{FL_a^2}\left(c-1-\sqrt{c(c-1)}+\frac{1}{2}\right)$$

$$\implies \frac{8\pi\epsilon_0 EIr}{FL_a^2}\left(c-\frac{1}{2}-\sqrt{c(c-1)}\right)$$

$$\boxed{C_1 = \frac{8\pi\epsilon_0 EIr}{FL_a^2}\left(\frac{d_0 EI}{rFL_a^2}-\frac{L_a}{3r}-\frac{1}{2}-\sqrt{\left(\frac{d_0 EI}{rFL_a^2}-\frac{L_a}{3r}\right)\left(\frac{d_0 EI}{rFL_a^2}-\frac{L_a}{3r}-1\right)}\right)} \tag{B.0.1}$$

We can simplify Equation (B.0.1) a bit by performing a Taylor expansion on the square root:

$$C_1 = \frac{8\pi\epsilon_0 EIr}{FL_a^2}\left(c-\frac{1}{2}-\sqrt{c(c-1)}\right) = \frac{8\pi\epsilon_0 EIr}{FL_a^2}\left(c-\frac{1}{2}-c\sqrt{1-\frac{1}{c}}\right)$$

$$\implies \frac{8\pi\epsilon_0 EIrc}{FL_a^2}\left(1-\frac{1}{2c}-\sqrt{1-\frac{1}{c}}\right) \approx \frac{8\pi\epsilon_0 EIrc}{FL_a^2}\left(1-\frac{1}{2c}-\left(1-\frac{1}{2c}-\frac{1}{8c^2}+\mathcal{O}\left(c^{-3}\right)\right)\right)$$

$$\implies \frac{8\pi\epsilon_0 EIrc}{FL_a^2}\frac{1}{8c^2} = \frac{\pi\epsilon_0 EIr}{FL_a^2 c} = \frac{\pi\epsilon_0 EIr}{FL_a^2\left(\frac{d_0 EI}{rFL_a^2}-\frac{L_a}{3r}\right)} = \frac{\epsilon_0 EI\overbrace{\pi r^2}^{A}}{d_0 EI - \frac{FL_a^3}{3}}$$

$$\boxed{C_1 = \frac{\epsilon_0 A}{d_0 - \frac{FL_a^3}{3EI}}} \tag{B.0.2}$$

Appendix C

Schematic representation of full VSM setup

On the next page we present a full schematic overview (not to scale) of the Vibrating Sample Magnetometer (VSM) setup at HFML-FELIX. A controlling computer (top left) drives the motor which will move the sample between the pickup cols (bottom left). The potentiometer (powered by a battery) vibrates along with the motor. We then use a "splitter box" to separate the AC and DC component of this vibration, which are then measured with a lock-in amplifier and digital multimeter respectively. The oscillating signal from the sum of all pickup coils is measured on a second lock-in amplifier, using the first lock-in amplifier as a reference. Also depicted are the power supply for the motor, a monitoring oscilloscope, and a second multimeter for monitoring the depletion level of the potentiometer battery.

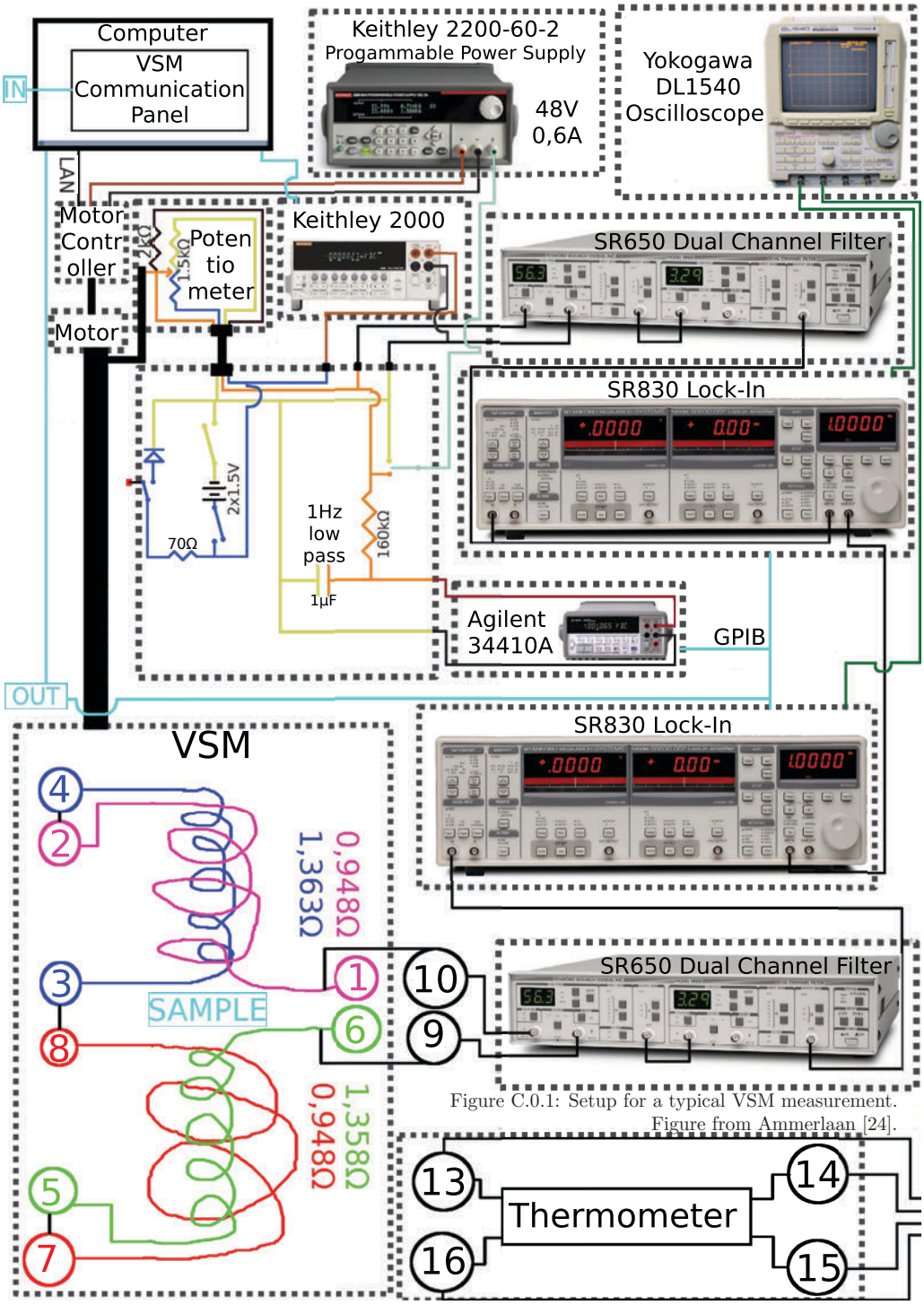

Figure C.0.1: Setup for a typical VSM measurement. Figure from Ammerlaan [24].

9 789465 152233

Radboud Universiteit